UNIVERSIDAD DE CONCEPCIÓN

Centro de Investigación en Ingeniería Matemática (CI^{2}MA)

A mixed hybrid high-order formulation for linear interior transmission elliptic problems

Rommel Bustinza, Jonathan Munguia

PREPRINT 2020-10

SERIE DE PRE-PUBLICACIONES

A mixed Hybrid High-Order formulation for linear interior transmission elliptic problems*

ROMMEL BUSTINZA† and JONATHAN MUNGUIA-LA-COTERA‡

Abstract

In this paper, we analyse a linear transmission elliptic problem in a bounded domain, applying the already known Hybrid High-Order (HHO) method. This approach gives approximation of unknowns in the interior volume of each element and on the faces of its boundary, in the following sense: obtaining L^2-projection on the space of polynomials of total degree at most k on the mesh elements and faces. Thus, we obtain a non-conforming discrete formulation, which is well posed, and after a condensation process, we can reduced it to another scheme defined on the skeleton induced by the mesh. This allows us to obtain a more compact system and reduce significantly the number of unknowns. We point out that we need to introduce an auxiliary unknown in order to deal with the non homogeneous transmission conditions, that will act as Lagrange multiplier. We prove that the method is optimally convergent in the energy norm, as well as in the L^2-norm for the potential and a weighted L^2-norm for the Lagrange multiplier, for smooth enough solutions. Finally, we include some numerical experiments that validate our theoretical results, even in situations not covered by the current analysis.

Keywords: Linear interior transmission elliptic problem, Polytopal Meshes, Hybrid High-Order method, Gradient reconstruction operator, Potential reconstruction operator.

1 Introduction

Transmission problems appear in many areas of engineering and science. They can involve multiple distinct materials or fluids with different densities, diffusions, conductivities, Youngs modulus, or Poisson ratio. For example, they appear in the calculation of magnetic fields of electromagnetic devices [51, 52], in problems of fluid mechanics and subsonic flow [38, 39, 14],

*This research has been partially supported by CONICYT / PIA / Concurso Apoyo a Centros Científicos y Tecnológicos de Excelencia con Financiamiento Basal AFB170001, by Vicerrectoría de Investigación y Desarrollo de la Universidad de Concepción (Chile) through project VRID-Enlace No. 218.013.044-1.0, and by Centro de Investigación en Ingeniería Matemática (CI^{2}MA), Universidad de Concepción (Chile), by CONCYTEC-Perú through FONDECYT project "Programas de Doctorado en Universidades Peruanas" CG-176-2015, Instituto de Matemática y Ciencias Afines (IMCA), and to Universidad Nacional de Ingeniería (Lima-Perú)

†Centro de Investigación en Ingeniería Matemática (CI^{2}MA) and Departamento de Ingeniería Matemática, Universidad de Concepción, Concepción, Chile, e-mail: rbustinz@ing-mat.udec.cl

‡Instituto de Matemática y Ciencias Afines (IMCA) and Universidad Nacional de Ingeniería (UNI), Lima, Perú, e-mail: jmunguial@uni.edu.pe

in incompressible multiphase flows [55], in models of electroporation [48] and electrohydrodynamic [53], and many other fields.

There are two types of transmission problems, exterior and interior. The work developed here corresponds to an interior one. In turn, interior transmission problems fit into interface problems, which can be found in material properties [61], modeling solid mechanics problems [59, 14], in fluid dynamics [37, 9], and many other important phenomena in science and engineering.

On the other hand, the numerical solution of exterior problems usually combines the Finite Element (FE) method with the Boundary Element (BE) method (see, e.g. [7, 43, 15]). FE method was proposed, for interface problems, in [59, 12, 22]. Also, it is possible to combine local discontinuous Galerkin (LDG) method with BE method, which does not require any continuity condition across the interelement boundaries, it is robust with respect to discontinuous coefficients, and it allows the use of different polynomial degrees in each element (see [16, 17, 45, 18]).

Moreover, interface problems are divided into interface-fitted and unfitted mesh. The former is built on body fitted mesh that does not allow the interface to cut across any of the elements in the mesh, while the latter does not impose that restriction. There exists several methods, such as immersed interface method [57, 46], fitted FE method [12], unfitted FE method [49], embedded FE method [35], multiscale finite element methods [23], extended finite element (XFE) method [5, 59], fitted HDG method [48], unfitted HDG method [64, 36], for example. Also, there are works considering a curve as interface. We can refer to the classical FE methods [4, 8], and HDG method [54, 63].

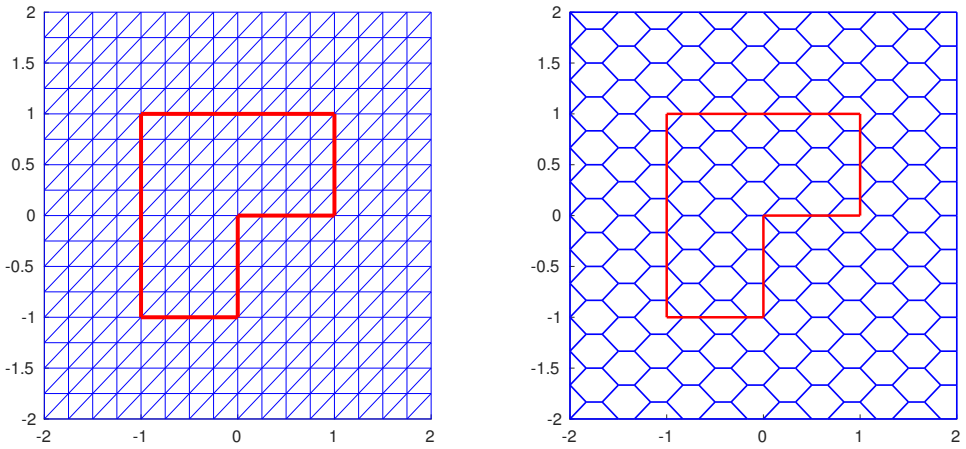

Figure 1: An interface-fitted mesh (left), and an unfitted mesh (right).

Interface-fitted mesh is also known as body-fitted or interface conforming, i.e. the meshes are tailored to fit the interface, (cf. left plot in Figure 1). Besides, the jump conditions across the

interface can be easily incorporated into a standard FE formulation [12, 22]. There are sophisticated use of approximate interface-fitted meshes [65] and the use of Virtual element methods on an interface-fitted mesh [21].

However, interface-unfitted mesh is more used in time dependent problems, where the interface moves with time or during iteration (free-boundary), and when the boundary or the internal interface is curved. This is caused since generating a body fitted mesh of relatively high quality is challenging and computationally costly, especially when complex and/or moving interfaces are involved. In this sense, it may be advantageous to use the same mesh on the domain for different, nearby, locations of the interface.

A well-known disadvantage for unfitted mesh approach, is the difficulty to capture the complex geometry of the interface and to enforce jump conditions across the interface accurately. The resulting linear system may not be always symmetric and its conditioning has a strong dependence on how the interface cuts the mesh cells. Furthermore, a rigorous error analysis is difficult to perform.

In this work, we consider an interface-fitted mesh, since we handle with a polygonal interface. In transmission problems, in general, it is identified/recognized an internal domain, a transmission or internal boundary, and an external (annular) domain. In the existing bibliography only Dirichlet and mixed conditions on the external boundary are addressed. In this paper we consider pure non-homogeneous Neumann condition on the exterior boundary. This work is not addressed to non mathching transmision mesh, although it is possible to extend our study, following the analysis in [50].

Now, we focus on the well known Hybrid High Order (HHO) method, introduced in [32, 31], which has been applied to a great variety of problems, thanks to its ability to handle physical parameters. We can mention, for example, linear diffusion problems [32, 31], quasi-incompressible linear elasticity [30], nonlinear elasticity problems in the small deformation regime [11], nonlinear Leray–Lions problems [26, 27], Stokes problem [2], incompressible Navier-Stokes equations [10], and finite deformations of hyperelastic materials [1], among other problems.

Its design relies on discrete unknowns that are broken polynomials on the mesh and on its skeleton, from which two key ingredients are devised:

(i) Local reconstructions, that are performed by solving small, parallel problems inside each element, and conceived so that their composition with the natural interpolator of sufficiently smooth functions yields a projector on local polynomial spaces (see Lemma 3.3).

(ii) Stabilisation terms that penalise residuals, and are defined at the element level, so they ensure stability while preserving the approximation properties of the reconstruction.

These ingredients are combined to formulate local contributions, which are then assembled as in standard Finite Element methods. We mention several advantageous features. Management of polytopal meshes (with possibly hanging nodes), which is an actual topic that is considered to deal with cracks and other kinds of discontinuities induced by material defects [59].

Support arbitrary approximation orders in any space dimension, and exhibits a reduced computational cost, thanks to the compact stencil, along with the possibility to locally eliminate a large portion of the unknowns (see Section 5 in [19]), is achieved. Then, we deal with a (linear) system defined on the skeleton of the mesh.

In lowest-order version ($k = 0$), HHO method can be linked with the unified framework Hybrid Mixed Mimetic (HMM) method [28]. In high-order, there is a link of HHO approach with HDG method [24], a connection with High-Order mimetic (HOM) [58], and with the non-conforming version of the Virtual Element (VE) method [3]. In addition, we find a description of the relation between HHO and VE methods in [56], with an analysis that differs from the standard VE method described in [62].

We point out that a transmission problem with curved interface, has been studied in [13], applying an unfitted finite element method (introduced in [49]), with the philosophy of HHO method. However, we point-wise that this paper does not include numerical experiments. In this work, we applied the standard HHO method for a linear transmission problem with non homogeneous transmission conditions, extending the application of the HHO approach described in [32]. We remark that the analysis here is quite different to the presented in [13], since we introduce an auxiliary unknown living on the transmission interface, that acts as a Lagrange multiplier. As result, we derive a discrete mixed HHO formulation.

The rest of this paper is organized as follows. In Section 2, we introduce the model problem and discuss its well-posedness, at continuous level. In Section 3, we describe the main analysis tools, the Degrees of Freedom (DOFs) in the context of HHO method, and the potential reconstruction operator, with its key properties. In Section 4, we introduce the discrete problem and study its stability. In Section 5, we perform the a priori error analysis, first in the energy-norm, and then in the L^2-norm under additional elliptic regularity assumptions. In Section 6, we discuss the aspects of the computational implementation. Finally, in Section 7, we present some numerical experiments, which are in agreement with our theoretical results.

2 Continuous settings

In this paper, we will work with two disjoint domains. Let Ω_1 be a bounded and simply connected domain in $\mathbb{R}^d$, $d \in \{2, 3\}$, with Lipschitz-continuous boundary $\Gamma_1 := \partial\Omega_1$. Let Ω_2 be the annular region bounded by Γ_1 and a second Lipschitz-continuous curve Γ_2, that is strictly contained in $\mathbb{R}^2 - \bar{\Omega}_1$ (see Figure 2). For any connected subset $X \subset \bar{\Omega}$ with nonzero Lebesgue measure, the inner product and norm of the Lebesgue space $L^2(X)$ are denoted by $(\cdot, \cdot)_X$ and $||\cdot||_X$, respectively.

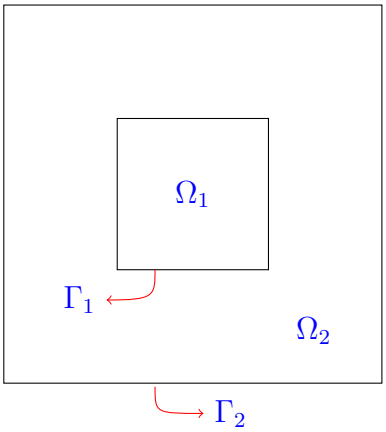

Figure 2: Geometry of the problem

Next, we consider the following transmission interior model problem: Find $u_1 : \Omega_1 \to \mathbb{R}$ and $u_2 : \Omega_2 \to \mathbb{R}$ such that

$$-\Delta u_1 = f_1 \text{ in } \Omega_1\,, \tag{1a}$$
$$-\Delta u_2 = f_2 \text{ in } \Omega_2\,, \tag{1b}$$
$$u_1 - u_2 = g \text{ on } \Gamma_1\,, \tag{1c}$$
$$\nabla u_1 \cdot \boldsymbol{n}_1 + \nabla u_2 \cdot \boldsymbol{n}_2 = g_1 \text{ on } \Gamma_1\,, \tag{1d}$$
$$\nabla u_2 \cdot \boldsymbol{n}_2 = g_2 \text{ on } \Gamma_2\,, \tag{1e}$$
$$\int_{\Omega_1} u_1 + \int_{\Omega_2} u_2 = 0\,, \tag{1f}$$

where $f_1 \in L^2(\Omega_1)$ and $f_2 \in L^2(\Omega_2)$ are the forcing terms, $g \in H^{1/2}(\Gamma_1)$ is the jump of traces of solutions on Γ_1, $g_1 \in H^{-1/2}(\Gamma_1)$ and $g_2 \in H^{-1/2}(\Gamma_2)$ are the jump of normal component of fluxes on Γ_1, and the normal component of u_2 on Γ_2. Here, $\boldsymbol{n}_1$ represents the unit outward normal to the boundary of Ω_1, while $\boldsymbol{n}_2$ denotes the unit outward normal to the boundary of Ω_2 given by $\partial\Omega_2 := \Gamma_1 \cup \Gamma_2$. Also we impose the following compatibility condition

$$\int_{\Omega_1} f_1 + \int_{\Omega_2} f_2 + \langle g_1, 1\rangle_{\Gamma_1} + \langle g_2, 1\rangle_{\Gamma_2} = 0\,, \tag{2}$$

for the well-posedness of problem (1).

The starting point of the HHO method relies on finding a primal-mixed variational formulation of (1). We consider the equations $-\Delta u_i = f_i$ in Ω_i, $i \in \{1, 2\}$, and after integrating by parts, we deduce that

$$(\nabla u_1, \nabla v_1)_{\Omega_1} - \langle \nabla u_1 \cdot \boldsymbol{n}_1, \gamma_0^-(v_1)\rangle_{\Gamma_1} = (f_1, v_1)_{\Omega_1}\,, \tag{3}$$
$$(\nabla u_2, \nabla v_2)_{\Omega_2} - \langle \nabla u_2 \cdot \boldsymbol{n}_2, \gamma_0^+(v_2)\rangle_{\Gamma_1} - \langle \nabla u_2 \cdot \boldsymbol{n}_2, \gamma_0^+(v_2)\rangle_{\Gamma_2} = (f_2, v_2)_{\Omega_2}\,, \tag{4}$$

for all $(v_1, v_2) \in H^1(\Omega_1) \times H^1(\Omega_2)$, where $\langle\cdot,\cdot\rangle_{\Gamma_1}$ denotes the duality pairing of $H^{-1/2}(\Gamma_1)$ and $H^{1/2}(\Gamma_1)$ with respect to the $L^2(\Gamma_1)$-inner product, and analogously for $\langle\cdot,\cdot\rangle_{\Gamma_2}$. In addition, $\gamma_0^- : H^1(\Omega_1) \to H^{1/2}(\partial\Omega_1)$ and $\gamma_0^+ : H^1(\Omega_2) \to H^{1/2}(\partial\Omega_2)$ correspond to the trace operators

on each subdomain. Then, using (1d), introducing the auxiliary unknown $\xi := \nabla u_1 \cdot \boldsymbol{n}_1 \in H^{-1/2}(\Gamma_1)$, and taking into account (1e), (3), and (4), we obtain

$$\sum_{i=1}^{2}(\nabla u_i, \nabla v_i)_{\Omega_i} - \langle g_1, \gamma_0^+(v_2)\rangle_{\Gamma_1} - \langle g_2, \gamma_0^+(v_2)\rangle_{\Gamma_2} - \langle \xi, \gamma_0^-(v_1) - \gamma_0^+(v_2)\rangle_{\Gamma_1} = \sum_{i=1}^{2}(f_i, v_i)_{\Omega_i}\,. \tag{5}$$

Further, we can formulate the jump of the traces of u_1 and u_2 on Γ_1, as

$$\langle \lambda, \gamma_0^-(u_1) - \gamma_0^+(u_2)\rangle_{\Gamma_1} = \langle \lambda, g\rangle_{\Gamma_1} \quad \forall\, \lambda \in H^{-1/2}(\Gamma_1)\,. \tag{6}$$

We now introduce the Hilbert space

$$\mathbf{U} := \left\{(v_1, v_2) \in H^1(\Omega_1) \times H^1(\Omega_2) \,:\, (v_1, 1)_{\Omega_1} + (v_2, 1)_{\Omega_2} = 0\right\}\,, \tag{7}$$

provided with the norm $||(v_1, v_2)||^2_{\mathbf{U}} := ||v_1||^2_{1,\Omega_1} + ||v_2||^2_{1,\Omega_2}$ and $Q := H^{-1/2}(\Gamma_1)$, with its usual norm $||\cdot||_{-1/2,\Gamma_1}$. Then, the variational formulation reads as: Find $((u_1, u_2), \xi) \in \mathbf{U} \times Q$ such that

$$a((u_1, u_2), (v_1, v_2)) + b((v_1, v_2), \xi) = F(v_1, v_2) \quad \forall (v_1, v_2) \in \mathbf{U}, \tag{8a}$$

$$-b((u_1, u_2), \lambda) = G(\lambda) \qquad \forall \lambda \in Q. \tag{8b}$$

where $a : \mathbf{U} \times \mathbf{U} \to \mathbb{R}$ and $b : \mathbf{U} \times Q \to \mathbb{R}$ are bilinear forms defined as

$$a((w_1, w_2), (v_1, v_2)) := (\nabla w_1, \nabla v_1)_{\Omega_1} + (\nabla w_2, \nabla v_2)_{\Omega_2} \quad \forall\, (w_1, w_2)\,,\, (v_1, v_2) \in \mathbf{U} \times \mathbf{U}\,,$$

$$b((v_1, v_2), \lambda) := \langle \lambda, \gamma_0^+(v_2) - \gamma_0^-(v_1)\rangle_{\Gamma_1} \quad \forall\, ((v_1, v_2), \lambda) \in \mathbf{U} \times Q\,,$$

while the linear functionals $F : \mathbf{U} \to \mathbb{R}$ and $G : Q \to \mathbb{R}$, are given by

$$F(v_1, v_2) := (f_1, v_1)_{\Omega_1} + (f_2, v_2)_{\Omega_2} + \langle g_1, \gamma_0^+(v_2)\rangle_{\Gamma_1} + \langle g_2, \gamma_0^+(v_2)\rangle_{\Gamma_2} \quad \forall\,,\,(v_1, v_2) \in \mathbf{U}\,,$$

$$G(\lambda) := \langle \lambda, g\rangle_{\Gamma_1} \quad \forall\, \lambda \in Q\,.$$

Lemma 2.1 *b is bounded.*

Proof. First, we fix $((v_1, v_2), \lambda) \in \mathbf{U} \times Q$. Then, we have

$$\begin{aligned} b((v_1, v_2), \lambda) &\leq ||\lambda||_{-1/2,\Gamma_1}\,(||\gamma_0^+(v_2)||_{1/2,\Gamma_1} + ||\gamma_0^-(v_1)||_{1/2,\Gamma_1}) \\ &\leq ||\lambda||_{-1/2,\Gamma_1}\,||(v_1, v_2)||_{\mathbf{U}}\,, \end{aligned}$$

and we conclude the statement. □

Remark 2.1 *Thanks to the boundedness of bilinear form b, we can define a bounded linear operator $\boldsymbol{B} : \mathbf{U} \to Q'$, induced by the bilinear form b, such that*

$$[\boldsymbol{B}(v_1, v_2), \lambda] := b((v_1, v_2), \lambda) \quad \forall\, (v_1, v_2) \in \mathbf{U}\,, \forall\, \lambda \in Q\,,$$

where $[\cdot, \cdot]$ stands for the duality pairing induced by the operator and functional used in this case. It is not difficult to deduce that $\boldsymbol{B}((v_1, v_2)) := \mathcal{R}^*(\gamma_0^+(v_2) - \gamma_0^-(v_1)) \quad \forall\, (v_1, v_2) \in \mathbf{U}$, where $\mathcal{R} : H^{-1/2}(\Gamma_1) \to H^{1/2}(\Gamma_1)$ represents the canonical Riesz operator between $H^{-1/2}(\Gamma_1)$ and $H^{1/2}(\Gamma_1)$, while $\mathcal{R}^* : H^{1/2}(\Gamma_1) \to H^{-1/2}(\Gamma_1)$ corresponds to the adjoint (Hilbert) Riesz operator of $\mathcal{R}$. Hereafter, $\langle \cdot, \cdot \rangle_{r,\Gamma_1}$ denotes the inner product on $H^r(\Gamma_1)$, $r \in \{-1/2, 1/2\}$. Finally, $\mathrm{Ker}(\boldsymbol{B})$ is characterized by

$$\mathbf{V} := \mathrm{Ker}(\boldsymbol{B}) := \{(v_1, v_2) \in \mathbf{U} : \gamma_0^-(v_1) = \gamma_0^+(v_2) \text{ on } \Gamma_1\}\,. \tag{9}$$

Lemma 2.2 *a is bounded in $\mathbf{U}\times\mathbf{U}$, and $\mathbf{V}$-elliptic.*

Proof. The continuity of bilinear form a follows from the Cauchy-Schwarz inequality. To prove the coerciveness of a on $\mathbf{V}$, we first set $\Omega := \Omega_1 \cup \Gamma_1 \cup \Omega_2$. Next, given $(v_1, v_2) \in \mathbf{V}$, we define the following measurable function

$$v := \begin{cases} v_1 & , \quad \text{a.e.} \in \Omega_1 \\ v_2 & , \quad \text{a.e.} \in \Omega_2. \end{cases} \tag{10}$$

Since $v_1 \in H^1(\Omega_1)$, $v_2 \in H^1(\Omega_2)$, and $\gamma_0^-(v_1) = \gamma_0^+(v_2)$ on Γ_1, we infer that $v \in H^1(\Omega)$, with $\int_\Omega v = 0$. Then, thanks to the Poincaré-Wintinger inequality, the seminorm $|\cdot|_{1,\Omega}$ is equivalent to $||\cdot||_{1,\Omega}$ in $H^1(\Omega)\cap L^2_0(\Omega)$, we deduce

$$\begin{aligned} a((u_1,u_2),(v_1,v_2)) &= \|\nabla v_1\|^2_{0,\Omega_1} + \|\nabla v_2\|^2_{0,\Omega_2} = \|\nabla v\|^2_{0,\Omega} \\ &\geq (1+C_p^2)^{-1}\|v\|^2_{1,\Omega} \\ &= (1+C_p^2)^{-1}\|(v_1,v_2)\|^2_{\mathbf{U}}, \end{aligned} \tag{11}$$

where $C_p > 0$ is the constant of Poincaré. □

Lemma 2.3 $\mathbf{B}$ *is surjective.*

Proof. Given $\lambda \in H^{-1/2}(\Gamma_1)$, there exists $z := -\left(\tilde{\gamma}_0^-\right)^{-1}\left(\mathcal{R}^*\right)^{-1}\lambda \in [H^1_0(\Omega_1)]^\perp \subset H^1(\Omega_1)$, such that $\lambda = \mathcal{R}^*(\gamma_0^-(z))$, where $\tilde{\gamma_0} := \gamma_0|_{[H^1_0(\Omega_1)]^\perp}$. For more details, we refer to [41] (pages 196-198). Now, by setting $c := -\dfrac{1}{|\Omega_1|+|\Omega_2|}\displaystyle\int_{\Omega_1} z$, we introduce $(v_1,v_2)\in H^1(\Omega_1)\times H^1(\Omega_2)$ such that $v_1 := z + c$ and $v_2 := c$, which in addition verifies that $(v_1,1)_{\Omega_1} + (v_2,1)_{\Omega_2} = 0$, letting us to conclude that $(v_1,v_2)\in\mathbf{U}$. Then, since $\gamma_0^+(v_2) - \gamma_0^-(v_1) = \gamma_0^-(-z)$ on Γ_1, we infer that

$$\mathbf{B}(v_1,v_2) = \mathcal{R}^*(\gamma_0^+(v_2) - \gamma_0^-(v_1)) = \mathcal{R}^*(\gamma_0^-(-z)) = \lambda\,.$$

□

We now establish the unique solvability of the variational problem.

Theorem 2.1 (Well-posedness) *The continuous problem* (8) *is well-posed.*

Proof. Taking into account Lemmas 2.1, 2.2 and 2.3, we invoke well known Babuška-Brezzi's theory, to conclude that the variational problem (8) is well-posed. □

Remark 2.2 *For $\lambda \in H^{1/2}(\Gamma_1)$ given, and $(v_1,v_2)\in\mathbf{U}$ defined as in the proof of Lemma 2.3, there holds*

$$\begin{aligned} b((v_1,v_2),\lambda) &= \langle\lambda\,,\,\gamma_0^+(v_2)-\gamma_0^-(v_1)\rangle_{\Gamma_1} = \langle\lambda\,,\,\gamma_0^-(-z)\rangle_{\Gamma_1} \\ &= \langle\lambda\,,\,\left(\mathcal{R}^*\right)^{-1}\lambda\rangle_{\Gamma_1} = ||\lambda||^2_{-1/2,\Gamma_1}\,. \end{aligned}$$

In addition, there exists $C_{\texttt{INF}} = C_{\texttt{INF}}(|\Omega_1|,|\Omega_2|) > 0$ such that

$$||(v_1,v_2)||^2_{\mathbf{U}} \leq C_{\texttt{INF}}\,||z||^2_{1,\Omega_1}\,.$$

As result, we can establish the so called inf-sup condition for b:

$$\sup_{(w_1,w_2)\in\mathbf{U}\setminus\{0\}}\frac{b((w_1,w_2),\lambda)}{||(w_1,w_2)||_{\mathbf{U}}} \geq \frac{b((v_1,v_2),\lambda)}{||(v_1,v_2)||_{\mathbf{U}}} \geq C_{\texttt{INF}}^{-1/2}\,\frac{||\lambda||^2_{-1/2,\Gamma_1}}{||z||_{1,\Omega_1}} = C_{\texttt{INF}}^{-1/2}\,||\lambda||_{-1/2,\Gamma_1}\,. \tag{12}$$

3 Discrete settings

We begin this section giving a general description of the discrete spaces, operators that we need to introduce for the discretization of the transmission problem, including some approximation properties. For simplicity, we let Ω be a domain with polygonal boundary. Then, we introduce $\mathcal{H} \subset \mathbb{R}^+$ as a countable set of meshsizes having 0 as its unique accumulation point and $\{\mathcal{T}_h\}_{h\in\mathcal{H}}$ be an h-refined admissible mesh sequence of $\bar{\Omega}$ (see Section 1.4 in [29]). Each mesh $\mathcal{T}_h$ is a finite collection $\{T\}$ of nonempty, disjoint, open, polytopal elements such that $\overline{\Omega} = \bigcup_{T\in\mathcal{T}_h} \overline{T}$. In addition, there is a matching simplicial submesh of $\mathcal{T}_h$ with locally equivalent meshsize and which is shape-regular in the usual sense. We also assume (for simplicity) that for each $T \in \mathcal{T}_h$, either $T \subset \bar{\Omega}_1$ or $T \subset \bar{\Omega}_2$, and that there are no hanging nodes on the transmission boundary Γ_1. We call a face, any hyperplanar closed connected subset F of $\overline{\Omega}$ with positive $(d-1)$-dimensional measure, such that (i) either there exist T_1, $T_2 \in \mathcal{T}_h$ with $F \subset \partial T_1 \cap \partial T_2$ (and F is called an interface) or (ii) there exists $T \in \mathcal{T}_h$ such that $F \subset \partial T \cap \partial\Omega$ (and F is called a boundary face). Interfaces are collected in the set $\mathcal{F}_h^{\mathtt{int}}$, boundary faces in $\mathcal{F}_h^{\mathtt{b}}$, and we set the list of faces on skeletal induced by $\mathcal{T}_h$ as $\mathcal{F}_h := \mathcal{F}_h^{\mathtt{int}} \cup \mathcal{F}_h^{\mathtt{b}}$.

On the other hand, given $T \in \mathcal{T}_h$, $\mathcal{F}_T := \{F \in \mathcal{F}_h \,|\, F \subset \partial T\}$ denotes the set of faces lying on the boundary of T and, for each $F \in \mathcal{F}_T$, $\boldsymbol{n}_{TF}$ is the unit normal to F pointing out of T. In an admissible mesh sequence, the diameters of the elements (h_T) and the diameters of the faces (h_F), linked to each element, are uniformly comparable, card($\mathcal{F}_T$) is uniformly bounded, the usual discrete and multiplicative trace inequalities hold on element faces, and the L^2-orthogonal projector onto polynomial spaces enjoys optimal approximation properties on each mesh element. In what follows, $A \lesssim B$ denotes the inequality $A \leq CB$ with positive constant C independent of the polynomial degree k, and the meshsize h of $\mathcal{T}_h$, which is set as $h := \max_{T\in\mathcal{T}_h} h_T$.

Lemma 3.1 (Approximation property of Orthogonal projector) *Given an integer $l \geq 0$, there exists a real positive number C_a, depending on ρ (mesh regularity parameter) and l, such that, for all $h \in \mathcal{H}$, and all $T \in \mathcal{T}_h$, denoting by π_T^l the L^2-orthogonal projector on $\mathbb{P}_d^l(T)$, and for all $s, t \in \mathbb{R}$ such that $0 \leq s \leq t \leq l+1$, there holds*

$$|v - \pi_T^l v|_{s,T} \leq C_a h_T^{t-s} |v|_{t,T}, \quad \forall\, v \in H^t(T)\,. \tag{13}$$

Moreover, there exists $\tilde{C}_a > 0$, such that, for all $1/2 < t \leq l+1$, there holds

$$\|v - \pi_T^l v\|_{0,\partial T} \leq \tilde{C}_a h_T^{t-1/2} |v|_{t,T}, \quad \forall\, v \in H^t(T), \tag{14}$$

where, given $r \geq 0$, $|\cdot|_{r,T}$ denotes the usual seminorm on Sobolev spaces $H^r(T)$.

Proof. We refer to the proofs of Theorems 3.2 and 3.3 in [44]. □

3.1 Degrees of freedom

Let a polynomial degree $k \geq 0$ be fixed. For each $T \in \mathcal{T}_h$, we define the local space of DOFs as $\underline{\mathbf{U}}_T^k := \mathbb{P}_d^k(T) \times \big(\prod_{F\in\mathcal{F}_T} \mathbb{P}_{d-1}^k(F)\big)$, where $\mathbb{P}_d^k(T)$ (resp., $\mathbb{P}_{d-1}^k(F)$) is spanned by the restrictions

to T (resp., F) of d-variate (resp., $(d-1)$-variate) polynomials of total degree $\leq k$. The global space of DOFs on the domain Ω is then defined as,

$$\underline{\mathbf{U}}_{\mathcal{T}_h}^k := \left(\prod_{T\in\mathcal{T}_h} \mathbb{P}_d^k(T) \right) \times \left(\prod_{F\in\mathcal{F}_h} \mathbb{P}_{d-1}^k(F) \right) .$$

Given $\underline{\mathbf{v}}_h := \Big((v_T)_{T\in\mathcal{T}_h}, (v_F)_{F\in\mathcal{F}_h} \Big) \in \underline{\mathbf{U}}_{\mathcal{T}_h}^k$, we introduce its restriction to the element $T \in \mathcal{T}_h$ as $\underline{\mathbf{v}}_T := \Big(v_T, (v_F)_{F\in\mathcal{F}_T} \Big) \in \underline{\mathbf{U}}_T^k$. In addition, by v_h we denote the function belonging to $\mathbb{P}_d^k(\mathcal{T}_h)$, such that $v_h|_T = v_T \quad \forall\, T \in \mathcal{T}_h$. These notations allow us to introduce the usual seminorm on $\underline{\mathbf{U}}_{\mathcal{T}_h}^k$ (see Lemma 4 in [32])

$$\|\underline{\mathbf{v}}_h\|_{1,\mathcal{T}_h}^2 := \sum_{T\in\mathcal{T}_h} \|\underline{\mathbf{v}}_T\|_{1,T}^2 \quad , \quad \|\underline{\mathbf{v}}_T\|_{1,T}^2 := \|\nabla v_T\|_{0,T}^2 + |\underline{\mathbf{v}}_T|_{1,\partial T}^2 , \tag{15}$$

for all $\underline{\mathbf{v}}_h \in \underline{\mathbf{U}}_{\mathcal{T}_h}^k$ and all $\underline{\mathbf{v}}_T \in \underline{\mathbf{U}}_T^k$, where

$$|\underline{\mathbf{v}}_T|_{1,\partial T}^2 := \sum_{F\in\mathcal{F}_T} h_F^{-1} \|v_F - v_T\|_{0,F}^2 .$$

Now, for each $T \in \mathcal{T}_h$, we define the local reduction operator $\underline{\mathbf{I}}_T^k : H^1(T) \to \underline{\mathbf{U}}_T^k$ such that, for each $v \in H^1(T)$,

$$\underline{\mathbf{I}}_T^k v := (\pi_T^k v, (\pi_F^k v)_{F\in\mathcal{F}_T}), \tag{16}$$

where π_T^k and π_F^k are the L^2-orthogonal projectors onto $\mathbb{P}_d^k(T)$ and $\mathbb{P}_{d-1}^k(F)$, respectively. The corresponding global reduction operator $\underline{\mathbf{I}}_{\mathcal{T}_h}^k : H^1(\Omega) \to \underline{\mathbf{U}}_{\mathcal{T}_h}^k$ is defined by

$$\underline{\mathbf{I}}_{\mathcal{T}_h}^k v := ((\pi_T^k v)_{T\in\mathcal{T}_h}, (\pi_F^k v)_{F\in\mathcal{F}_h}) \quad \forall\, v \in H^1(\Omega) . \tag{17}$$

3.2 Local Gradient reconstruction

For all $T \in \mathcal{T}_h$, we define the local gradient reconstruction operator $G_T^k : \underline{\mathbf{U}}_T^k \to \nabla\mathbb{P}_d^{k+1}(T)$ such that, for all $\underline{\mathbf{v}}_T := (v_T, (v_F)_{F\in\mathcal{F}_T}) \in \underline{\mathbf{U}}_T^k$ and all $w \in \mathbb{P}_d^{k+1}(T)$,

$$(G_T^k \underline{\mathbf{v}}_T, \nabla w)_T = (\nabla v_T, \nabla w)_T + \sum_{F\in\mathcal{F}_T} (v_F - v_T, \nabla w \cdot \boldsymbol{n}_{TF})_F, \tag{18}$$

where $\boldsymbol{n}_{TF}$ is the unit normal to face F pointing out of element T. We define the potential reconstruction operator $p_T^{k+1} : \underline{\mathbf{U}}_T^k \to \mathbb{P}_d^{k+1}(T)$ such that, for all $\underline{\mathbf{v}}_T \in \underline{\mathbf{U}}_T^k$,

$$\nabla p_T^{k+1} \underline{\mathbf{v}}_T = G_T^k \underline{\mathbf{v}}_T \qquad \int_T p_T^{k+1} \underline{\mathbf{v}}_T = \int_T v_T . \tag{19}$$

Lemma 3.2 (Characterization of $p_T^{k+1}\underline{\mathbf{I}}_T^k$ and polynomial consistency) *The following property holds for all $v \in H^1(T)$:*

$$(\nabla(v - p_T^{k+1}\underline{\mathbf{I}}_T^k v), \nabla w)_T = 0 \quad \forall\, w \in \mathbb{P}_d^{k+1}(T). \tag{20}$$

Consequently, for all $v \in \mathbb{P}_d^{k+1}(T)$, we have

$$p_T^{k+1}\underline{\mathbf{I}}_T^k v = v. \tag{21}$$

Proof. We refer to the proof of Lemma 3.1 in [34]. □

Lemma 3.3 (Approximation properties for $p_T^{k+1}\underline{\mathbf{I}}_T^k$). *Let a polynomial degree $k \geq 0$, an integer $q \in \{0, \cdots, k\}$, and $\delta \in (1/2, 1]$ be given. There exists a real number $C > 0$, depending on ρ (mesh regularity parameter), possibly on d, k, q, and δ, but independent of h_T, such that, for all $h \in \mathcal{H}$, for all $T \in \mathcal{T}_h$, and all $v \in H^{q+1+\delta}(T)$, there holds:*

$$\begin{aligned}&\left\|v - p_T^{k+1}\underline{\mathbf{I}}_T^k v\right\|_{0,T} + h_T^{1/2}\left\|v - p_T^{k+1}\underline{\mathbf{I}}_T^k v\right\|_{0,\partial T}\\ &+ h_T\left\|\nabla(v - p_T^{k+1}\underline{\mathbf{I}}_T^k v)\right\|_{0,T} + h_T^{3/2}\left\|\nabla(v - p_T^{k+1}\underline{\mathbf{I}}_T^k v)\right\|_{0,\partial T} \leq C h_T^{q+1+\delta}\left\|v\right\|_{q+1+\delta,T}. \end{aligned} \tag{22}$$

Proof. We adapt the proof of Lemma 3 in [32]. First, we fix $v \in H^{q+1+\delta}(T)$, with $q \in \{0, ..., k\}$, and notice from the orthogonality property (20), that

$$\begin{aligned}\|\nabla(v - p_T^{k+1}\underline{\mathbf{I}}_T^k v)\|_{0,T} &= \sup_{z \in \mathbb{P}_d^{k+1}(T)} \|\nabla v - \nabla z\|_{0,T}\\ &\leq \|\nabla(v - \pi_T^{k+1} v)\|_{0,T} \lesssim h_T^{q+\delta}\|v\|_{q+1+\delta,T}, \end{aligned} \tag{23}$$

where we have used the approximation property (13) of π_T^{k+1} (with $t = q + 1 + \delta$ and $s = 1$).

Now, from the definition of p_T^{k+1} and $\underline{\mathbf{I}}_T^k$, we observe that $v - p_T^{k+1}\underline{\mathbf{I}}_T^k v \in L_0^2(T)$. Then, applying the very well known inequality $||z||_{0,T} \lesssim h_T|z|_{1,T}$, $\forall\, z \in H^1(T) \cap L_0^2(T)$, togehter with (23), we infer that

$$\|v - p_T^{k+1}\underline{\mathbf{I}}_T^k v\|_{0,T} \lesssim h_T\|\nabla(v - p_T^{k+1}\underline{\mathbf{I}}_T^k v)\|_{0,T} \lesssim h_T^{q+1+\delta}\|v\|_{q+1+\delta,T}. \tag{24}$$

The consecutive use of a continuous trace inequality, (23) and (24), yields

$$h_T\|v - p_T^{k+1}\underline{\mathbf{I}}_T^k v\|_{0,\partial T}^2 \lesssim \|v - p_T^{k+1}\underline{\mathbf{I}}_T^k v\|_{0,T}^2 + h_T^2\|\nabla(v - p_T^{k+1}\underline{\mathbf{I}}_T^k v)\|_{0,T}^2 \lesssim h_T^{2(q+1+\delta)}\|v\|_{q+1+\delta,T}^2. \tag{25}$$

Finally, for to bound $h_T^{3/2}\|\nabla(v - p_T^{k+1}\underline{\mathbf{I}}_T^k v)\|_{0,\partial T}$, we introduce $\pm\pi_T^k\nabla v$ inside the norm, obtaining

$$h_T^{3/2}\left\|\nabla(v - p_T^{k+1}\underline{\mathbf{I}}_T^k v)\right\|_{0,\partial T} \leq h_T^{3/2}\left\|\nabla v - \pi_T^k\nabla v\right\|_{0,\partial T} + h_T^{3/2}\left\|\pi_T^k\nabla v - \nabla p_T^{k+1}\underline{\mathbf{I}}_T^k v\right\|_{0,\partial T}.$$

Using the approximation property (14) of π_T^k (applied componentwise to ∇v with $t = q + \delta$ and $s = 0$), we infer that

$$h_T\left\|\nabla v - \pi_T^k\nabla v\right\|_{0,\partial T}^2 \lesssim h_T^{2(q+\delta)}\|v\|_{q+1+\delta,T}^2. \tag{26}$$

Now, we apply the discrete trace inequality, using the fact that $\mathrm{card}(\mathcal{F}_T)$ is uniformly bounded, and that $\nabla p_T^{k+1}\underline{\mathbf{I}}_T^k v \in \left[\mathbb{P}_d^k(T)\right]^d$, to infer

$$\|\pi_T^k\nabla v - \nabla p_T^{k+1}\underline{\mathbf{I}}_T^k v\|_{0,\partial T} \lesssim h_T^{-1/2}\|\nabla(v - p_T^{k+1}\underline{\mathbf{I}}_T^k v)\|_{0,T} \lesssim h_T^{q+\delta-1/2}\|v\|_{q+1+\delta,T}. \tag{27}$$

Finally, the proof is concluded from (26) and (27). □

4 HHO formulation

From here on, we consider $g_1 \in L^2(\Gamma_1)$, $g_2 \in L^2(\Omega_2)$, $\Omega := \Omega_1 \cup \Gamma_1 \cup \Omega_2$, and let $\mathcal{T}_h$ be a triangulation of $\bar{\Omega}$, satisfying the geometric assumptions given in Section 3. Next, we introduce the triangulations induced by $\mathcal{T}_h$, of each subdomain $\bar{\Omega}_i$, $i \in \{1,2\}$, that is

$$\mathcal{T}_{i,h} := \{T \in \mathcal{T}_h \,:\, T \subset \Omega_i\}\,,$$

with $\mathcal{F}_{i,h}$ being the list of faces on skeleton, induced by $\mathcal{T}_{i,h}$, $i \in \{1,2\}$. Moreover, by $\Gamma_{1,h}$ and $\Gamma_{2,h}$, we denote the partitions of Γ_1 and Γ_2, respectively, induced by $\mathcal{T}_{2,h}$. At this point we require also that the partition of transmission boundary Γ_1 inherited by $\mathcal{T}_h$, $\Gamma_{1,h}$, is quasi-uniform in the sense: considering $h_{\Gamma_1} := \max_{F\in\mathcal{F}_{1,h}} h_F$, there exists $C_{\mathtt{qu}} > 0$, independent of the meshsize, such that

$$C_{\mathtt{qu}}\, h_{\Gamma_1} \,\leq\, h_F \quad \forall\, F \in \Gamma_{1,h}\,. \tag{28}$$

These notations allow us to introduce the discrete spaces

$$\underline{\mathbf{U}}^k_{\mathcal{T}_{i,h}} := \left(\prod_{T\in\mathcal{T}_{i,h}} \mathbb{P}^k_d(T)\right) \times \left(\prod_{F\in\mathcal{F}_{i,h}} \mathbb{P}^k_{d-1}(F)\right), \quad i \in \{1,2\}\,.$$

Then, each element $\underline{\mathbf{v}}_{i,h} \in \underline{\mathbf{U}}^k_{\mathcal{T}_{i,h}}$ is characterized by $\underline{\mathbf{v}}_{i,h} := \Big((v_{i,T})_{T\in\mathcal{T}_{i,h}}, (v_{i,F})_{F\in\mathcal{F}_{i,h}}\Big)$, $i \in \{1,2\}$. Now, we set our discrete approximation space, as $\underline{\mathbf{U}}^{k,0}_{\mathcal{T}_h} \times Q^k_h$, where

$$\underline{\mathbf{U}}^{k,0}_{\mathcal{T}_h} := \left\{ \underline{\mathbf{v}}_h := (\underline{\mathbf{v}}_{1,h}, \underline{\mathbf{v}}_{2,h}) \in \underline{\mathbf{U}}^k_{\mathcal{T}_{1,h}} \times \underline{\mathbf{U}}^k_{\mathcal{T}_{2,h}} \,:\, \sum_{i=1}^{2} \sum_{T\in\mathcal{T}_{i,h}} (v_{i,T}, 1)_T \,=\, 0 \right\},$$

and $Q^k_h := \mathbb{P}^k_{d-1}(\Gamma_{1,h})$. From here on, we adopt the following notation. Given $\lambda_h \in Q^k_h$, we set $\lambda_F := \lambda_h|_F$, for all $F \in \Gamma_{1,h}$. Then, we introduce the characterization $\lambda_h := (\lambda_F)_{F\in\Gamma_{1,h}}$. The space Q^k_h is provided with the weighted L^2-norm

$$\|\lambda_h\|^2_{\Gamma_{1,h}} := \sum_{F\in\Gamma_{1,h}} h_F \|\lambda_F\|^2_{0,F}\,, \quad \forall\, \lambda_h := (\lambda_F)_{F\in\Gamma_{1,h}} \in Q^k_h\,. \tag{29}$$

We introduce the seminorm $|\!|\!| \cdot |\!|\!|_h \,:\, \underline{\mathbf{U}}^k_{\mathcal{T}_{1,h}} \times \underline{\mathbf{U}}^k_{\mathcal{T}_{2,h}} \to \mathbb{R}$, which is given, for each $(\underline{\mathbf{v}}_{1,h}, \underline{\mathbf{v}}_{2,h}) \in \underline{\mathbf{U}}^k_{\mathcal{T}_{1,h}} \times \underline{\mathbf{U}}^k_{\mathcal{T}_{2,h}}$, by

$$|\!|\!|(\underline{\mathbf{v}}_{1,h}, \underline{\mathbf{v}}_{2,h})|\!|\!|^2_h := \|\underline{\mathbf{v}}_{1,h}\|^2_{1,\mathcal{T}_{1,h}} + \|\underline{\mathbf{v}}_{2,h}\|^2_{1,\mathcal{T}_{2,h}} + \sum_{F\in\Gamma_{1,h}} h_F^{-1} \|v_{1,F} - v_{2,F}\|^2_{0,F}. \tag{30}$$

Proposition 4.1 *The map $|\!|\!| \cdot |\!|\!|_h$ defines a norm on $\underline{\mathbf{U}}^{k,0}_{\mathcal{T}_h}$.*

Proof. It is enough to check that, for all $(\underline{\mathbf{v}}_{1,h}, \underline{\mathbf{v}}_{2,h}) \in \underline{\mathbf{U}}_{\mathcal{T}_h}^{k,0}$: $|||(\underline{\mathbf{v}}_{1,h}, \underline{\mathbf{v}}_{2,h})|||_h = 0 \Rightarrow (\underline{\mathbf{v}}_{1,h}, \underline{\mathbf{v}}_{2,h}) = (\underline{\mathbf{0}}, \underline{\mathbf{0}})$. Let $(\underline{\mathbf{v}}_{1,h}, \underline{\mathbf{v}}_{2,h}) \in \underline{\mathbf{U}}_{\mathcal{T}_h}^{k,0}$ be such that $|||(\underline{\mathbf{v}}_{1,h}, \underline{\mathbf{v}}_{2,h})|||_h = 0$. By definition of $|||\cdot|||_h$, this implies

$$\forall T \in \mathcal{T}_{1,h} \quad \nabla v_{1,T} \equiv 0 \quad , \quad \forall F \in \mathcal{F}_T \quad v_{1,T}|_F = v_{1,F} \tag{31a}$$

$$\forall S \in \mathcal{T}_{2,h} \quad \nabla v_{2,S} \equiv 0 \quad , \quad \forall F \in \mathcal{F}_S \quad v_{2,S}|_F = v_{2,F} \tag{31b}$$

$$\forall F \in \Gamma_{1,h} \quad v_{1,F} = v_{2,F}. \tag{31c}$$

We have from (31a), that $v_{1,T}$ is constant on each $T \in \mathcal{T}_{1,h}$, and that on each interior face $F \in \mathcal{F}_{1,h}$, there exist $T_1, T_2 \in \mathcal{T}_{1,h}$ with $F \subset \partial T_1 \cap \partial T_2$, such that $v_{1,T_1}|_F = v_{1,F} = v_{1,T_2}|_F$. Then, we infer that, there exists a constant $C_1 > 0$ such that $v_{1,F} = C_1 \; \forall \, F \in \mathcal{F}_{1,h}$. In a similar way, we can deduce from (31b), that there exists $C_2 > 0$ such that $v_{2,F} = C_2 \; \forall \, F \in \mathcal{F}_{2,h}$. Now by (31c), we have that on each transmission face $F \in \Gamma_{1,h}$, there exist $T \in \mathcal{T}_{1,h}$ and $S \in \mathcal{T}_{2,h}$ with $F \subset \partial T \cap \partial S$ such that,

$$C_1 = v_{1,T}|_F = v_{1,F} = v_{2,F} = v_{2,S}|_F = C_2 \,,$$

which allows us to state that $v_{1,T} = v_{2,S} \equiv C_1 \quad \forall \, (T, S) \in \mathcal{T}_{1,h} \times \mathcal{T}_{2,h}$. Finally, due to the condition $\sum_{T \in \mathcal{T}_{1,h}} (v_{1,T}, 1)_T + \sum_{S \in \mathcal{T}_{2,h}} (v_{2,S}, 1)_S = 0$, we deduce that $C_1 = C_2 = 0$, and we conclude the proof. □

Now, for each $T \in \mathcal{T}_h$, we introduce $a_T : \underline{\mathbf{U}}_T^k \times \underline{\mathbf{U}}_T^k \to \mathbb{R}$ given by

$$a_T(\underline{\mathbf{u}}_T, \underline{\mathbf{v}}_T) := \Big(G_T^k \underline{\mathbf{u}}_T, G_T^k \underline{\mathbf{v}}_T \Big)_T + j_T(\underline{\mathbf{u}}_T, \underline{\mathbf{v}}_T) \,, \tag{32}$$

where

$$j_T(\underline{\mathbf{u}}_T, \underline{\mathbf{v}}_T) := \sum_{F \in \mathcal{F}_T} h_F^{-1} (\pi_F^k (u_F - R_T^{k+1} \underline{\mathbf{u}}_T), \pi_F^k (v_F - R_T^{k+1} \underline{\mathbf{v}}_T))_F \,,$$

with

$$R_T^{k+1} \underline{\mathbf{v}}_T := v_T + (p_T^{k+1} \underline{\mathbf{v}}_T - \pi_T^k p_T^{k+1} \underline{\mathbf{v}}_T) \,.$$

Then, we set the bilinear form $a_h : \underline{\mathbf{U}}_{\mathcal{T}_h}^{k,0} \times \underline{\mathbf{U}}_{\mathcal{T}_h}^{k,0} \to \mathbb{R}$, as

$$a_h((\underline{\mathbf{u}}_{1,h}, \underline{\mathbf{u}}_{2,h}), (\underline{\mathbf{v}}_{1,h}, \underline{\mathbf{v}}_{2,h})) = \sum_{T \in \mathcal{T}_{1,h}} a_T(\underline{\mathbf{u}}_{1,T}, \underline{\mathbf{v}}_{1,T}) + \sum_{S \in \mathcal{T}_{2,h}} a_S(\underline{\mathbf{u}}_{2,S}, \underline{\mathbf{v}}_{2,S}), \tag{33}$$

which can also be written as

$$a_h((\underline{\mathbf{u}}_{1,h}, \underline{\mathbf{u}}_{2,h}), (\underline{\mathbf{v}}_{1,h}, \underline{\mathbf{v}}_{2,h})) = A_h((\underline{\mathbf{u}}_{1,h}, \underline{\mathbf{u}}_{2,h}), (\underline{\mathbf{v}}_{1,h}, \underline{\mathbf{v}}_{2,h})) + j_h((\underline{\mathbf{u}}_{1,h}, \underline{\mathbf{u}}_{2,h}), (\underline{\mathbf{v}}_{1,h}, \underline{\mathbf{v}}_{2,h})) \,, \tag{34}$$

where the consistency contribution $A_h : \underline{\mathbf{U}}_{\mathcal{T}_h}^{k,0} \times \underline{\mathbf{U}}_{\mathcal{T}_h}^{k,0} \to \mathbb{R}$ and the stability contribution $j_h : \underline{\mathbf{U}}_{\mathcal{T}_h}^{k,0} \times \underline{\mathbf{U}}_{\mathcal{T}_h}^{k,0} \to \mathbb{R}$ are, respectively, defined as

$$A_h((\underline{\mathbf{u}}_{1,h}, \underline{\mathbf{u}}_{2,h}), (\underline{\mathbf{v}}_{1,h}, \underline{\mathbf{v}}_{2,h})) := \sum_{T \in \mathcal{T}_h} \Big(G_T^k \underline{\mathbf{u}}_T, G_T^k \underline{\mathbf{v}}_T \Big)_T \tag{35}$$

and

$$j_h((\underline{\mathbf{u}}_{1,h}, \underline{\mathbf{u}}_{2,h}), (\underline{\mathbf{v}}_{1,h}, \underline{\mathbf{v}}_{2,h})) := \sum_{T \in \mathcal{T}_h} j_T(\underline{\mathbf{u}}_T, \underline{\mathbf{v}}_T) \,. \tag{36}$$

We also introduce the bilinear form $b_h : \underline{\mathbf{U}}_{\mathcal{T}_h}^{k,0} \times Q_h^k \to \mathbb{R}$, which is defined as

$$b_h((\underline{\mathbf{v}}_{1,h}, \underline{\mathbf{v}}_{2,h}), \lambda_h) := \sum_{F \in \Gamma_{1,h}} (\lambda_F, v_{2,F} - v_{1,F})_F \quad \forall\, (\underline{\mathbf{v}}_{1,h}, \underline{\mathbf{v}}_{2,h}) \in \underline{\mathbf{U}}_{\mathcal{T}_h}^{k,0},\ \lambda_h := (\lambda_F)_{F \in \Gamma_{1,h}} \in Q_h^k\,. \tag{37}$$

Then, the discrete scheme associated to (8) reads as follows: Find $((\underline{\mathbf{u}}_{1,h}, \underline{\mathbf{u}}_{2,h}), \xi_h) \in \underline{\mathbf{U}}_{\mathcal{T}_h}^{k,0} \times Q_h^k$ such that

$$a_h((\underline{\mathbf{u}}_{1,h}, \underline{\mathbf{u}}_{2,h}), (\underline{\mathbf{v}}_{1,h}, \underline{\mathbf{v}}_{2,h})) + b_h((\underline{\mathbf{v}}_{1,h}, \underline{\mathbf{v}}_{2,h}), \xi_h) = F_h((\underline{\mathbf{v}}_{1,h}, \underline{\mathbf{v}}_{2,h}))\ \forall (\underline{\mathbf{v}}_{1,h}, \underline{\mathbf{v}}_{2,h}) \in \underline{\mathbf{U}}_{\mathcal{T}_h}^{k,0}\,, \tag{38a}$$

$$-b_h((\underline{\mathbf{u}}_{1,h}, \underline{\mathbf{u}}_{2,h}), \lambda_h) = G_h(\lambda_h)\ \forall \lambda_h \in Q_h^k\,, \tag{38b}$$

where, for each $(\underline{\mathbf{v}}_{1,h}, \underline{\mathbf{v}}_{2,h}) \in \underline{\mathbf{U}}_{\mathcal{T}_h}^{k}$ and $\lambda_h \in Q_h^k$, we define the discrete linear functionals as:

$$F_h(\underline{\mathbf{v}}_{1,h}, \underline{\mathbf{v}}_{2,h}) := \sum_{T \in \mathcal{T}_{1,h}} (f_1, v_{1,T})_T + \sum_{S \in \mathcal{T}_{2,h}} (f_2, v_{2,S})_S + \sum_{F \in \Gamma_{1,h}} (g_1, v_{2,F})_F + \sum_{F \in \Gamma_{2,h}} (g_2, v_{2,F})_F, \tag{39}$$

and $G_h(\lambda_h) := (\lambda_h, g)_{\Gamma_{1,h}}$. In what follows, we recall the well known relationships between $||\cdot||_{0,\Gamma_1}$ and $||\cdot||_{-1/2,\Gamma_1}$.

Lemma 4.1 *There holds*

$$||\tilde{g}||_{-1/2,\Gamma_1} \lesssim ||\tilde{g}||_{0,\Gamma_1} \quad \forall\, \tilde{g} \in L^2(\Gamma_1)\,, \tag{40}$$

$$||\lambda_h||_{0,\Gamma_1} \lesssim h_{\Gamma_1}^{-1/2}\, ||\lambda_h||_{-1/2,\Gamma_1} \quad \forall\, \lambda_h \in Q_h^k\,. \tag{41}$$

Proof. A proof of (40) is available in [60] (page 115), while (41) can be proven in the same spirit of the proof of Lemma 4.6 in [42]. □

From here on, given $\underline{\mathbf{v}}_h \in \underline{\mathbf{U}}_{\mathcal{T}_h}^{k}$, we denote by v_h the $L^2(\Omega)$ function such that $v_h|_T = v_T$, for all $T \in \mathcal{T}_h$. Next result, which can be seen as the corresponding to Lemma 8.3 in [33] for Neumann boundary condition, will be useful for proving the continuity of linear functional F_h.

Lemma 4.2 *There holds*

$$||v_h||_{0,\Omega} \lesssim |\!|\!|\underline{\mathbf{v}}_h|\!|\!|_h \quad \forall\, \underline{\mathbf{v}}_h \in \underline{\mathbf{U}}_{\mathcal{T}_h}^{k,0}\,. \tag{42}$$

Proof. The proof for general domain Ω is provided in the appendix of this paper. However, when Ω is convex, the proof of (42) can be done usign a different argument, more constructive, which is described next.

Let $\underline{\mathbf{v}}_h \in \underline{\mathbf{U}}_{\mathcal{T}_h}^{k,0}$. Since $v_h \in L_0^2(\Omega)$, there exists a unique weak solution $z \in H^1(\Omega)$ of

$$-\Delta z = v_h \quad \text{in} \quad \Omega\,, \quad \frac{\partial z}{\partial \boldsymbol{\nu}} = 0 \quad \text{on} \quad \partial\Omega\,. \tag{43}$$

Since Ω is convex, we can ensure that $z \in H^2(\Omega)$ and $||z||_{2,\Omega} \lesssim ||v_h||_{0,\Omega}$ (cf. [47]). This allows us to introduce $\boldsymbol{\tau}_v := -\nabla z \in [H^1(\Omega)]^2$, which satisfies:

$$\mathrm{div}(\boldsymbol{\tau}_v) = v_h \quad \text{in} \quad \Omega\,, \quad \boldsymbol{\tau}_v \cdot \boldsymbol{\nu} = 0 \quad \text{on} \quad \partial\Omega\,, \quad \text{and} \quad ||\boldsymbol{\tau}_v||_{1,\Omega} \lesssim ||v_h||_{0,\Omega}\,. \tag{44}$$

Then, taking into account the fact that $\boldsymbol{\tau}_v \in H(\mathrm{div};\Omega)$, and the first two statements in (44), we have

$$
\begin{aligned}
||v_h||^2_{0,\Omega} =& (v_h, \mathrm{div}(\boldsymbol{\tau}_v))_\Omega \,=\, (v_h, \mathrm{div}(\boldsymbol{\tau}_v))_{\Omega_1} \,+\, (v_h, \mathrm{div}(\boldsymbol{\tau}_v))_{\Omega_2} \\
&= \sum_{T\in\mathcal{T}_{1,h}} \left\{ -(\nabla v_{1,T}, \boldsymbol{\tau}_v)_T \,+\, \sum_{F\in\mathcal{F}_T} (\boldsymbol{\tau}_v\cdot\boldsymbol{n}_{TF}, v_{1,T})_F \right\} \\
&\quad + \sum_{T\in\mathcal{T}_{2,h}} \left\{ -(\nabla v_{2,T}, \boldsymbol{\tau}_v)_T \,+\, \sum_{F\in\mathcal{F}_T} (\boldsymbol{\tau}_v\cdot\boldsymbol{n}_{TF}, v_{2,T})_F \right\} \\
&= \sum_{T\in\mathcal{T}_{1,h}} \left\{ -(\nabla v_{1,T}, \boldsymbol{\tau}_v)_T \,+\, \sum_{F\in\mathcal{F}_T} (\boldsymbol{\tau}_v\cdot\boldsymbol{n}_{TF}, v_{1,T}-v_{1,F})_F \right\} \\
&\quad + \sum_{T\in\mathcal{T}_{2,h}} \left\{ -(\nabla v_{2,T}, \boldsymbol{\tau}_v)_T \,+\, \sum_{F\in\mathcal{F}_T} (\boldsymbol{\tau}_v\cdot\boldsymbol{n}_{TF}, v_{2,T}-v_{2,F})_F \right\} \\
&\quad + \sum_{F\in\Gamma_{1,h}} (\boldsymbol{\tau}_v\cdot\boldsymbol{n}_1, v_{1,F}-v_{2,F})_F \,. \qquad (45)
\end{aligned}
$$

Now, applying Cauchy-Schwarz, Minkowski and continuous local trace inequalities, we notice

$$
\begin{aligned}
&\sum_{T\in\mathcal{T}_{1,h}} \left\{ -(\nabla v_{1,T}, \boldsymbol{\tau}_v)_T \,+\, \sum_{F\in\mathcal{F}_T} (\boldsymbol{\tau}_v\cdot\boldsymbol{n}_{TF}, v_{1,T}-v_{1,F})_F \right\} \\
&\le \sum_{T\in\mathcal{T}_{1,h}} \left(||\nabla v_{1,T}||_{0,T}||\boldsymbol{\tau}_v||_{0,T} \,+\, \sum_{F\in\mathcal{F}_T} \left(h_F^{-1/2}||v_{1,T}-v_{1,F}||_{0,F}\right)\left(h_F^{1/2}||\boldsymbol{\tau}_v||_{0,F}\right)\right) \\
&\le ||\underline{v}_{1,h}||_{1,\mathcal{T}_{1,h}} \left\{ \sum_{T\in\mathcal{T}_{1.h}} \left(||\boldsymbol{\tau}_v||^2_{0,T} \,+\, h_T||\boldsymbol{\tau}_v||^2_{0,\partial T}\right)\right\}^{1/2} \\
&\lesssim ||\underline{v}_{1,h}||_{1,\mathcal{T}_{1,h}} \left\{ \sum_{T\in\mathcal{T}_{1.h}} \left(||\boldsymbol{\tau}_v||^2_{0,T} \,+\, ||\boldsymbol{\tau}_v||^2_{0,T} + h_T^2|\boldsymbol{\tau}_v|^2_{1,T}\right)\right\}^{1/2} \\
&\lesssim ||\underline{v}_{1,h}||_{1,\mathcal{T}_{1,h}}\, ||\boldsymbol{\tau}_v||_{1,\Omega_1} \,.
\end{aligned}
$$

Proceeding in analogous way, we deduce that

$$
\sum_{T\in\mathcal{T}_{2,h}} \left\{ -(\nabla v_{2,T}, \boldsymbol{\tau}_v)_T \,+\, \sum_{F\in\mathcal{F}_T} (\boldsymbol{\tau}_v\cdot\boldsymbol{n}_{TF}, v_{2,T}-v_{2,F})_F \right\} \lesssim ||\underline{v}_{2,h}||_{1,\mathcal{T}_{2,h}}\, ||\boldsymbol{\tau}_v||_{1,\Omega_2} \,,
$$

and

$$
\sum_{F\in\Gamma_{1,h}} (\boldsymbol{\tau}_v\cdot\boldsymbol{n}_1, v_{1,F}-v_{2,F})_F \lesssim \left(\sum_{F\in\Gamma_{1,h}} h_F^{-1}||v_{1,F}-v_{2,F}||^2_{0,F} \right)^{1/2} ||\boldsymbol{\tau}_v||_{1,\Omega_1} \,.
$$

Considering these relationships, and applying Minkowski inequality one more time and the regularity property in (44), (45) yields to

$$||v_h||^2_{0,\Omega} \lesssim |\!|\!|\underline{v}_h|\!|\!|_h \, ||v_h||_{0,\Omega} \,,$$

and we conclude the proof. □

Lemma 4.3 *Bilinear forms a_h and b_h, as well as linear functionals F_h and G_h, are continuous.*

Proof. Let us establish the continuity of the discrete bilinear forms a_h and b_h. Thanks to the continuity of a_T (see [32]), and applying Cauchy-Schwarz and Minkowski inequalities, we have

$$\begin{aligned} |a_h((\underline{\mathbf{u}}_{1,h}, \underline{\mathbf{u}}_{2,h}), (\underline{\mathbf{v}}_{1,h}, \underline{\mathbf{v}}_{2,h}))| &\lesssim \|\underline{\mathbf{u}}_{1,h}\|_{1,\mathcal{T}_{1,h}} \cdot \|\underline{\mathbf{v}}_{1,h}\|_{1,\mathcal{T}_{1,h}} + \|\underline{\mathbf{u}}_{2,h}\|_{1,\mathcal{T}_{2,h}} \cdot \|\underline{\mathbf{v}}_{2,h}\|_{1,\mathcal{T}_{2,h}} \\ &\leq \left(\|\underline{\mathbf{u}}_{1,h}\|^2_{1,\mathcal{T}_{1,h}} + \|\underline{\mathbf{u}}_{2,h}\|^2_{1,\mathcal{T}_{2,h}}\right)^{1/2} \left(\|\underline{\mathbf{v}}_{1,h}\|^2_{1,\mathcal{T}_{1,h}} + \|\underline{\mathbf{v}}_{2,h}\|^2_{1,\mathcal{T}_{1,h}}\right)^{1/2} \\ &\leq |\!|\!|(\underline{\mathbf{u}}_{1,h}, \underline{\mathbf{u}}_{2,h})|\!|\!|_h \, |\!|\!|(\underline{\mathbf{v}}_{1,h}, \underline{\mathbf{v}}_{2,h})|\!|\!|_h \,. \end{aligned}$$

Now, for b_h, after applying Cauchy-Schwarz and Minkowski inequalities, and Lemma 4.1, we obtain

$$\begin{aligned} |b_h((\underline{\mathbf{u}}_{1,h}, \underline{\mathbf{u}}_{2,h}), \lambda_h)| &\leq \left(\sum_{F\in\Gamma_{1,h}} h_F^{-1}\|u_{1,F} - u_{2,F}\|^2_{0,F}\right)^{1/2} \left(\sum_{F\in\Gamma_{1,h}} h_F\|\lambda_F\|^2_{0,F}\right)^{1/2} \\ &\leq |\!|\!|(\underline{\mathbf{u}}_{1,h}, \underline{\mathbf{u}}_{2,h})|\!|\!|_h \, \|\lambda_h\|_{\Gamma_{1,h}} \,. \end{aligned} \tag{46}$$

Next, we prove the continuity of the discrete linear functional F_h. First, we notice that

$$\sum_{F\in\mathcal{F}_{1,h}} (g_1, v_{2,F})_F = \sum_{F\in\mathcal{F}_{1,h}} (g_1, v_{2,F} - c_2)_F + c_2\langle g_1, 1\rangle_{\Gamma_1} \tag{47}$$

$$\sum_{F\in\mathcal{F}_{2,h}} (g_2, v_{2,F})_F = \sum_{F\in\mathcal{F}_{2,h}} (g_2, v_{2,F} - c_2)_F + c_2\langle g_2, 1\rangle_{\Gamma_2} \,, \tag{48}$$

where $c_2 := \dfrac{1}{|\Omega_2|}\displaystyle\int_{\Omega_2} v_{2,h}$.

Applying Cauchy-Schwarz inequality appropriately, we have

$$\begin{aligned} |F_h(\underline{\mathbf{v}}_{1,h}, \underline{\mathbf{v}}_{2,h})| &\leq \|f_1\|_{0,\Omega_1} \left(\sum_{T\in\mathcal{T}_{1,h}} \|v_{1,T}\|^2_{0,T}\right)^{1/2} + \|f_2\|_{0,\Omega_2} \left(\sum_{S\in\mathcal{T}_{2,h}} \|v_{2,S}\|^2_{0,S}\right)^{1/2} \\ &+ ||g_1||_{0,\Gamma_1} \left(\sum_{F\in\Gamma_{1,h}} \|v_{2,F} - c_2\|^2_{0,F}\right)^{1/2} + |c_2|\,|\Omega_2|^{1/2}\,||g_1||_{-1/2,\Gamma_1} \\ &+ ||g_2||_{0,\Gamma_2} \left(\sum_{F\in\Gamma_{2,h}} \|v_{2,F} - c_2\|^2_{0,F}\right)^{1/2} + |c_2|\,|\Omega_2|^{1/2}\,||g_2||_{-1/2,\Gamma_2} \,. \end{aligned} \tag{49}$$

Thanks to Minkowski inequality, (47), and the fact that $|c_2| \leq |\Omega_2|^{-1/2}\,||v_{2,h}||_{0,\Omega_2}$, we obtain

$$|F_h(\underline{\mathbf{v}}_{1,h},\underline{\mathbf{v}}_{2,h})| \leq C\left(||v_{1,h}||^2_{0,\Omega_1}+||v_{2,h}||^2_{0,\Omega_2}+\sum_{F\in\Gamma_{1,h}\cup\Gamma_{2,h}}\|v_{2,F}-c_2\|^2_{0,F}\right)^{1/2}, \quad (50)$$

where $C := \left(\|f_1\|^2_{0,\Omega_1}+\|f_2\|^2_{0,\Omega_2}+||g_1||^2_{-1/2,\Gamma_1}+||g_2||^2_{-1/2,\Gamma_2}+||g_1||^2_{0,\Gamma_1}+||g_2||^2_{0,\Gamma_2}\right)^{1/2}$.

Now, we bound the right hand side of (50). First, since $\underline{\mathbf{v}}_h \in \underline{\mathbf{U}}^{k,0}_{\mathcal{T}_h}$, we apply Lemma 4.2, and get

$$||v_{1,h}||^2_{0,\Omega_1}+||v_{2,h}||^2_{0,\Omega_2} = ||v_h||^2_{0,\Omega} \lesssim |\!|\!|\underline{\mathbf{v}}_h|\!|\!|^2_h\,. \quad (51)$$

On the other hand, considering $\underline{\mathbf{z}}_h := \left((v_{2,T}-c_2)_{T\in\mathcal{T}_{2,h}},(v_{2,F}-c_2)_{F\in\mathcal{F}_{2,h}}\right) \in \underline{\mathbf{U}}^{k,0}_{\mathcal{T}_{2,h}}$, and denoting by $\gamma_h(\underline{\mathbf{z}}_h)$ the discrete trace of $\underline{\mathbf{z}}_h$, such that $\gamma_h(\underline{\mathbf{z}}_h)|_F = v_{2,F}-c_2$, on each $F\in\mathcal{F}_{2,h}$, we apply Theorem 6.7 in [33], and deduce

$$\sum_{F\in\Gamma_{1,h}\cup\Gamma_{2,h}}||v_{2,F}-c_2||^2_{0,F} = ||\gamma_h(\underline{\mathbf{z}}_h)||^2_{0,\partial\Omega_2} \lesssim ||\underline{\mathbf{z}}_h||^2_{1,\mathcal{T}_{2,h}} = ||\underline{\mathbf{v}}_{2,h}||^2_{1,\mathcal{T}_{2,h}}\,. \quad (52)$$

Finally, taking into account (51) and (52), we conclude from (50)

$$|F_h(\underline{\mathbf{v}}_{1,h},\underline{\mathbf{v}}_{2,h})| \lesssim |\!|\!|(\underline{\mathbf{v}}_{1,h},\underline{\mathbf{v}}_{2,h})|\!|\!|_h\,, \quad (53)$$

which ensures the continuity of F_h.
Now, for the continuity of the discrete linear functional G_h, we recall that $g\in H^{1/2}(\Gamma_1)\subset L^2(\Gamma_1)$. Then, we have

$$|G_h(\lambda_h)| = \sum_{F\in\Gamma_{1,h}}(h_F^{1/2}\lambda_T\,,\,h_F^{-1/2}g)_F \leq ||\alpha^{1/2}\,g||_{0,\Gamma_1}\,||\lambda_h||_{\Gamma_{1,h}}\,, \quad (54)$$

where α is a parameter defined on $\Gamma_{1,h}$ such that $\alpha|_F := h_F^{-1}$ for each $F\in\Gamma_{1,h}$. □

Remark 4.1 *The linear operator $\mathbf{B}_h : \underline{\mathbf{U}}^{k,0}_{\mathcal{T}_h} \to Q^k_h$, induced by b_h, is characterized by*

$$\mathbf{B}_h(\underline{\mathbf{v}}_{1,h},\underline{\mathbf{v}}_{2,h}) := (v_{2,F}-v_{1,F})_{F\in\Gamma_{1,h}} \quad \forall\,(\underline{\mathbf{v}}_{1,h},\underline{\mathbf{v}}_{2,h})\in\underline{\mathbf{U}}^{k,0}_{\mathcal{T}_h}\,. \quad (55)$$

Introducing $\mathbf{V}_h := \mathrm{Ker}(\mathbf{B}_h)$, we establish the following result.

Lemma 4.4 (Ellipticity). *a_h is $\mathbf{V}_h$-elliptic.*

Proof. From (37), we characterize the kernel of $\mathbf{B}_h$, as

$$\mathbf{V}_h := \{(\underline{\mathbf{v}}_{1,h},\underline{\mathbf{v}}_{2,h})\in\underline{\mathbf{U}}^{k,0}_{\mathcal{T}_h} : v_{1,F}=v_{2,F} \quad \forall F\in\Gamma_{1,h}\}\,.$$

Now, taking $(\underline{\mathbf{v}}_{1,h},\underline{\mathbf{v}}_{2,h})\in\mathbf{V}_h$ and considering the fact that $||\cdot||_{1,\mathcal{T}_{i,h}}$ is equivalent to $||\cdot||_{a,\mathcal{T}_{i,h}}$ (cf. Lemma 4 in [32]), we have

$$\begin{aligned} a_h((\underline{\mathbf{v}}_{1,h},\underline{\mathbf{v}}_{2,h}),(\underline{\mathbf{v}}_{1,h},\underline{\mathbf{v}}_{2,h})) &= \|\underline{\mathbf{v}}_{1,h}\|^2_{a,\mathcal{T}_{1,h}}+\|\underline{\mathbf{v}}_{2,h}\|^2_{a,\mathcal{T}_{2,h}} \\ &\gtrsim \|\underline{\mathbf{v}}_{1,h}\|^2_{1,\mathcal{T}_{1,h}}+\|\underline{\mathbf{v}}_{2,h}\|^2_{1,\mathcal{T}_{2,h}} \\ &= |\!|\!|(\underline{\mathbf{v}}_{1,h},\underline{\mathbf{v}}_{2,h})|\!|\!|^2_h\,. \end{aligned} \quad (56)$$

□

Lemma 4.5 $\mathbf{B}_h$ *is a surjective operator.*

Proof. Given $\lambda_h \in Q_h^k$, we can define $(\underline{\mathbf{v}}_{1,h}, \underline{\mathbf{v}}_{2,h}) \in \underline{\mathbf{U}}_{\mathcal{T}_h}^{k,0}$, such that $v_{1,T} \equiv 0, \forall T \in \mathcal{T}_{1,h}$, $v_{1,F} = \begin{cases} -\lambda_F & , \ F \in \Gamma_{1,h} \\ 0 & , \ F \in \mathcal{F}_{1,h} \backslash \Gamma_{1,h} \end{cases}$, and $\underline{\mathbf{v}}_{2,h} = \underline{0}_{2,h}$. Then, the operator $\mathbf{B}_h$ is surjective. □

As in the continuous case, here we can establish also the so called discrete inf-sup condition, which will help us later to obtain an a priori error estimate corresponding to λ_h.

Lemma 4.6 *There exists $C > 0$, independent of the meshsize, such that*

$$\sup_{\underline{\mathbf{v}}_h \in \underline{\mathbf{U}}_{\mathcal{T}_h}^{k,0} \backslash \{0\}} \frac{b_h(\underline{\mathbf{v}}_h, \lambda_h)}{|||\underline{\mathbf{v}}_h|||_h} \geq C \, ||\lambda_h||_{\Gamma_{1,h}} \quad \forall \, \lambda_h \in Q_h^k \, . \tag{57}$$

Proof. Let $\lambda_h := (\lambda_F)_{F \in \Gamma_{1,h}} \in Q_h^k \backslash \{0\}$. Then, we construct $\underline{\mathbf{w}}_h := (\underline{\mathbf{w}}_{1,h}, \underline{\mathbf{w}}_{2,h}) \in \underline{\mathbf{U}}_{\mathcal{T}_h}^{k,0} \backslash \{0\}$ as in the proof of Lemma 4.5, and we notice that

$$|||\underline{\mathbf{w}}_h|||_h^2 = 2 \sum_{F \in \Gamma_{1,h}} h_F^{-1} ||\lambda_F||_{0,F}^2 \lesssim h_{\Gamma_1}^{-1} ||\lambda_h||_{0,\Gamma_1}^2 \, . \tag{58}$$

Then, taking into account (58) and the fact that $h_{\Gamma_1} \lesssim h_F$, for all $F \in \Gamma_{1,h}$, we have

$$\sup_{\underline{\mathbf{v}}_h \in \underline{\mathbf{U}}_{\mathcal{T}_h}^{k,0} \backslash \{0\}} \frac{b_h(\underline{\mathbf{v}}_h, \lambda_h)}{|||\underline{\mathbf{v}}_h|||_h} \geq \frac{b_h(\underline{\mathbf{w}}_h, \lambda_h)}{|||\underline{\mathbf{w}}_h|||_h} \gtrsim h_{\Gamma_1}^{1/2} \frac{||\lambda_h||_{0,\Gamma_1}^2}{||\lambda_h||_{0,\Gamma_1}} \gtrsim ||\lambda_h||_{\Gamma_{1,h}} \, . \tag{59}$$

This allows us to conclude the result. □

Proposition 4.2 (meshsize). *The discrete problem (38) is well-posed.*

Proof. It is a straightforward consequence of Lemmas 4.3, 4.4 and 4.5. We omit further details. □

It is important to notice that bilinear form a_h induces another seminorm on $\underline{\mathbf{U}}_{\mathcal{T}_{1,h}}^k \times \underline{\mathbf{U}}_{\mathcal{T}_{2,h}}^k$, that is given by

$$\|(\underline{\mathbf{v}}_{1,h}, \underline{\mathbf{v}}_{2,h})\|_{a,h}^2 := a_h((\underline{\mathbf{v}}_{1,h}, \underline{\mathbf{v}}_{2,h}), (\underline{\mathbf{v}}_{1,h}, \underline{\mathbf{v}}_{2,h})) \, , \quad \forall \, (\underline{\mathbf{v}}_{1,h}, \underline{\mathbf{v}}_{2,h}) \in \underline{\mathbf{U}}_{\mathcal{T}_{1,h}}^k \times \underline{\mathbf{U}}_{\mathcal{T}_{2,h}}^k \, . \tag{60}$$

Next result could be useful in the rest of this work.

Corollary 4.1 *There exists $\eta > 1$, independent of the meshsize, such that*

$$\eta^{-1} |||(\underline{\mathbf{v}}_{1,h}, \underline{\mathbf{v}}_{2,h})|||_h \leq \|(\underline{\mathbf{v}}_{1,h}, \underline{\mathbf{v}}_{2,h})\|_{a,h} \quad \forall \, (\underline{\mathbf{v}}_{1,h}, \underline{\mathbf{v}}_{2,h}) \in \mathbf{V}_h \, , \tag{61}$$

$$\|(\underline{\mathbf{v}}_{1,h}, \underline{\mathbf{v}}_{2,h})\|_{a,h} \leq \eta |||(\underline{\mathbf{v}}_{1,h}, \underline{\mathbf{v}}_{2,h})|||_h \quad \forall \, (\underline{\mathbf{v}}_{1,h}, \underline{\mathbf{v}}_{2,h}) \in \underline{\mathbf{U}}_{\mathcal{T}_h}^{k,0} \, . \tag{62}$$

Proof. (61) follows straightforwardly from the $\mathbf{V}_h$-ellipticity of a_h (56), while (62) has been established in the proof of Lemma 4.3. We omit further details. □

5 A priori error analysis

From here on, we assume that exact solution $u_i \in H^{1+\delta_i}(\Omega_i)$, and $\delta_i \in (1/2, 1]$, and $\Delta u_i \in L^2(\Omega)$ for $i \in \{1,2\}$. These assumptions allow us to see ξ belonging to $L^2(\Gamma_1)$, and consider g_1 and g_2 as elements in $L^2(\Gamma_1)$ and $L^2(\Gamma_2)$, respectively. In addition, we introduce $\widehat{\underline{\mathbf{u}}}_{1,h} := \underline{\mathbf{I}}^k_{\mathcal{T}_{1,h}} u_1 \in \underline{\mathbf{U}}^k_{\mathcal{T}_{1,h}}$, $\widehat{\underline{\mathbf{u}}}_{2,h} := \underline{\mathbf{I}}^k_{\mathcal{T}_{2,h}} u_2 \in \underline{\mathbf{U}}^k_{\mathcal{T}_{2,h}}$, where $\underline{\mathbf{I}}^k_{\mathcal{T}_{i,h}}$, for $i \in \{1,2\}$, denotes the global interpolation operator that is defined in the same spirit as in (17), and $\widehat{\xi}_h \in Q^k_h$ is such that $\widehat{\xi}_h|_F := \pi^k_F(\xi)$, for each $F \in \Gamma_{1,h}$. It is not difficult to check that $(\widehat{\underline{\mathbf{u}}}_{1,h}, \widehat{\underline{\mathbf{u}}}_{2,h}) \in \underline{\mathbf{U}}^{k,0}_{\mathcal{T}_h}$. We recall again that, given $i \in \{1,2\}$, $\underline{\mathbf{v}}_{i,h} := \Big((v_{i,T})_{T\in\mathcal{T}_{i,h}}, (v_{i,F})_{F\in\mathcal{F}_{i,h}}\Big) \in \underline{\mathbf{U}}^k_{\mathcal{T}_{i,h}}$, and we set $v_{i,h} \in \mathbb{P}^k_d(\mathcal{T}_{i,h})$ such that $v_{i,h}|_T = v_{i,T} \quad \forall\, T \in \mathcal{T}_{i,h}$.

Now, we introduce the product space $\mathbf{X}_h := \underline{\mathbf{U}}^{k,0}_{\mathcal{T}_h} \times Q^k_h$, provided with the norm

$$||((\underline{\mathbf{v}}_{1,h}, \underline{\mathbf{v}}_{2,h}), \lambda_h)||_{\mathbf{X}_h} := \Big(|||(\underline{\mathbf{v}}_{1,h}, \underline{\mathbf{v}}_{2,h})|||^2_h + ||\lambda_h||^2_{\Gamma_{1,h}}\Big)^{1/2} \quad \forall\, ((\underline{\mathbf{v}}_{1,h}, \underline{\mathbf{v}}_{2,h}), \lambda_h) \in \mathbf{X}_h\,,$$

and the *consistency error* as the linear functional $\mathcal{E}_h(((u_1,u_2),\xi);\cdot) : \mathbf{X}_h \to \mathbb{R}$ such that, for each $((\underline{\mathbf{v}}_{1,h}, \underline{\mathbf{v}}_{2,h}), \lambda_h) \in \mathbf{X}_h$:

$$\begin{aligned}\mathcal{E}_h(((u_1,u_2),\xi);((\underline{\mathbf{v}}_{1,h}, \underline{\mathbf{v}}_{2,h}), \lambda_h)) :=& a_h((\widehat{\underline{\mathbf{u}}}_{1,h}, \widehat{\underline{\mathbf{u}}}_{2,h}), (\underline{\mathbf{v}}_{1,h}, \underline{\mathbf{v}}_{2,h})) + b_h((\underline{\mathbf{v}}_{1,h}, \underline{\mathbf{v}}_{2,h})), \widehat{\xi}_h) \\ &- b_h((\widehat{\underline{\mathbf{u}}}_{1,h}, \widehat{\underline{\mathbf{u}}}_{2,h}), \lambda_h) + G_h(\lambda_h) - F_h(\underline{\mathbf{v}}_{1,h}, \underline{\mathbf{v}}_{2,h})\,.\end{aligned}$$

In our case, we notice that

$$\begin{aligned} b_h((\widehat{\underline{\mathbf{u}}}_{1,h}, \widehat{\underline{\mathbf{u}}}_{2,h}), \lambda_h) &= \sum_{F\in\Gamma_{1,h}} (\pi^k_F u_2 - \pi^k_F u_1, \lambda_F)_F \\ &= \sum_{F\in\Gamma_{1,h}} (\lambda_F, \gamma_0^+(u_2) - \gamma_0^-(u_1))_F = (\lambda_h, g)_{\Gamma_1} = G_h(\lambda_h) \quad \forall\, \lambda_h \in Q^k_h\,,\end{aligned}$$

and thus, the consistency error reduces to

$$\begin{aligned}\mathcal{E}_h(((u_1,u_2),\xi);((\underline{\mathbf{v}}_{1,h}, \underline{\mathbf{v}}_{2,h}), \lambda_h)) =& a_h((\widehat{\underline{\mathbf{u}}}_{1,h}, \widehat{\underline{\mathbf{u}}}_{2,h}), (\underline{\mathbf{v}}_{1,h}, \underline{\mathbf{v}}_{2,h})) + b_h((\underline{\mathbf{v}}_{1,h}, \underline{\mathbf{v}}_{2,h})), \widehat{\xi}_h) \\ &- F_h(\underline{\mathbf{v}}_{1,h}, \underline{\mathbf{v}}_{2,h}) =: \widetilde{\mathcal{E}}_h(((u_1,u_2),\xi);(\underline{\mathbf{v}}_{1,h}, \underline{\mathbf{v}}_{2,h}))\,.\end{aligned} \tag{63}$$

The latter implies that

$$||\mathcal{E}_h(((u_1,u_2),\xi);\cdot)||_{\mathbf{X}^*_h} = ||\widetilde{\mathcal{E}}_h(((u_1,u_2),\xi);\cdot)||_{\underline{\mathbf{U}}^{k,0,*}_{\mathcal{T}_h}}\,, \tag{64}$$

with $\mathbf{X}^*_h$ and $\underline{\mathbf{U}}^{k,0,*}_{\mathcal{T}_h}$ denoting the dual space of $\mathbf{X}_h$ and $\underline{\mathbf{U}}^{k,0}_{\mathcal{T}_h}$, respectively. The following result will help us to bound (64).

Lemma 5.1 *There holds, for each* $(\underline{\mathbf{v}}_{1,h}, \underline{\mathbf{v}}_{2,h}) \in \underline{\mathbf{U}}^{k,0}_{\mathcal{T}_h}$:

$$\begin{aligned} F_h(\underline{\mathbf{v}}_{1,h}, \underline{\mathbf{v}}_{2,h}) - b_h((\underline{\mathbf{v}}_{1,h}, \underline{\mathbf{v}}_{2,h}), \widehat{\xi}_h) =& \sum_{T\in\mathcal{T}_{1,h}} (\nabla v_{1,T}, \nabla u_1)_T + \sum_{T\in\mathcal{T}_{1,h}} \sum_{F\in\mathcal{F}_T} (\nabla u_1 \cdot \boldsymbol{n}_{TF}, v_{1,F} - v_{1,T})_F \\ &+ \sum_{S\in\mathcal{T}_{2,h}} (\nabla v_{2,S}, \nabla u_2)_S + \sum_{S\in\mathcal{T}_{2,h}} \sum_{F\in\mathcal{F}_S} (\nabla u_2 \cdot \boldsymbol{n}_{SF}, v_{2,F} - v_{2,S})_F.\end{aligned} \tag{65}$$

Proof. Since $f_i = -\Delta u_i$ in Ω_i (weak sense), and after performing an element-wise integration by parts in $(f_i, v_{i,h})_{\Omega_i}$, with $i \in \{1,2\}$, we obtain that two first addends of F_h (cf. (39)) can be written as

$$(f_1, v_{1,h})_{\Omega_1} = \sum_{T\in\mathcal{T}_{1,h}} (\nabla u_1, \nabla v_{1,T})_T - \sum_{T\in\mathcal{T}_{1,h}} \sum_{F\in\mathcal{F}_T} (\nabla u_1 \cdot \boldsymbol{n}_{TF}, v_{1,T})_F, \tag{66}$$

$$(f_2, v_{2,h})_{\Omega_2} = \sum_{S\in\mathcal{T}_{2,h}} (\nabla u_2, \nabla v_{2,S})_S - \sum_{S\in\mathcal{T}_{2,h}} \sum_{F\in\mathcal{F}_S} (\nabla u_2 \cdot \boldsymbol{n}_{SF}, v_{2,S})_F. \tag{67}$$

Now, using the fact that $\nabla u_1 \cdot \boldsymbol{n}_1 + \nabla u_2 \cdot \boldsymbol{n}_2 = g_1$ a.e. on Γ_1, and $\nabla u_2 \cdot \boldsymbol{n}_2 = g_2$ a.e. on Γ_2, and that there exist $T \in \mathcal{T}_{1,h}$ and $S \in \mathcal{T}_{2,h}$, such that $\boldsymbol{n}_1 = \boldsymbol{n}_{TF}$ on $\partial\Omega_1$ and $\boldsymbol{n}_2 = \boldsymbol{n}_{SF}$ on $\partial\Omega_2$, we can write the last two addends of F_h as

$$\sum_{F\in\Gamma_{1,h}} (g_1, v_{2,F})_F = \sum_{F\in\Gamma_{1,h}} (\nabla u_1 \cdot \boldsymbol{n}_{TF}, v_{2,F})_F + \sum_{F\in\Gamma_{1,h}} (\nabla u_2 \cdot \boldsymbol{n}_{SF}, v_{2,F})_F, \tag{68}$$

$$\sum_{F\in\Gamma_{2,h}} (g_2, v_{2,F})_F = \sum_{F\in\Gamma_{2,h}} (\nabla u_2 \cdot \boldsymbol{n}_{SF}, v_{2,F})_F. \tag{69}$$

From the definition of $\widehat{\xi}_h$, property of π_F^k, the fact that $\xi = \nabla u_1 \cdot \boldsymbol{n}_1$ a.e. on Γ_1, and that there exist $T \in \mathcal{T}_{1,h}$ and $S \in \mathcal{T}_{2,h}$, such that $\boldsymbol{n}_1 = \boldsymbol{n}_{TF} = -\boldsymbol{n}_{SF}$ on Γ_1, we derive

$$b_h((\underline{\mathbf{v}}_{1,h}, \underline{\mathbf{v}}_{2,h}), \widehat{\xi}_h) = \sum_{F\in\Gamma_{1,h}} (\nabla u_1 \cdot \boldsymbol{n}_{TF}, v_{2,F})_F - \sum_{F\in\Gamma_{1,h}} (\nabla u_1 \cdot \boldsymbol{n}_{TF}, v_{1,F})_F. \tag{70}$$

Finally, from equations (66)-(70), knowing that $v_{i,F}$ is single-valued, and the normal component of ∇u_i is continuous on skeletal induced by $\mathcal{T}_{i,h}$, $i \in \{1,2\}$, we conclude the proof. □

Lemma 5.2 *Assuming that $u_i \in H^{q+1+\delta_i}(\mathcal{T}_{i,h})$, $i \in \{1,2\}$, and $q \in \{0,...,k\}$, there exists $C > 0$, independent of the meshsize, such that*

$$||\mathcal{E}_h(((u_1,u_2),\xi);\cdot)||_{\mathbf{X}_h^*} \leq C \left(h_1^{2(q+\delta_1)} \|u_1\|^2_{H^{q+1+\delta_1}(\mathcal{T}_{1,h})} + h_2^{2(q+\delta_2)} \|u_2\|^2_{H^{q+1+\delta_2}(\mathcal{T}_{2,h})} \right)^{1/2}, \tag{71}$$

where $h_i := \max_{T\in\mathcal{T}_{i,h}} h_T$, $i = 1,2$.

Proof. First, we take $(\underline{\mathbf{v}}_{1,h}, \underline{\mathbf{v}}_{2,h}) \in \underline{\mathbf{U}}_{\mathcal{T}_h}^{k,0}$. Then, after noticing that $G_T^k \underline{\mathbf{I}}_T^k(w) = \nabla p_T^{k+1} \underline{\mathbf{I}}_T^k(w)$, for any $w \in H^1(T)$, $T \in \mathcal{T}_h$, and introducing $\breve{u}_{1,T} := p_T^{k+1} \underline{\mathbf{I}}_T^k(u_1|_T)$, for each $T \in \mathcal{T}_{1,h}$ and $\breve{u}_{2,S} := p_S^{k+1} \underline{\mathbf{I}}_S^k(u_2|_S)$, for all $S \in \mathcal{T}_{2,h}$, we have

$$\begin{aligned}
a_h((\widehat{\underline{\mathbf{u}}}_{1,h}, \widehat{\underline{\mathbf{u}}}_{2,h}), (\underline{\mathbf{v}}_{1,h}, \underline{\mathbf{v}}_{2,h})) &= \sum_{T\in\mathcal{T}_{1,h}} (G_T^k \widehat{\underline{\mathbf{u}}}_{1,T}, G_T^k \underline{\mathbf{v}}_{1,T})_T + \sum_{T\in\mathcal{T}_{1,h}} j_T(\widehat{\underline{\mathbf{u}}}_{1,T}, \underline{\mathbf{v}}_{1,T}) \\
&\quad + \sum_{S\in\mathcal{T}_{h,2}} (G_S^k \widehat{\underline{\mathbf{u}}}_{2,S}, G_S^k \underline{\mathbf{v}}_{2,S})_S + \sum_{S\in\mathcal{T}_{2,h}} j_S(\widehat{\underline{\mathbf{u}}}_{2,S}, \underline{\mathbf{v}}_{2,S}) \\
&= \sum_{T\in\mathcal{T}_{1,h}} (\nabla v_{1,T}, \nabla \breve{u}_{1,T})_T + \sum_{T\in\mathcal{T}_{1,h}} \sum_{F\in\mathcal{F}_T} (v_{1,F} - v_{1,T}, \nabla \breve{u}_{1,T} \cdot \boldsymbol{n}_{TF})_F \\
&\quad + \sum_{S\in\mathcal{T}_{2,h}} (\nabla v_{2,S}, \nabla \breve{u}_{2,S})_S + \sum_{S\in\mathcal{T}_{2,h}} \sum_{F\in\mathcal{F}_S} (v_{2,F} - v_{2,S}, \nabla \breve{u}_{2,S} \cdot \boldsymbol{n}_{SF})_F \\
&\quad + \sum_{T\in\mathcal{T}_{1,h}} j_T(\widehat{\underline{\mathbf{u}}}_{1,T}, \underline{\mathbf{v}}_{1,T}) + \sum_{S\in\mathcal{T}_{2,h}} j_S(\widehat{\underline{\mathbf{u}}}_{2,S}, \underline{\mathbf{v}}_{2,S}) \,.
\end{aligned} \tag{72}$$

At this point, from (72) and Lemma 5.1 , we can write the consistency error as

$$\begin{aligned}
&\widetilde{\mathcal{E}}_h(((u_1,u_2),\xi);(\underline{\mathbf{v}}_{1,h},\underline{\mathbf{v}}_{2,h}))\\
=\ &\underbrace{\sum_{T\in\mathcal{T}_{1,h}}(\nabla v_{1,T},\nabla(\breve{u}_{1,T}-u_1))_T}_{\mathfrak{T}_1}+\underbrace{\sum_{T\in\mathcal{T}_{1,h}}\sum_{F\in\mathcal{F}_T}(v_{1,F}-v_{1,T},\nabla(\breve{u}_{1,T}-u_1)\cdot\boldsymbol{n}_{TF})_F}_{\mathfrak{T}_2}\\
&+\underbrace{\sum_{S\in\mathcal{T}_{2,h}}(\nabla v_{2,S},\nabla(\breve{u}_{2,S}-u_2))_S}_{\mathfrak{T}_3}+\underbrace{\sum_{S\in\mathcal{T}_{2,h}}\sum_{F\in\mathcal{F}_S}(v_{2,F}-v_{2,S},\nabla(\breve{u}_{2,S}-u_2)\cdot\boldsymbol{n}_{SF})_F}_{\mathfrak{T}_4}\\
&+\underbrace{\sum_{T\in\mathcal{T}_{1,h}}j_T(\widehat{\underline{\mathbf{u}}}_{1,T},\underline{\mathbf{v}}_{1,T})}_{\mathfrak{T}_5}+\underbrace{\sum_{S\in\mathcal{T}_{2,h}}j_S(\widehat{\underline{\mathbf{u}}}_{2,S},\underline{\mathbf{v}}_{2,S})}_{\mathfrak{T}_6}\ .
\end{aligned}\tag{73}$$

Applying Cauchy-Schwarz inequality, followed by the approximation properties of $p_T^{k+1}\underline{\mathbf{I}}_T^k$ (cf. (22)), with T either in $\mathcal{T}_{1,h}$ or in $\mathcal{T}_{2,h}$, and the definition of the norm $||\cdot||_{1,\mathcal{T}_{i,h}}$, we can estimate $\mathfrak{T}_1$, $\mathfrak{T}_2$, $\mathfrak{T}_3$, and $\mathfrak{T}_4$ as

$$|\mathfrak{T}_1|+|\mathfrak{T}_2|\lesssim||\underline{\mathbf{v}}_{1,h}||_{1,\mathcal{T}_{1,h}}\cdot h_1^{q+\delta_1}|u_1|_{H^{q+1+\delta_1}(\mathcal{T}_{1,h})}\,,\tag{74}$$

$$|\mathfrak{T}_3|+|\mathfrak{T}_4|\lesssim||\underline{\mathbf{v}}_{2,h}||_{1,\mathcal{T}_{2,h}}\cdot h_2^{q+\delta_2}|u_2|_{H^{q+1+\delta_2}(\mathcal{T}_{2,h})}\,.\tag{75}$$

Invoking now Theorem 8 in [32], we deduce $h_F^{-1/2}||\pi_F^k(\widehat{u}_{i,F}-R_T^{k+1}\widehat{\underline{\mathbf{u}}}_{i,T})||_F\lesssim h_i^{q+\delta_i}|u_i|_{H^{q+1+\delta_i}(T)}$, $\forall\,F\in\mathcal{F}_T$, where $T\in\mathcal{T}_{i,h}$, $i\in\{1,2\}$. This allows us to estimate $\mathfrak{T}_5$ and $\mathfrak{T}_6$ as

$$|\mathfrak{T}_5|\lesssim||\underline{\mathbf{v}}_{1,h}||_{1,\mathcal{T}_{1,h}}\cdot h_1^{q+\delta_1}|u_1|_{H^{q+1+\delta_1}(\mathcal{T}_{1,h})}\,,\tag{76}$$

$$|\mathfrak{T}_6|\lesssim||\underline{\mathbf{v}}_{2,h}||_{1,\mathcal{T}_{2,h}}\cdot h_2^{q+\delta_2}|u_2|_{H^{q+1+\delta_2}(\mathcal{T}_{2,h})}\,.\tag{77}$$

Then, from (74)-(77), we deduce that for each $(\underline{\mathbf{v}}_{1,h},\underline{\mathbf{v}}_{2,h})\in\underline{\mathbf{U}}_{\mathcal{T}_h}^{k,0}$:

$$\begin{aligned}
&\widetilde{\mathcal{E}}_h(((u_1,u_2),\xi);(\underline{\mathbf{v}}_{1,h},\underline{\mathbf{v}}_{2,h}))\\
\lesssim\ &|\!|\!|(\underline{\mathbf{v}}_{1,h},\underline{\mathbf{v}}_{2,h})|\!|\!|_h\left(h_1^{2(q+\delta_1)}|u_1|^2_{H^{q+1+\delta_1}(\mathcal{T}_{1,h})}+h_2^{2(q+\delta_2)}|u_2|^2_{H^{q+1+\delta_2}(\mathcal{T}_{2,h})}\right)^{1/2}.
\end{aligned}\tag{78}$$

Finally, (78) yields to an upper bound for $||\widetilde{\mathcal{E}}_h(((u_1,u_2),\xi);\cdot)||_{\underline{\mathbf{U}}_{\mathcal{T}_h}^{k,0,*}}$, and thanks to (64), we conclude (71). □

Theorem 5.1 (Energy error estimate). *Assuming that $(u_1,u_2)\in H^{q+1+\delta_1}(\mathcal{T}_{1,h})\times H^{q+1+\delta_2}(\mathcal{T}_{2,h})$, with $q\in\{0,...,k\}$, there exists $C>0$, independent of the meshsize, such that:*

$$\begin{aligned}
&\|((\widehat{\underline{\mathbf{u}}}_{1,h},\widehat{\underline{\mathbf{u}}}_{2,h})-(\underline{\mathbf{u}}_{1,h},\underline{\mathbf{u}}_{2,h})),\widehat{\xi}_h-\xi_h)\|_{\mathbf{X}_h}\\
&\le C\left(h_1^{2(q+\delta_1)}\|u_1\|^2_{H^{q+1+\delta_1}(\mathcal{T}_{1,h})}+h_2^{2(q+\delta_2)}\|u_2\|^2_{H^{q+1+\delta_2}(\mathcal{T}_{2,h})}\right)^{1/2},
\end{aligned}\tag{79}$$

where $h_i:=\max\limits_{T\in\mathcal{T}_{i,h}}h_T$, $i=1,2$. Moreover, applying Lemma 3.3, there also holds

$$\sum_{i=1}^{2}\sum_{T\in\mathcal{T}_{i,h}}||\nabla u_i-\nabla p_T^{k+1}\underline{\mathbf{u}}_{i,T}||^2_{0,T}\ \le\ C\left(h_1^{2(q+\delta_1)}\|u_1\|^2_{H^{q+1+\delta_1}(\mathcal{T}_{1,h})}+h_2^{2(q+\delta_2)}\|u_2\|^2_{H^{q+1+\delta_2}(\mathcal{T}_{2,h})}\right).\tag{80}$$

Proof. Since bilinear form a_h is coercive on $\mathbf{V}_h$ and b_h satisfies a discrete inf-sup condition, with corresponding constants that are independent of the meshsize, we can apply a variant of Lemma A.11 in the appendix in [33], which is valid according to Remark A.12 in this same appendix. As result, we can establish a global discrete inf-sup condition: For any $((\underline{\mathbf{w}}_{1,h}, \underline{\mathbf{w}}_{2,h}), \zeta_h) \in \mathbf{X}_h$:

$$||((\underline{\mathbf{w}}_{1,h}, \underline{\mathbf{w}}_{2,h}), \zeta_h)||_{\mathbf{X}_h} \lesssim \sup_{((\underline{\mathbf{v}}_{1,h}, \underline{\mathbf{v}}_{2,h}), \lambda_h) \in \mathbf{X}_h \setminus \{0\}} \frac{\mathtt{A}_h(((\underline{\mathbf{w}}_{1,h}, \underline{\mathbf{w}}_{2,h}), \zeta_h), ((\underline{\mathbf{v}}_{1,h}, \underline{\mathbf{v}}_{2,h}), \lambda_h))}{||((\underline{\mathbf{v}}_{1,h}, \underline{\mathbf{v}}_{2,h}), \lambda_h)||_{\mathbf{X}_h}}, \quad (81)$$

where the bilinear form $\mathtt{A}_h : \mathbf{X}_h \times \mathbf{X}_h \to \mathbb{R}$ is given by

$$\begin{aligned} \mathtt{A}_h(((\underline{\mathbf{w}}_{1,h}, \underline{\mathbf{w}}_{2,h}), \zeta_h), ((\underline{\mathbf{v}}_{1,h}, \underline{\mathbf{v}}_{2,h}), \lambda_h)) &:= a_h((\underline{\mathbf{w}}_{1,h}, \underline{\mathbf{w}}_{2,h}), (\underline{\mathbf{v}}_{1,h}, \underline{\mathbf{v}}_{2,h})) \\ &+ b_h((\underline{\mathbf{v}}_{1,h}, \underline{\mathbf{v}}_{2,h}), \zeta_h) - b_h((\underline{\mathbf{w}}_{1,h}, \underline{\mathbf{w}}_{2,h}), \lambda_h). \end{aligned} \quad (82)$$

This allows us to apply Corollary A.13 in the appendix in [33], with $\mathtt{l}_h := F_h$ and $\mathtt{m}_h := G_h$, which yields us to

$$||((\widehat{\underline{\mathbf{u}}}_{1,h}, \widehat{\underline{\mathbf{u}}}_{2,h}) - (\underline{\mathbf{u}}_{1,h}, \underline{\mathbf{u}}_{2,h})), \widehat{\xi}_h - \xi_h)||_{\mathbf{X}_h} \lesssim ||\mathcal{E}_h(((u_1, u_2), \xi); \cdot)||_{\mathbf{X}_h^*}.$$

Then, (79) follows straightforwardly from Lemma 5.2.

Finally, in order to derive (80), we realize, after applying triangle inequality, that

$$||\nabla u_i - \nabla p_T^{k+1} \underline{\mathbf{u}}_{i,T}||_{0,T} \leq ||\nabla u_i - \nabla p_T^{k+1} \underline{\mathbf{I}}_T^k(u_i|_T)||_{0,T} + ||\nabla p_T^{k+1} \underline{\mathbf{I}}_T^k(u_i|_T) - \nabla p_T^{k+1} \underline{\mathbf{u}}_{i,T}||_{0,T}, \quad (83)$$

for each $T \in \mathcal{T}_{i,h}$, $i \in \{1, 2\}$. Thus, (80) is deduced from (83), after invoking (79) and Lemma 3.3. We omit further details. □

Remark 5.1 (L^2-error estimate of the projection of the trace error). *Concerning the L^2-norm of $\widehat{\xi}_h - \xi_h$, Theorem 5.1 establishes that, for $q \in \{0, ..., k\}$:*

$$||\widehat{\xi}_h - \xi_h||_{\Gamma_{1,h}} \lesssim h_1^{q+\delta_1} ||u_1||_{q+1+\delta_1, \mathcal{T}_{1,h}} + h_2^{q+\delta_2} ||u_1||_{q+1+\delta_2, \mathcal{T}_{2,h}}. \quad (84)$$

On the other hand, we know that

$$h_{\Gamma_1}^{1/2} ||\widehat{\xi}_h - \xi_h||_{0,\Gamma_1} \lesssim ||\widehat{\xi}_h - \xi_h||_{\Gamma_{1,h}}, \quad (85)$$

since we are assuming that the partition on Γ_1 is quasi-uniform (cf. (28)*). Then, from* (84) *and* (85)*, we deduce that*

$$||\widehat{\xi}_h - \xi_h||_{0,\Gamma_1} \lesssim h_{\Gamma_1}^{-1/2} \left(h_1^{q+\delta_1} ||u_1||_{q+1+\delta_1, \mathcal{T}_{1,h}} + h_2^{q+\delta_2} ||u_1||_{q+1+\delta_2, \mathcal{T}_{2,h}} \right). \quad (86)$$

Our next aim, is to provide an error estimate in the L^2-norm of the projection of the errors $e_{i,h} := \pi_{\mathcal{T}_{i,h}}^k u_i - u_{i,h}$ for each $i \in \{1, 2\}$, where given $\underline{\mathbf{u}}_{i,h} := \left((u_{i,T})_{T \in \mathcal{T}_{i,h}}, (u_{i,F})_{F \in \mathcal{F}_{i,h}} \right)$, we define $u_{i,h}$ as an element of $L^2(\Omega_i)$, such that

$$u_{i,h}|_T := u_{i,T} \quad \text{and} \quad \left(\pi_{\mathcal{T}_{i,h}}^k u_i \right)\Big|_T := \pi_T^k u_i \quad \forall\, T \in \mathcal{T}_{i,h}, \, i \in \{1, 2\}. \quad (87)$$

To this end, we introduce the following auxiliar problem: *Given* $(w_1, w_2) \in L^2(\Omega_1) \times L^2(\Omega_2)$ *with* $(w_1, 1)_{0,\Omega_1} + (w_2, 1)_{0,\Omega_2} = 0$*, we look for* $(z_1, z_2) \in \mathbf{U}$*, such that, in weak sense, verifies*

$$-\Delta\, z_1 = w_1 \text{ in } \Omega_1\,, \tag{88a}$$
$$-\Delta\, z_2 = w_2 \text{ in } \Omega_2\,, \tag{88b}$$
$$z_1 - z_2 = 0 \text{ on } \Gamma_1\,, \tag{88c}$$
$$\nabla z_1 \cdot \boldsymbol{n}_1 + \nabla z_2 \cdot \boldsymbol{n}_2 = 0 \text{ on } \Gamma_1\,, \tag{88d}$$
$$\nabla z_2 \cdot \boldsymbol{n}_2 = 0 \text{ on } \Gamma_2\,. \tag{88e}$$

Since the transmission conditions in (88) *are homogeneous, it is known that* (88) *is equivalent to: Find* $z \in H^1(\Omega) \cap L^2_0(\Omega)$ *such that:*

$$\begin{aligned} -\Delta z \;&= w \text{ in } \Omega \;:=\; \Omega_1 \cup \Gamma_1 \cup \Omega_2\,,\\ \frac{\partial z}{\partial \boldsymbol{n}_2} \;&= 0 \text{ on } \Gamma_2 \;:=\; \partial\Omega\,, \end{aligned} \tag{89}$$

with $w \in L^2_0(\Omega)$ *such that* $w|_{\Omega_1} = w_1$ *and* $w|_{\Omega_2} = w_2$*. In this case,* $z|_{\Omega_1} = z_1$ *and* $z|_{\Omega_2} = z_2$*. Then, we assume further regularity on* z*, the weak solution of* (89)*, so that* $z \in H^2(\Omega) \cap L^2_0(\Omega)$*, and there exists* $C > 0$*, independent of the meshsize, such that*

$$||z||^2_{2,\Omega} \;\leq\; C\, ||w||^2_{0,\Omega}\,,$$

or, equivalently

$$\|z_1\|^2_{2,\Omega_1} + \|z_2\|^2_{2,\Omega_2} \;\leq\; C\left(\|w_1\|^2_{0,\Omega_1} + \|w_2\|^2_{0,\Omega_2}\right)\,. \tag{90}$$

We remark that this assumption holds when, for example, the domain $\Omega := \Omega_1 \cup \Gamma_1 \cup \Omega_2$ *is convex. From here on, we introduce* $h := \max\{h_1, h_2\}$*.*

Theorem 5.2 (convergence estimate of the projection of the potential error). *Assuming that the exact solution* $(u_1, u_2) \in H^{q+1+\delta_1}(\mathcal{T}_{1,h}) \times H^{q+1+\delta_2}(\mathcal{T}_{2,h})$*, with* $q \in \{0, ..., k\}$*, and there holds the elliptic regularity property* (90)*, we have, for* $k \geq 1$*:*

$$\begin{aligned} &\|\pi^k_{\mathcal{T}_{1,h}} u_1 - u_{1,h}\|_{0,\Omega_1} + \|\pi^k_{\mathcal{T}_{2,h}} u_2 - u_{2,h}\|_{0,\Omega_2}\\ \lesssim\; & h\,\left(h_1^{2(q+\delta_1)}\,||u_1||^2_{q+1+\delta_1,\mathcal{T}_{1,h}} \;+\; h_2^{2(q+\delta_2)}\,||u_2||^2_{q+1+\delta_2,\mathcal{T}_{2,h}}\right)^{1/2}\,. \end{aligned} \tag{91}$$

For $k = 0$*, assuming in addition that* $f_i \in H^{\delta_i}(\mathcal{T}_{i,h})$*, for* $i \in \{1, 2\}$*,* $g_1 \in \mathbb{P}_0(\Gamma_{1,h})$ *and* $g_2 \in \mathbb{P}_0(\Gamma_{2,h})$*, there holds*

$$\begin{aligned} &\|\pi^0_{\mathcal{T}_{1,h}} u_1 - u_{1,h}\|_{0,\Omega_1} + \|\pi^0_{\mathcal{T}_{2,h}} u_2 - u_{2,h}\|_{0,\Omega_2}\\ \lesssim\; & h\,\left(h_1^{2(\delta_1)}\,||u_1||^2_{1+\delta_1,\mathcal{T}_{1,h}} \;+\; h_2^{2(\delta_2)}\,||u_2||^2_{1+\delta_2,\mathcal{T}_{2,h}}\right)^{1/2}\\ &+\left(h_1^{2(1+\delta_1)}||f_1||^2_{\delta_1,\mathcal{T}_{1,h}} \;+\; h_2^{2(1+\delta_2)}||f_2||^2_{\delta_2,\mathcal{T}_{2,h}}\right)^{1/2}\,. \end{aligned} \tag{92}$$

Proof. *Let* $((z_1, z_2), \eta) \in \mathbf{X} := \mathbf{U} \times H^{-1/2}(\Gamma_1)$ *be the solution of the corresponding mixed variational formulation associated to* (88)*, where* $\eta := \nabla z_1 \cdot \boldsymbol{n}_1$ *on* Γ_1 *is introduced as auxiliary*

unknown. This formulation can be seen as (8)*, with* $F(v_1, v_2) := (w_1, v_1)_{\Omega_1} + (w_2, v_2)_{\Omega_2}$*, and* $G(\lambda) := 0$*. Next, we denote by* $((\underline{\mathbf{z}}_{1,h}, \underline{\mathbf{z}}_{2,h}), \eta_h) \in \mathbf{X}_h$ *the unique solution of the mixed HHO scheme corresponding to* (88)*, that is*

$$\mathtt{A}_h(((\underline{\mathbf{z}}_{1,h}, \underline{\mathbf{z}}_{2,h}), \eta_h), ((\underline{\mathbf{v}}_{1,h}, \underline{\mathbf{v}}_{2,h}), \lambda_h)) \;=\; (w_1, v_{1,h})_{\Omega_1} \;+\; (w_2, v_{2,h})_{\Omega_2} \quad \forall ((\underline{\mathbf{v}}_{1,h}, \underline{\mathbf{v}}_{2,h}), \lambda_h) \in \mathbf{X}_h\,. \tag{93}$$

We notice that there holds $\forall ((\underline{\mathbf{v}}_{1,h}, \underline{\mathbf{v}}_{2,h}), \lambda_h)\,,\; ((\underline{\mathbf{w}}_{1,h}, \underline{\mathbf{w}}_{2,h}), \zeta_h) \in \mathbf{X}_h$*:*

$$\mathtt{A}_h(((\underline{\mathbf{w}}_{1,h}, \underline{\mathbf{w}}_{2,h}), \zeta_h), ((\underline{\mathbf{v}}_{1,h}, \underline{\mathbf{v}}_{2,h}), \lambda_h)) \;=\; \mathtt{A}_h(((\underline{\mathbf{v}}_{1,h}, \underline{\mathbf{v}}_{2,h}), -\lambda_h), ((\underline{\mathbf{w}}_{1,h}, \underline{\mathbf{w}}_{2,h}), -\zeta_h))\,. \tag{94}$$

As a result, we notice that (93) *can also be written as*

$$\mathtt{A}_h(((\underline{\mathbf{v}}_{1,h}, \underline{\mathbf{v}}_{2,h}), \lambda_h), ((\underline{\mathbf{z}}_{1,h}, \underline{\mathbf{z}}_{2,h}), -\eta_h)) \;=\; (w_1, v_{1,h})_{\Omega_1} \;+\; (w_2, v_{2,h})_{\Omega_2} \quad \forall ((\underline{\mathbf{v}}_{1,h}, \underline{\mathbf{v}}_{2,h}), \lambda_h) \in \mathbf{X}_h\,. \tag{95}$$

This lets us to state that the dual consistency error is given by

$$\begin{aligned}\mathcal{E}_h^{\mathtt{d}}(((z_1, z_2), \eta), ((\underline{\mathbf{v}}_{1,h}, \underline{\mathbf{v}}_{2,h}), \lambda_h)) \;:=\; &\mathtt{A}_h(((\underline{\mathbf{v}}_{1,h}, \underline{\mathbf{v}}_{2,h}), \lambda_h), ((\widehat{\underline{\mathbf{z}}}_{1,h}, \widehat{\underline{\mathbf{z}}}_{2,h}), -\widehat{\eta}_h))) \\ &- (w_1, v_{1,h})_{\Omega_1} - (w_2, v_{2,h})_{\Omega_2}\,,\end{aligned}$$

where $\widehat{\underline{\mathbf{z}}}_{i,h} := \underline{\mathbf{I}}^k_{\mathcal{T}_{i,h}}(z_i) \in \underline{\mathbf{U}}^k_{\mathcal{T}_{i,h}}$*,* $i \in \{1, 2\}$*, and* $\widehat{\eta}_h \;=\; \left(\pi^k_F(\eta|_F)\right)_{F \in \Gamma_{1,h}} \in Q^k_h$*. Thanks to* (94)*, it is not difficult to check that* $\forall ((\underline{\mathbf{v}}_{1,h}, \underline{\mathbf{v}}_{2,h}), \lambda_h) \in \mathbf{X}_h$ *there holds*

$$\begin{aligned}\mathcal{E}_h^{\mathtt{d}}(((z_1, z_2), \eta), ((\underline{\mathbf{v}}_{1,h}, \underline{\mathbf{v}}_{2,h}), -\lambda_h)) \;&=\mathtt{A}_h(((\widehat{\underline{\mathbf{z}}}_{1,h}, \widehat{\underline{\mathbf{z}}}_{2,h}), \widehat{\eta}_h), ((\underline{\mathbf{v}}_{1,h}, \underline{\mathbf{v}}_{2,h}), \lambda_h)) \\ &\quad - (w_1, v_{1,h})_{\Omega_1} - (w_2, v_{2,h})_{\Omega_2} \\ &=: \mathcal{E}_h(((z_1, z_2), \eta), ((\underline{\mathbf{v}}_{1,h}, \underline{\mathbf{v}}_{2,h}), \lambda_h))\,.\end{aligned} \tag{96}$$

Now, invoking Lemma A.14 in the appendix in [33] with $\mathtt{U} := \mathbf{U}$*,* $\mathtt{P} := H^{-1/2}(\Gamma_1)$*,* $\mathtt{U}_h := \underline{\mathbf{U}}^{k,0}_{\mathcal{T}_h}$*, provided with the* $|\!|\!| \cdot |\!|\!|_h$*−norm and interpolator* $\mathtt{I}_h := \underline{\mathbf{I}}^k_{\mathcal{T}_h}$ *(cf.* (17)*),* $\mathtt{P}_h := Q^k_h$*, equipped with* $||\cdot||_{\Gamma_{1,h}}$*−norm and interpolator* $\mathtt{J}_h := \pi^k_{\Gamma_{1,h}} := \left(\pi^k_F\right)_{F \in \Gamma_{1,h}}$*,* $\mathtt{a}_h := a_h$*, and* $\mathtt{b}_h := b_h$*. In addition, we introduce* $\mathtt{L} := L^2_0(\Omega)$*, with the reconstruction operator* $\mathtt{r}_h : \mathtt{U}_h \to \mathtt{L}$ *such that* $\mathtt{r}_h(\underline{\mathbf{v}}_h) := v_h$*. Then, the error estimate (A.30) in [33] reads as*

$$\begin{aligned}&||\pi^k_{\mathcal{T}_{1,h}} u_1 - u_{1,h}||_{0,\Omega_1} \;+\; ||\pi^k_{\mathcal{T}_{2,h}} u_2 - u_{2,h}||_{0,\Omega_2} \\ \leq\; &\underbrace{|\!|\!|((\underline{\mathbf{u}}_{1,h}, \underline{\mathbf{u}}_{2,h}), \xi_h) - ((\widehat{\underline{\mathbf{u}}}_{1,h}, \widehat{\underline{\mathbf{u}}}_{2,h}), \widehat{\xi}_h)|\!|\!|_{\mathbf{X}_h} \sup_{(w_1,w_2) \in L^2_0(\Omega)\,,\, ||w||_\Omega = 1} ||\mathcal{E}_h^{\mathtt{d}}(((z_1, z_2), \eta), \cdot)||_{\mathbf{X}_h^*}}_{\mathfrak{T}_1} \\ &+ \underbrace{\sup_{(w_1,w_2) \in L^2_0(\Omega)\,,\, ||w||_\Omega = 1} \mathcal{E}_h(((u_1, u_2), \xi), ((\widehat{\underline{\mathbf{z}}}_{1,h}, \widehat{\underline{\mathbf{z}}}_{2,h}), \widehat{\eta}_h))}_{\mathfrak{T}_2}\end{aligned} \tag{97}$$

Then (91) *and* (92) *are obtained after bounding the terms on the right hand side of* (97)*.*

i) **Bounding $\mathfrak{T}_1$.** *From* (79) *in Theorem 5.1, we have*

$$\begin{aligned} &||((\underline{\mathbf{u}}_{1,h},\underline{\mathbf{u}}_{2,h}),\xi_h)-((\widehat{\underline{\mathbf{u}}}_{1,h},\widehat{\underline{\mathbf{u}}}_{2,h}),\widehat{\xi}_h)||_{\mathbf{X}_h} \\ &\lesssim h_1^{q+\delta_1}||u_1||_{q+1+\delta_1,\mathcal{T}_{1,h}} + h_2^{q+\delta_2}||u_2||_{q+1+\delta_2,\mathcal{T}_{2,h}}\,. \end{aligned} \tag{98}$$

From (96)*, we notice that*

$$||\mathcal{E}_h^{\mathtt{d}}(((z_1,z_2),\eta),\cdot)||_{\mathbf{X}_h^*} = ||\mathcal{E}_h(((z_1,z_2),\eta),\cdot)||_{\mathbf{X}_h^*}\,,$$

which is estimated by applying Lemma 5.2 with $q=0$ and $\delta_1=\delta_2=1$, yielding to

$$\begin{aligned} ||\mathcal{E}_h(((z_1,z_2),\eta),\cdot)||_{\mathbf{X}_h^*} &\lesssim (h_1\,||z_1||_{2,\Omega_1} + h_2\,||z_2||_{2,\Omega_2}) \\ &\lesssim h\,(||w_1||_{0,\Omega_1} + ||w_2||_{0,\Omega_2})\,, \end{aligned} \tag{99}$$

where the last inequality has been obtained after applying the ellipticity property (90)*. Then, from* (98) *and* (99)*, we deduce*

$$|\mathfrak{T}_1| \lesssim h\,\left(h_1^{q+\delta_1}||u_1||_{q+1+\delta_1,\mathcal{T}_{1,h}} + h_2^{q+\delta_2}||u_2||_{q+1+\delta_2,\mathcal{T}_{2,h}}\right)\,. \tag{100}$$

ii) **Bounding $\mathfrak{T}_2$.** *At this point, we need to consider two cases: $k\geq 1$ and $k=0$.*

ii.A) The case $k\geq 1$. Taking into account (63) *and the orthogonality property of p_T^{k+1}* (20)*, we proceed as in the derivation of* (73)*, and obtain*

$$\begin{aligned} \widetilde{\mathcal{E}}_h(((u_1,u_2),\xi),((\widehat{\underline{\mathbf{z}}}_{1,h},\widehat{\underline{\mathbf{z}}}_{2,h}))) &= \underbrace{\sum_{T\in\mathcal{T}_{1,h}}\sum_{F\in\mathcal{F}_T}(\pi_F^k z_1-\pi_T^k z_1,\nabla(\breve{u}_{1,T}-u_1)\cdot\boldsymbol{n}_{TF})_F}_{\mathfrak{E}_1} \\ &\quad+\underbrace{\sum_{S\in\mathcal{T}_{2,h}}\sum_{F\in\mathcal{F}_S}(\pi_F^k z_2-\pi_S^k z_2,\nabla(\breve{u}_{2,S}-u_2)\cdot\boldsymbol{n}_{SF})_F}_{\mathfrak{E}_2} \\ &\quad+\underbrace{\sum_{T\in\mathcal{T}_{1,h}} j_T(\widehat{\underline{\mathbf{u}}}_{1,T},\widehat{\underline{\mathbf{z}}}_{1,T})}_{\mathfrak{E}_3}+\underbrace{\sum_{S\in\mathcal{T}_{2,h}} j_S(\widehat{\underline{\mathbf{u}}}_{2,S},\widehat{\underline{\mathbf{z}}}_{2,S})}_{\mathfrak{E}_4}\,. \end{aligned} \tag{101}$$

Now, taking into account (22) *and* (14) *(with $l=q\geq 1$ and $t=2$), we deduce*

$$|\mathfrak{E}_1| \lesssim \sum_{T\in\mathcal{T}_{1,h}} h_T^{q+1+\delta_1}\,||u_1||_{q+1+\delta_1,T}\,||z_1||_{2,T}\,. \tag{102}$$

On the other hand, we notice that

$$\begin{aligned} j_T(\widehat{\underline{\mathbf{u}}}_{1,T},\widehat{\underline{\mathbf{z}}}_{1,T}) &\leq j_T(\widehat{\underline{\mathbf{u}}}_{1,T},\widehat{\underline{\mathbf{u}}}_{1,T})^{1/2} j_T(\widehat{\underline{\mathbf{z}}}_{1,T},\widehat{\underline{\mathbf{z}}}_{1,T})^{1/2} \\ &\lesssim (h_T^{q+\delta_1}\,|u_1|_{q+1+\delta_1})(h_T\,|z_1|_{2,T})\,, \end{aligned} \tag{103}$$

and then we derive

$$|\mathfrak{E}_3| \lesssim \sum_{T\in\mathcal{T}_{1,h}} h_T^{q+1+\delta_1} ||u_1||_{q+1+\delta_1,T} \, ||z_1||_{2,T} \, . \tag{104}$$

Proceeding in analogous way, we find that

$$|\mathfrak{E}_2| \lesssim \sum_{T\in\mathcal{T}_{2,h}} h_T^{q+1+\delta_2} \, ||u_2||_{q+1+\delta_2,T} \, ||z_2||_{2,T} \, , \tag{105}$$

$$|\mathfrak{E}_4| \lesssim \sum_{T\in\mathcal{T}_{2,h}} h_T^{q+1+\delta_2} ||u_2||_{q+1+\delta_2,T} \, ||z_2||_{2,T} \, . \tag{106}$$

Now, thanks to (102), (105), (104), (106)*, and the elliptic regularity property* (90)*, we are able to bound*
$\widetilde{\mathcal{E}}_h(((u_1,u_2),\xi),((\widehat{\underline{\mathbf{z}}}_{1,h},\widehat{\underline{\mathbf{z}}}_{2,h})))$ *(cf.* (101)*), and then* $\mathfrak{T}_2$*, arriving to*

$$|\mathfrak{T}_2| \lesssim \left(\sum_{T\in\mathcal{T}_{1,h}} h_T^{2(q+1+\delta_1)} \, ||u_1||^2_{q+1+\delta_1,T} + \sum_{T\in\mathcal{T}_{2,h}} h_T^{2(q+1+\delta_2)} \, ||u_2||^2_{q+1+\delta_2,T} \right)^{1/2} . \tag{107}$$

ii.B) The case $k=0$*. It is not difficult to establish*

$$(f_1,\pi_T^0 z_1)_T \, = \, (\pi_T^0 f_1, z_1)_T \, = \, (\pi_T^0 f_1 - f_1, z_1 - \pi_T^0 z_1)_T \, + \, (f_1,z_1)_T \quad \forall \, T \in \mathcal{T}_{1,h} \, , \tag{108}$$

$$(f_2,\pi_S^0 z_2)_S \, = \, (\pi_S^0 f_2, z_2)_S \, = \, (\pi_S^0 f_2 - f_2, z_2 - \pi_S^0 z_2)_S \, + \, (f_2,z_2)_S \quad \forall \, S \in \mathcal{T}_{2,h} \, , \tag{109}$$

$$(g_1,\pi_F^0 z_2)_F \, = \, (g_1,z_2)_F \quad \forall \, F \in \Gamma_{1,h} \, , \tag{110}$$

$$(g_2,\pi_F^0 z_2)_F \, = \, (g_2,z_2)_F \quad \forall \, F \in \Gamma_{2,h} \, . \tag{111}$$

Now, taking $(v_1,v_2) := (z_1,z_2) \in U$ *in* (8a)*, we have*

$$\begin{aligned} &(f_1,z_1)_{\Omega_1} \, + \, (f_2,z_2)_{\Omega_2} \, + \, \langle g_1, \gamma_0^+(z_2)\rangle_{\Gamma_1} \, + \, \langle g_2, \gamma_0^+(z_2)\rangle_{\Gamma_2} \\ &= \, (\nabla u_1, \nabla z_1)_{\Omega_1} \, + \, (\nabla u_2, \nabla z_2)_{\Omega_2} \, + \, \langle \xi, \underbrace{\gamma_0^+(z_2) - \gamma_0^-(z_1)}_{=0} \rangle_{\Gamma_1} \, , \end{aligned}$$

and from (108)-(111)*, we deduce that*

$$\begin{aligned} &\sum_{T\in\mathcal{T}_{1,h}} (f_1,\pi_T^0 z_1)_T \, + \, \sum_{S\in\mathcal{T}_{2,h}} (f_2,\pi_S^0 z_2)_S \, + \, \sum_{F\in\Gamma_{1,h}} (g_1,\pi_F^0 z_2)_F \, + \, \sum_{F\in\Gamma_{2,h}} (g_2,\pi_F^0 z_2)_F \\ &\qquad = \sum_{T\in\mathcal{T}_{1,h}} (\pi_T^0 f_1 - f_1, z_1 - \pi_T^0 z_1)_T \, + \, \sum_{S\in\mathcal{T}_{2,h}} (\pi_S^0 f_2 - f_2, z_2 - \pi_S^0 z_2)_S \\ &\qquad\qquad + (\nabla u_1, \nabla z_1)_{\Omega_1} + (\nabla u_2, \nabla z_2)_{\Omega_2} \, . \end{aligned} \tag{112}$$

Then, taking into account (63) *and* (112)*, we have*

$$\begin{aligned}
&\mathcal{E}_h(((u_1,u_2),\xi),((\widehat{\underline{\mathbf{z}}}_{1,h},\widehat{\underline{\mathbf{z}}}_{2,h}),\widehat{\eta}_h))\\
&= \underbrace{\sum_{T\in\mathcal{T}_{1,h}}\left[(\nabla p_T^1\underline{\mathbf{I}}_T^0u_1,\nabla p_T^1\underline{\mathbf{I}}_T^0z_1)_T-(\nabla u_1,\nabla z_1)_T\right]}_{\mathfrak{E}_1}\\
&+ \underbrace{\sum_{S\in\mathcal{T}_{2,h}}\left[(\nabla p_S^1\underline{\mathbf{I}}_S^0u_1,\nabla p_S^1\underline{\mathbf{I}}_S^0z_1)_S-(\nabla u_2,\nabla z_2)_S\right]}_{\mathfrak{E}_2}\\
&+ \underbrace{\sum_{T\in\mathcal{T}_{1,h}} j_T(\widehat{\underline{\mathbf{u}}}_{1,T},\widehat{\underline{\mathbf{z}}}_{1,T})}_{\mathfrak{E}_3} + \underbrace{\sum_{S\in\mathcal{T}_{2,h}} j_S(\widehat{\underline{\mathbf{u}}}_{2,S},\widehat{\underline{\mathbf{z}}}_{2,S})}_{\mathfrak{E}_4}\\
&- \underbrace{\sum_{T\in\mathcal{T}_{1,h}}(\pi_T^0f_1-f_1,z_1-\pi_T^0z_1)_T}_{\mathfrak{E}_5} - \underbrace{\sum_{S\in\mathcal{T}_{2,h}}(\pi_S^0f_2-f_2,z_2-\pi_S^0z_2)_S}_{\mathfrak{E}_6}. \qquad (113)
\end{aligned}$$

In order to bound $\mathfrak{E}_1$*, we first notice that*

$$(\nabla u_1,\nabla z_1)_T-(\nabla p_T^1\underline{\mathbf{I}}_T^0u_1,\nabla p_T^1\underline{\mathbf{I}}_T^0z_1)_T=(\nabla u_1-\nabla p_T^1\underline{\mathbf{I}}_T^0u_1,\nabla z_1-\nabla p_T^1\underline{\mathbf{I}}_T^0z_1)_T,$$

and, after take into consideration (22)*, we deduce*

$$|\mathfrak{E}_1|\lesssim\left(\sum_{T\in\mathcal{T}_{1,h}}h_T^{2(1+\delta_1)}||u_1||_{1+\delta_1,T}^2\right)^{1/2}|z_1|_{2,\Omega_1}. \qquad (114)$$

Proceeding in similar way, we also derive

$$|\mathfrak{E}_2|\lesssim\left(\sum_{S\in\mathcal{T}_{2,h}}h_S^{2(1+\delta_2)}||u_2||_{1+\delta_2,S}^2\right)^{1/2}|z_2|_{2,\Omega_2}. \qquad (115)$$

Next, applying (103) *with* $k=0$*, we obtain*

$$|\mathfrak{E}_3|\lesssim\left(\sum_{T\in\mathcal{T}_{1,h}}h_T^{2(1+\delta_1)}||u_1||_{1+\delta_1,T}^2\right)^{1/2}|z_1|_{2,\Omega_1}, \qquad (116)$$

$$|\mathfrak{E}_4|\lesssim\left(\sum_{T\in\mathcal{T}_{2,h}}h_T^{2(1+\delta_2)}||u_2||_{1+\delta_2,T}^2\right)^{1/2}|z_2|_{2,\Omega_1}. \qquad (117)$$

For $\mathfrak{E}_5$, we apply Cauchy-Schwarz inequality, and approximation theory, to have

$$\begin{aligned}|\mathfrak{E}_5| &\leq \sum_{T\in\mathcal{T}_{1,h}} ||\pi_T^0 f_1 - f_1||_T||z_1 - \pi_T^0 z_1||_T \\ &\leq \sum_{T\in\mathcal{T}_{1,h}} \left(h_T^{\delta_1}||f_1||_{\delta_1,T}\right)\,(h_T|z_1|_{1,T}) \\ &\lesssim \left(\sum_{T\in\mathcal{T}_{1,h}} h_T^{2(1+\delta_1)}||f_1||_{\delta_1,T}^2\right)^{1/2} |z_1|_{1,\Omega_1}\,. \end{aligned} \tag{118}$$

Analogously, we derive

$$|\mathfrak{E}_6| \lesssim \left(\sum_{T\in\mathcal{T}_{2,h}} h_T^{2(1+\delta_1)}||f_2||_{\delta_2,T}^2\right)^{1/2} |z_2|_{1,\Omega_2}\,. \tag{119}$$

Then, $\mathfrak{T}_2$ is bounded from (114)-(119)*. Finally, the conclusion is also achieved in this case, thanks to* (100) *(which also holds for $k=0$). We omit further details.*

□

Following the ideas given in the proof of Theorem 2.32 in [33] (see also the proof of Theorem 6.3 in [20]), and with the help of Theorem 5.2, we can establish a super convergent L^2-error estimate of the reconstructive potential error.

Theorem 5.3 (L^2-error estimate). *Assuming that $(u_1,u_2)\in H^{q+1+\delta_1}(\mathcal{T}_{1,h})\times H^{q+1+\delta_2}(\mathcal{T}_{2,h})$, with $q\in\{0,...,k\}$, and the elliptic regularity property* (90)*, we have, for $k\geq 1$:*

$$\begin{aligned}&\|p_h^{k+1}\underline{\mathbf{u}}_{1,h} - u_1\|_{0,\Omega_1} + \|p_h^{k+1}\underline{\mathbf{u}}_{2,h} - u_2\|_{0,\Omega_2} \\ \lesssim\, & h\left(h_1^{2(q+\delta_1)}\,||u_1||_{q+1+\delta_1,\mathcal{T}_{1,h}}^2 + h_2^{2(q+\delta_2)}\,||u_2||_{q+1+\delta_2,\mathcal{T}_{2,h}}^2\right)^{1/2}, \end{aligned} \tag{120}$$

For $k=0$, assuming in addition that $f_i\in H^{\delta_i}(\mathcal{T}_{i,h})$, for $i\in\{1,2\}$, $g_1\in\mathbb{P}_0(\Gamma_{1,h})$ and $g_2\in\mathbb{P}_0(\Gamma_{2,h})$, there holds

$$\begin{aligned}&\|p_h^1\underline{\mathbf{u}}_{1,h} - u_1\|_{0,\Omega_1} + \|p_h^1\underline{\mathbf{u}}_{2,h} - u_2\|_{0,\Omega_2} \\ \lesssim\, & h\left(h_1^{2\delta_1}\,||u_1||_{1+\delta_1,\mathcal{T}_{1,h}}^2 + h_2^{2\delta_2}\,||u_2||_{1+\delta_2,\mathcal{T}_{2,h}}^2\right)^{1/2} \\ +\, & \left(h_1^{2(1+\delta_1)}||f_1||_{\delta_1,\mathcal{T}_{1,h}}^2 + h_2^{2(1+\delta_2)}||f_2||_{\delta_2,\mathcal{T}_{2,h}}^2\right)^{1/2}. \end{aligned} \tag{121}$$

6 Computational implementation aspects

We start remarking that the condition $(v_{1,h},1)_{\Omega_1}+(v_{2,h},1)_{\Omega_2}=0$ given in the definition of discrete space $\underline{\mathbf{U}}_{\mathcal{T}_h}^{k,0}$, make it difficult to find a basis. Then, we impose this restriction in the HHO variational formulation with the help of a Lagrange multiplier. This procedure yields to

the following equivalent discrete scheme: Find $(\underline{\mathbf{u}}_{1,h}, \underline{\mathbf{u}}_{2,h}, \alpha, \xi_h) \in \underline{\mathbf{U}}^k_{\mathcal{T}_{1,h}} \times \underline{\mathbf{U}}^k_{\mathcal{T}_{2,h}} \times \mathbb{R} \times Q^k_h$ *such that*

$$\begin{aligned}
&\sum_{T\in\mathcal{T}_{1,h}} a_T(\underline{\mathbf{u}}_{1,T}, \underline{\mathbf{v}}_{1,T}) + \alpha\left(\sum_{T\in\mathcal{T}_{1,h}} (v_{1,T},1)_T + \sum_{S\in\mathcal{T}_{2,h}} (v_{2,S},1)_S\right) + \sum_{F\in\Gamma_{1,h}} (v_{2,F}-v_{1,F},\xi_F)_F \\
&+ \sum_{S\in\mathcal{T}_{2,h}} a_S(\underline{\mathbf{u}}_{2,S}, \underline{\mathbf{v}}_{2,S}) + \beta\left(\sum_{T\in\mathcal{T}_{1,h}} (u_{1,T},1)_T + \sum_{S\in\mathcal{T}_{2,h}} (u_{2,S},1)_S\right) + \sum_{F\in\Gamma_{1,h}} (u_{2,F}-u_{1,F},\lambda_F)_F \\
&= F_h(\underline{\mathbf{v}}_{1,h}, \underline{\mathbf{v}}_{2,h}) - G_h(\lambda_h) \qquad \forall (\underline{\mathbf{v}}_{1,h}, \underline{\mathbf{v}}_{2,h}, \beta, \lambda_h) \in \underline{\mathbf{U}}^k_{\mathcal{T}_{1,h}} \times \underline{\mathbf{U}}^k_{\mathcal{T}_{2,h}} \times \mathbb{R} \times Q^k_h, \qquad (122)
\end{aligned}$$

where we rewrite (39) as

$$\begin{aligned}
F_h(\underline{\mathbf{v}}_{1,h}, \underline{\mathbf{v}}_{2,h}) &= \sum_{T\in\mathcal{T}_{1,h}} \left\{ (f_1, v_{1,T})_T + \sum_{F\in\mathcal{F}_T\cap\Gamma_{1,h}} (g_1, v_{2,F})_F \right\} \\
&\quad + \sum_{S\in\mathcal{T}_{2,h}} \left\{ (f_2, v_{2,S})_S + \sum_{F\in\mathcal{F}_S\cap\Gamma_{2,h}} (g_2, v_{2,F})_F \right\}, \\
&= \sum_{T\in\mathcal{T}_{1,h}} F^1_T(\underline{\mathbf{v}}_{1,T}) + \sum_{S\in\mathcal{T}_{2,h}} F^2_S(\underline{\mathbf{v}}_{2,S}), \qquad (123)
\end{aligned}$$

and

$$G_h(\lambda_h) = \sum_{F\in\Gamma_{1,h}} (\lambda_F, g)_F \quad \forall\, \lambda_h := (\lambda_F)_{F\in\Gamma_{1,h}} \in Q^k_h\,. \qquad (124)$$

For integers $l \geq 0$ *and* $n \geq 0$*, we denote by* $N^l_n := \begin{pmatrix} l+n \\ l \end{pmatrix}$ *the dimension of the space polynomial in* $\mathbb{R}^n$*, of degree at most* l*.*

Now, given $\underline{\mathbf{v}}_{i,h}$ *in the global discrete space* $\underline{\mathbf{U}}^k_{\mathcal{T}_{i,h}}$*, we collect its components with respect to the polynomial bases attached to the mesh cells and faces, in a global component vector denoted by* $V_{\mathcal{TF}}(i) \in \mathbb{R}^{N^k_{\mathcal{T}}(i)}$*, with*

$$N^k_{\mathcal{T}}(i) := \dim(\underline{\mathbf{U}}^k_{\mathcal{T}_{i,h}}) = \mathrm{card}(\mathcal{T}_{i,h}) \times N^k_d + \mathrm{card}(\mathcal{F}_{i,h}) \times N^k_{d-1} \text{ for } i \in \{1,2\}. \qquad (125)$$

Here, N^k_d *and* N^k_{d-1} *denote the dimension of the corresponding local cell and face bases (*d *represents the space dimension). We can decompose the global vector of coefficients as*

$$V_{\mathcal{TF}}(i) = \left[\begin{array}{c} V_{\mathcal{T}}(i) \\ \hdashline V_{\mathcal{F}}(i) \end{array}\right], \qquad (126)$$

where the vectors $V_{\mathcal{T}}(i)$ *and* $V_{\mathcal{F}}(i)$ *collect the coefficients associated to element-based and face-based DOFS for each subdomain, respectively.*

Also, the restriction of $V_{\mathcal{TF}}(i)$ *over their components associated to* T*,* ∂T *and* S*,* ∂S *are denoted by the local component vectors* $V_{T\mathcal{F}_T} \in \mathbb{R}^{N^k_T}$ *and* $V_{S\mathcal{F}_S} \in \mathbb{R}^{N^k_S}$*, respectively. In similar way, we can split these local vectors as*

$$V_{T\mathcal{F}_T} = \left[\begin{array}{c} V_T \\ \hdashline V_{\mathcal{F}_T} \end{array}\right] \quad \text{and} \quad V_{S\mathcal{F}_S} = \left[\begin{array}{c} V_S \\ \hdashline V_{\mathcal{F}_S} \end{array}\right], \qquad (127)$$

with V_T, $V_{\mathcal{F}_T}$, and V_S, $V_{\mathcal{F}_S}$, collecting the coefficients associated to the bases of the elements T, S, and their linked faces, correspondingly.

Expressing the functions in the discrete formulation (122) as a linear combination of its respective basis functions, we obtain the following problem: Find $(U_{\mathcal{TF}}(1), U_{\mathcal{TF}}(2), \alpha, \xi) \in \mathbb{R}^{N_{\mathcal{T}}^k(1)} \times \mathbb{R}^{N_{\mathcal{T}}^k(2)} \times \mathbb{R} \times \mathbb{R}^{N_{\mathcal{F}}^k}$ such that

$$\begin{aligned}
&\sum_{T\in\mathcal{T}_{1,h}} V_{T\mathcal{F}_T}^t A(T) U_{T\mathcal{F}_T} + \alpha\left(\sum_{T\in\mathcal{T}_{1,h}} V_T^t M_T + \sum_{S\in\mathcal{T}_{2,h}} V_S^t M_S\right) + \sum_{F\in\Gamma_{1,h}} [V_F^2 - V_F^1]^t M_{FF}\xi_F \\
&+ \sum_{S\in\mathcal{T}_{2,h}} V_{S\mathcal{F}_S}^t A(S) U_{S\mathcal{F}_S} + \beta\left(\sum_{T\in\mathcal{T}_{1,h}} M_T^t U_T + \sum_{S\in\mathcal{T}_{2,h}} M_S^t U_S\right) + \sum_{F\in\Gamma_{1,h}} \lambda_F^t M_{FF}[U_F^2 - U_F^1] \\
&= \sum_{T\in\mathcal{T}_{1,h}} V_{T\mathcal{F}_T}^t F(T) + \sum_{S\in\mathcal{T}_{2,h}} V_{S\mathcal{F}_S}^t F(S) - \sum_{F\in\Gamma_{1,h}} \lambda_F^t G_F, \qquad (128)
\end{aligned}$$

for all $(V_{\mathcal{TF}}(1), V_{\mathcal{TF}}(2), \beta, \lambda) \in \mathbb{R}^{N_{\mathcal{T}}^k(1)} \times \mathbb{R}^{N_{\mathcal{T}}^k(2)} \times \mathbb{R} \times \mathbb{R}^{N_{\mathcal{F}}^k}$, where $N_{\mathcal{F}}^k := \mathrm{card}(\Gamma_{1,h}) \times N_{d-1}^k$. Here, the local matrices $A(T)$, $A(S)$ represent the local bilinear forms a_T and a_S respectively. The local vector $F(T)$, $F(S)$ represent the linear functionals F_T^1 and F_S^2 in (123) respectively, and G_F represents the linear functional $(\lambda_F, g)_F$ in (124). The vector $M_T \in \mathbb{R}^{N_d^k}$ collects the average of the local base functions on T and for each $F \in \Gamma_{1,h}$, we define $M_{FF} := [(\psi_i, \psi_j)]_{1\le i,j\le N_{d-1}^k}$, where ψ_i represent the face polynomials on F.

In order to eliminate the element-based DOFS (by static condensation), we divide in blocks the following matrices

$$A(T) = \left[\begin{array}{c|c} A_{TT} & A_{T\mathcal{F}_T} \\ \hline A_{T\mathcal{F}_T}^t & A_{\mathcal{F}_T\mathcal{F}_T} \end{array}\right], \qquad F(T) = \left[\begin{array}{c} F_T \\ \hline F_{\mathcal{F}_T} \end{array}\right], \qquad (129)$$

$$A(S) = \left[\begin{array}{c|c} A_{SS} & A_{S\mathcal{F}_S} \\ \hline A_{S\mathcal{F}_S}^t & A_{\mathcal{F}_S\mathcal{F}_S} \end{array}\right], \qquad F(S) = \left[\begin{array}{c} F_S \\ \hline F_{\mathcal{F}_S} \end{array}\right], \qquad (130)$$

Arranging the equation (128) in a matrix form, where we collect/assemble the submatrices A_{TT}, $A_{T\mathcal{F}_T}$, $A_{\mathcal{F}_T\mathcal{F}_T}$, F_T, $F_{\mathcal{F}_T}$ in $A_{\mathcal{TT}}(1)$, $A_{\mathcal{TF}}(1)$, $A_{\mathcal{FF}}(1)$, $F_{\mathcal{T}}(1)$, $F_{\mathcal{F}}(1)$, and A_{SS}, $A_{S\mathcal{F}_S}$, $A_{\mathcal{F}_S\mathcal{F}_S}$, F_S, $F_{\mathcal{F}_S}$ in $A_{\mathcal{TT}}(2)$, $A_{\mathcal{TF}}(2)$, $A_{\mathcal{FF}}(2)$, $F_{\mathcal{T}}(2)$, $F_{\mathcal{F}}(2)$, respectively, we obtain the linear global system corresponding to the discrete problem (122):

$$\left[\begin{array}{cc|cc|cc} A_{\mathcal{TT}}(1) & 0 & A_{\mathcal{TF}}(1) & 0 & M_{\mathcal{T}}(1) & 0 \\ \hline 0 & A_{\mathcal{TT}}(2) & 0 & A_{\mathcal{TF}}(2) & M_{\mathcal{T}}(2) & 0 \\ \hline A_{\mathcal{TF}}^t(1) & 0 & A_{\mathcal{FF}}(1) & 0 & 0 & -M_{\Gamma\Gamma} \\ \hline 0 & A_{\mathcal{TF}}^t(2) & 0 & A_{\mathcal{FF}}(2) & 0 & M_{\Gamma\Gamma} \\ \hline M_{\mathcal{T}}^t(1) & M_{\mathcal{T}}^t(2) & 0 & 0 & 0 & 0 \\ \hline 0 & 0 & -M_{\Gamma\Gamma}^t & M_{\Gamma\Gamma}^t & 0 & 0 \end{array}\right] \left[\begin{array}{c} U_{\mathcal{T}}(1) \\ \hline U_{\mathcal{T}}(2) \\ \hline U_{\mathcal{F}}(1) \\ \hline U_{\mathcal{F}}(2) \\ \hline \alpha \\ \hline \xi_\Gamma \end{array}\right] = \left[\begin{array}{c} F_{\mathcal{T}}(1) \\ \hline F_{\mathcal{T}}(2) \\ \hline F_{\mathcal{F}}(1) \\ \hline F_{\mathcal{F}}(2) \\ \hline 0 \\ \hline -G_\Gamma \end{array}\right], \qquad (131)$$

where $M_{\mathcal{T}}(1)$, $M_{\mathcal{T}}(2)$, G_Γ and $M_{\Gamma\Gamma}$ collect the vectors M_T, M_S, G_F and the matrices M_{FF}, respectively. $U_{\mathcal{T}}(1)$, $U_{\mathcal{T}}(2)$, $U_{\mathcal{F}}(1)$, $U_{\mathcal{F}}(2)$ and ξ_Γ assemble the coefficients of the local unknowns U_T, U_S, $U_{\mathcal{F}_T}$, $U_{\mathcal{F}_S}$ and ξ_F, respectively. Now, we compact the system (131)*, as*

$$\left[\begin{array}{c|c:c:c} A_{\mathcal{T}\mathcal{T}} & A_{\mathcal{T}\mathcal{F}} & M_{\mathcal{T}} & 0 \\ \hline A^t_{\mathcal{T}\mathcal{F}} & A_{\mathcal{F}\mathcal{F}} & 0 & M_{\mathcal{F}\Gamma} \\ \hdashline M^t_{\mathcal{T}} & 0 & 0 & 0 \\ \hdashline 0 & M^t_{\mathcal{F}\Gamma} & 0 & 0 \end{array}\right] \left[\begin{array}{c} U_{\mathcal{T}} \\ \hdashline U_{\mathcal{F}} \\ \hdashline \alpha \\ \hdashline \xi_\Gamma \end{array}\right] = \left[\begin{array}{c} F_{\mathcal{T}} \\ \hdashline F_{\mathcal{F}} \\ \hdashline 0 \\ \hdashline -G_\Gamma \end{array}\right]. \tag{132}$$

Then, computing the Schur complement of the block $A_{\mathcal{T}\mathcal{T}}$ of the system (132), we deduce another linear system, on the skeleton, as follows:

$$\left[\begin{array}{c:c:c} A_{\mathcal{F}\mathcal{F}} - A^t_{\mathcal{T}\mathcal{F}}A^{-1}_{\mathcal{T}\mathcal{T}}A_{\mathcal{T}\mathcal{F}} & -A^t_{\mathcal{T}\mathcal{F}}A^{-1}_{\mathcal{T}\mathcal{T}}M_{\mathcal{T}} & M_{\mathcal{F}\Gamma} \\ \hdashline -M^t_{\mathcal{T}}A^{-1}_{\mathcal{T}\mathcal{T}}A_{\mathcal{T}\mathcal{F}} & -M^t_{\mathcal{T}}A^{-1}_{\mathcal{T}\mathcal{T}}M_{\mathcal{T}} & 0 \\ \hdashline M^t_{\mathcal{F}\Gamma} & 0 & 0 \end{array}\right] \left[\begin{array}{c} U_{\mathcal{F}} \\ \hdashline \alpha \\ \hdashline \xi_\Gamma \end{array}\right] = \left[\begin{array}{c} F_{\mathcal{F}} - A^t_{\mathcal{T}\mathcal{F}}A^{-1}_{\mathcal{T}\mathcal{T}}F_{\mathcal{T}} \\ \hdashline -M^t_{\mathcal{T}}A^{-1}_{\mathcal{T}\mathcal{T}}F_{\mathcal{T}} \\ \hdashline -G_\Gamma \end{array}\right], \tag{133}$$

Instead of solving the global system (132), whose size is

$$\sum_{i=1}^{2}\left[\mathrm{card}(\mathcal{T}_{i,h}) \times N^k_d + \mathrm{card}(\mathcal{F}_{i,h}) \times N^k_{d-1}\right] + N^k_{\mathcal{F}} + 1, \tag{134}$$

we solve the reduced system (133), whose DOF corresponds to the skeleton of the mesh, then its size is

$$\mathrm{card}(\mathcal{F}_{1,h}) \times N^k_{d-1} + \mathrm{card}(\mathcal{F}_{2,h}) \times N^k_{d-1} + N^k_{\mathcal{F}} + 1\,. \tag{135}$$

Therefore, we obtain $U_{\mathcal{F}}$, the vector of coefficients of variables polynomials faces and ξ_Γ, the vector of coefficients of the auxiliary variable transmission ξ. We remark that the faces on transmission boundary are counted three times, two times for the skeleton mesh of each subdomain, and one more for the transmission condition.

Denoting by $\underset{T\in\mathcal{T}_h}{\longleftarrow}$ the usual assembling procedure based on a global DOF map, we can assemble all matrix products appearing in (133) directly from their local counterparts for each T and S of their subdomains, as

$$F_{\mathcal{F}} - A^t_{\mathcal{T}\mathcal{F}}A^{-1}_{\mathcal{T}\mathcal{T}}F_{\mathcal{T}} \underset{T\in\mathcal{T}_h}{\longleftarrow} F_{\mathcal{F}_T} - A^t_{T\mathcal{F}_T}A^{-1}_{TT}F_T \quad , \quad A^t_{\mathcal{T}\mathcal{F}}A^{-1}_{\mathcal{T}\mathcal{T}}M_{\mathcal{T}} \underset{T\in\mathcal{T}_h}{\longleftarrow} A^t_{T\mathcal{F}_T}A^{-1}_{TT}M_T,$$
$$A_{\mathcal{F}\mathcal{F}} - A^t_{\mathcal{T}\mathcal{F}}A^{-1}_{\mathcal{T}\mathcal{T}}A_{\mathcal{T}\mathcal{F}} \underset{T\in\mathcal{T}_h}{\longleftarrow} A_{\mathcal{F}_T\mathcal{F}_T} - A^t_{T\mathcal{F}_T}A^{-1}_{TT}A_{T\mathcal{F}_T},$$

$$M^t_{\mathcal{T}}A^{-1}_{\mathcal{T}\mathcal{T}}M_{\mathcal{T}} = \sum_{T\in\mathcal{T}_{1,h}} M^t_T A^{-1}_{TT}M_T + \sum_{S\in\mathcal{T}_{2,h}} M^t_S A^{-1}_{SS}M_S,$$
$$\text{and} \quad M^t_{\mathcal{T}}A^{-1}_{\mathcal{T}\mathcal{T}}B_{\mathcal{T}} = \sum_{T\in\mathcal{T}_{1,h}} M^t_T A^{-1}_{TT}B_T + \sum_{S\in\mathcal{T}_{2,h}} M^t_S A^{-1}_{SS}B_S$$

Besides, from the static condensation (Schur complement), we can recover the global vector $U_{\mathcal{T}}$, obtaining

$$U_{\mathcal{T}} = A^{-1}_{\mathcal{T}\mathcal{T}}\left[F_{\mathcal{T}} - \widehat{A}_{\mathcal{T}\mathcal{F}}\widehat{U}_{\mathcal{F}}\right]. \tag{136}$$

Letting $\alpha = 0$ in $\widehat{U}_{\mathcal{F}}$, yields

$$U_{\mathcal{T}} = A_{\mathcal{T}\mathcal{T}}^{-1}\Big(F_{\mathcal{T}} - A_{\mathcal{T}\mathcal{F}}U_{\mathcal{F}}\Big), \tag{137}$$

After a post-processing procedure, we obtain the local vectors U_T and U_S in each subdomain, as follows

$$U_T = A_{TT}^{-1}\Big(F_T - A_{T\mathcal{F}_T}U_{\mathcal{F}_T}\Big), \quad U_S = A_{SS}^{-1}\Big(F_S - A_{S\mathcal{F}_S}U_{\mathcal{F}_S}\Big). \tag{138}$$

7 Numerical results

In this section we present a comprehensive set of numerical tests to assess the theoretical results we have obtained. In all cases, we consider a family of uniform simplicial meshes, piecewise polynomials of degree at most k, with $k \in \{0, 1, 2, 3, 4\}$ to approximate the exact solution. The experimental order of convergence (r), is computed as

$$r = \log(e_{\mathcal{T}}/e_{\widetilde{\mathcal{T}}})/\log(h_{\mathcal{T}}/h_{\widetilde{\mathcal{T}}}),$$

where $e_{\mathcal{T}}$ and $e_{\widetilde{\mathcal{T}}}$ are the errors associated to the corresponding variable considering two consecutive meshes $\mathcal{T}$ and $\widetilde{\mathcal{T}}$, respectively.

The numerical tests have been run considering a modification of the code used in [19], which is based, in turn, on the one developed by Di Pietro in [30, 32]. The implementation of local gradient reconstruction operator (18)*, L^2-orthogonal projectors π_T^k and π_F^k, are based on the linear algebra facilities (robust Cholesky factorization) provided by the Eigen3 library [40]. The reduced system on the skeleton (133) is solved by using SuperLU [25] through the PETSc 3.4 interface [6].*

From here on, given (u_1, u_2, ξ) and $(\underline{\mathbf{u}}_{1,h}, \underline{\mathbf{u}}_{2,h}, \xi_h)$ the unique solutions of (8) *and* (38)*, respectively, we introduce the potential error as*

- *Energy norm of the potential error:* $||(\widehat{\underline{\mathbf{u}}}_{1,h}, \widehat{\underline{\mathbf{u}}}_{2,h}) - (\underline{\mathbf{u}}_{1,h}, \underline{\mathbf{u}}_{2,h})||_{a,h}$,
- *L^2-norm of the flux error:* $\big(||\nabla u_1 - \nabla_h p_h^{k+1}\underline{\mathbf{u}}_{1,h}||_{0,\Omega_1}^2 + ||\nabla u_2 - \nabla_h p_h^{k+1}\underline{\mathbf{u}}_{2,h}||_{0,\Omega_2}^2\big)^{1/2}$,
- *Discrete norm of the projection of the trace error:* $||\widehat{\xi_h} - \xi_h||_{\Gamma_{1,h}}$,
- *L^2- norm of the projection of the trace error:* $||\widehat{\xi_h} - \xi_h||_{0,\Gamma_1}$,
- *L^2-norm of the potential error:*

$$\Big(||u_{1,h} - \pi_{\mathcal{T}_{1,h}}^k u_1||_{0,\Omega_1}^2 + ||u_{2,h} - \pi_{\mathcal{T}_{2,h}}^k u_2||_{0,\Omega_2}^2||\Big)^{1/2},$$

- *L^2-norm of the reconstructive potential error:*

$$\big(||u_1 - p_h^{k+1}\underline{\mathbf{u}}_{1,h}||_{0,\Omega_1}^2 + ||u_2 - p_h^{k+1}\underline{\mathbf{u}}_{2,h}||_{0,\Omega_2}^2\big)^{1/2},$$

where $\widehat{\underline{\mathbf{u}}}_{i,h} := \underline{\mathbf{I}}_{\mathcal{T}_{i,h}}^k u_i \in \underline{\mathbf{U}}_{\mathcal{T}_{i,h}}^k$, for $i \in \{1, 2\}$.

7.1 Example 1: Regular test case

We solve a transmission problem with subdomains $\Omega_1 := (0,1)^2$ *and* $\Omega_2 := (-1,2)^2 \setminus \overline{\Omega}_1$ *(see Figure 3), such that the exact solution is given by*

$$u_1(x,y) = (\mathrm{e}^x - 1)(x-1)(\mathrm{e}^y - 1)(y-1) - \mathrm{e}^2 + 5\mathrm{e} - \frac{25}{4} \quad , \quad u_2(x,y) = \sin(\pi x)\sin(\pi y). \tag{139}$$

On the transmission boundary, we have nonhomogeneous jump of trace of their potentials, and also nonhomogeneous jump of normal trace of their fluxes. Table 1 shows the histories of convergence of the energy norm of the potential error and the flux error vs meshsize, noticing that they converge at the optimal orders $k+1$*, when the exact solution is approximated by piecewise polynomials of degree at most* $k \in \{0, ..., 4\}$*. On the other hand, in Table 2, we show the corresponding history of convergence of the auxiliary unknown* ξ*, considering the discrete trace* (29) *and the standard* L^2-*norms. We observe convergence in both two cases, for* $k \in \{0, ..., 4\}$*, with orders* $k+3/2$ *and* $k+1$*, respectively. In Table 3, we include the histories of convergence in* L^2-*norm of the potential and reconstructive potential errors, which behave as* $\mathcal{O}(h^{k+2})$*. We remark that all these results are in agreement with Theorems 5.1, 5.2, and 5.3, as well as Remark 5.1, considering* $\delta_1 = \delta_2 = 1$*, and they can also be observed in Figures 4, 5 and 6. In the case of* ξ*, we notice that rate of convergence in* $||\cdot||_{\Gamma_{1,h}}$ *is* $1/2$ *faster than the predicted by Theorem 5.1.*

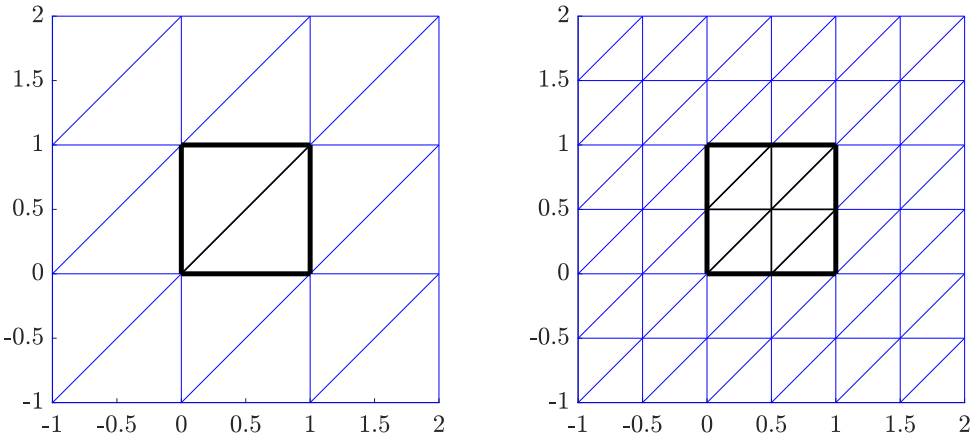

Figure 3: First two simplicial meshes for Example 1.

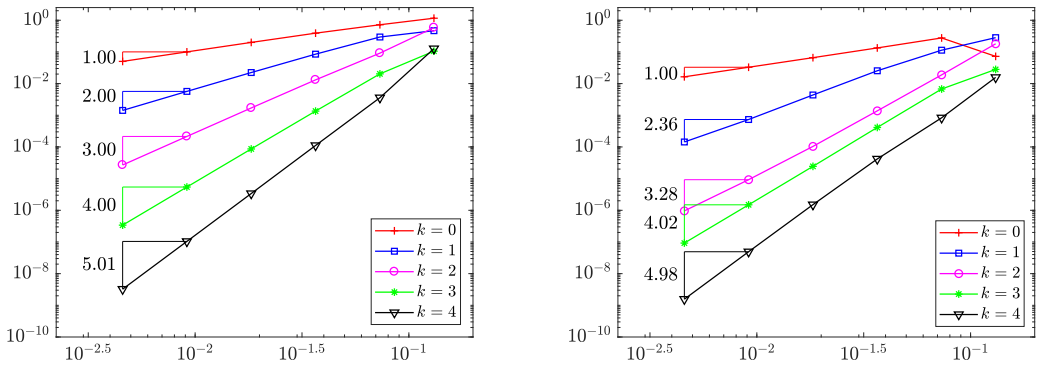

(a) Energy norm of the potential error vs. h (b) L^2-norm of the flux error vs. h

Figure 4: Rates of convergence of the (a) energy norm of the potential error, and (b) flux error (Example 1)

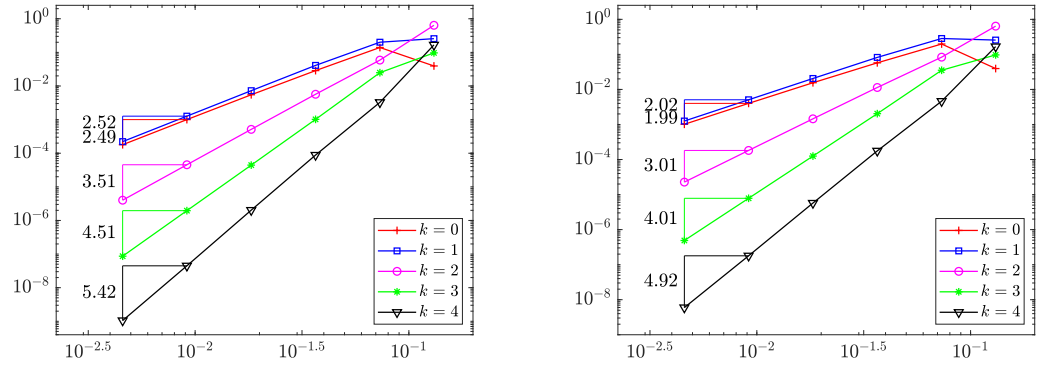

(a) $||\widehat{\xi}_h - \xi_h||_{\Gamma_{1,h}}$ vs. h (b) $||\widehat{\xi}_h - \xi_h||_{0,\Gamma_1}$ vs. h

Figure 5: Rates of convergence of the Lagrange multiplier considering the (a) Discrete trace norm $||\cdot||_{\Gamma_{1,h}}$, and (b) Standard L^2-norm (Example 1)

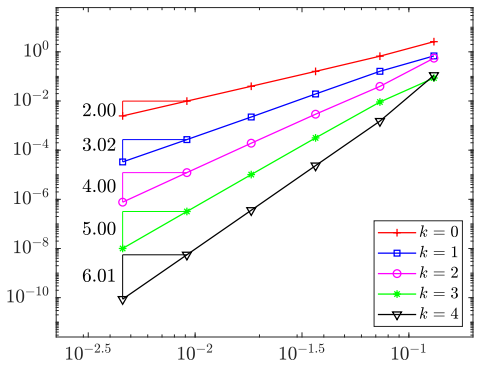

(a) L^2-norm of the potential error vs. h

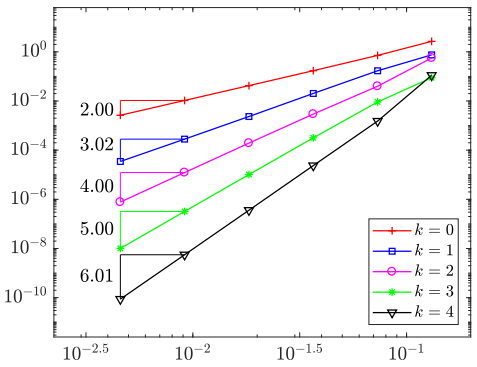

(b) L^2-norm of the reconstructive potential error vs. h

Figure 6: Rates of convergence of the L^2-norm of the (a) potential error, and (b) reconstructive potential error (Example 1).

Table 1: Histories of convergence of the energy norm of the potential error and L^2-norm of the flux error, considering $k \in \{0, 1, 2, 3, 4\}$ (Example 1)

Energy norm of the potential error										
	$k = 0$		$k = 1$		$k = 2$		$k = 3$		$k = 4$	
h	error	rate	error	rate	error	rate	error	rate	error	rate
1.31e-01	1.16e+00		4.68e-01		5.85e-01		1.05e-01		1.27e-01	
7.32e-02	7.21e-01	0.817	2.96e-01	0.790	9.15e-02	3.187	2.03e-02	2.835	3.59e-03	6.127
3.66e-02	3.91e-01	0.883	8.50e-02	1.798	1.31e-02	2.803	1.36e-03	3.903	1.11e-04	5.010
1.83e-02	2.00e-01	0.970	2.23e-02	1.928	1.70e-03	2.946	8.65e-05	3.970	3.38e-06	5.041
9.15e-03	1.00e-01	0.993	5.67e-03	1.978	2.15e-04	2.985	5.43e-06	3.993	1.04e-07	5.021
4.58e-03	5.02e-02	1.000	1.42e-03	1.997	2.69e-05	3.001	3.40e-07	4.005	3.24e-09	5.015
L^2-norm of the flux error										
	$k = 0$		$k = 1$		$k = 2$		$k = 3$		$k = 4$	
h	error	rate	error	rate	error	rate	error	rate	error	rate
1.31e-01	7.23e-02		2.82e-01		1.81e-01		2.80e-02		1.57e-02	
7.32e-02	2.76e-01	-2.302	1.13e-01	1.567	1.89e-02	3.883	6.74e-03	2.448	8.31e-04	5.047
3.66e-02	1.34e-01	1.047	2.54e-02	2.158	1.38e-03	3.774	4.13e-04	4.030	4.18e-05	4.314
1.83e-02	6.59e-02	1.021	4.37e-03	2.540	1.04e-04	3.727	2.44e-05	4.080	1.51e-06	4.795
9.15e-03	3.28e-02	1.006	7.35e-04	2.572	9.25e-06	3.492	1.49e-06	4.034	4.92e-08	4.937
4.58e-03	1.64e-02	1.003	1.44e-04	2.360	9.57e-07	3.278	9.23e-08	4.019	1.56e-09	4.984

Table 2: Histories of convergence of the L^2-projection of $\xi - \xi_h$ in $||\cdot||_{\Gamma_{1,h}}$ and $||\cdot||_{0,\Gamma_1}$ norms, for $k \in \{0,1,2,3,4\}$ (Example 1)

$\|\widehat{\xi_h} - \xi_h\|_{\Gamma_{1,h}}$										
	$k=0$		$k=1$		$k=2$		$k=3$		$k=4$	
h	error	rate	error	rate	error	rate	error	rate	error	rate
1.31e-01	3.94e-02		2.56e-01		6.39e-01		9.66e-02		1.67e-01	
7.32e-02	1.40e-01	-2.174	2.01e-01	0.419	5.89e-02	4.096	2.49e-02	2.329	3.26e-03	6.760
3.66e-02	2.87e-02	2.285	4.10e-02	2.291	5.68e-03	3.376	1.02e-03	4.613	8.82e-05	5.210
1.83e-02	5.48e-03	2.388	7.26e-03	2.499	5.13e-04	3.470	4.43e-05	4.523	2.02e-06	5.445
9.15e-03	1.00e-03	2.454	1.27e-03	2.518	4.54e-05	3.497	1.96e-06	4.501	4.47e-08	5.501
4.58e-03	1.79e-04	2.487	2.22e-04	2.519	4.01e-06	3.507	8.65e-08	4.506	1.05e-09	5.417
$\|\widehat{\xi_h} - \xi_h\|_{0,\Gamma_1}$										
	$k=0$		$k=1$		$k=2$		$k=3$		$k=4$	
h	error	rate	error	rate	error	rate	error	rate	error	rate
1.31e-01	3.94e-02		2.56e-01		6.39e-01		9.66e-02		1.67e-01	
7.32e-02	1.98e-01	-2.769	2.84e-01	-0.177	8.34e-02	3.500	3.52e-02	1.734	4.62e-03	6.164
3.66e-02	5.74e-02	1.785	8.20e-02	1.791	1.14e-02	2.876	2.04e-03	4.113	1.76e-04	4.710
1.83e-02	1.55e-02	1.888	2.05e-02	1.999	1.45e-03	2.970	1.25e-04	4.023	5.73e-06	4.945
9.15e-03	4.00e-03	1.954	5.07e-03	2.018	1.82e-04	2.997	7.82e-06	4.001	1.79e-07	5.001
4.58e-03	1.01e-03	1.986	1.25e-03	2.019	2.27e-05	3.006	4.89e-07	4.005	5.95e-09	4.916

Table 3: Histories of convergence of L^2-norm of the potential and reconstructive potential errors, considering $k \in \{0,1,2,3,4\}$ (Example 1)

L^2-norm of the potential error										
	$k=0$		$k=1$		$k=2$		$k=3$		$k=4$	
h	error	rate	error	rate	error	rate	error	rate	error	rate
1.31e-01	2.59e+00		6.82e-01		5.52e-01		8.61e-02		1.11e-01	
7.32e-02	6.65e-01	2.338	1.61e-01	2.477	3.93e-02	4.542	9.08e-03	3.864	1.52e-03	7.369
3.66e-02	1.60e-01	2.053	1.93e-02	3.064	2.90e-03	3.759	3.16e-04	4.848	2.35e-05	6.016
1.83e-02	3.97e-02	2.013	2.23e-03	3.111	1.92e-04	3.918	1.02e-05	4.956	3.59e-07	6.032
9.15e-03	9.90e-03	2.003	2.69e-04	3.054	1.22e-05	3.976	3.20e-07	4.988	5.54e-09	6.017
4.58e-03	2.47e-03	2.004	3.32e-05	3.022	7.66e-07	3.999	1.00e-08	5.004	8.68e-11	6.005
L^2-norm of the reconstructive potential error										
	$k=0$		$k=1$		$k=2$		$k=3$		$k=4$	
h	error	rate	error	rate	error	rate	error	rate	error	rate
1.31e-01	2.66e+00		7.52e-01		5.64e-01		8.86e-02		1.11e-01	
7.32e-02	7.15e-01	2.259	1.70e-01	2.559	3.99e-02	4.551	9.12e-03	3.906	1.52e-03	7.369
3.66e-02	1.71e-01	2.067	2.03e-02	3.065	2.93e-03	3.768	3.17e-04	4.849	2.36e-05	6.015
1.83e-02	4.22e-02	2.017	2.34e-03	3.116	1.93e-04	3.920	1.02e-05	4.957	3.60e-07	6.031
9.15e-03	1.05e-02	2.004	2.81e-04	3.057	1.23e-05	3.977	3.21e-07	4.988	5.57e-09	6.016
4.58e-03	2.63e-03	2.004	3.47e-05	3.023	7.72e-07	4.000	1.01e-08	5.005	8.71e-11	6.006

7.2 Example 2: Another regular test case

We solve (1) *with subdomains* $\Omega_1 := (1,2)^2$ *and* $\Omega_2 := (0,3)^2 \setminus \overline{\Omega}_1$, *and the data are such that the exact solution is*

$$u_1(x,y) = \sin(\pi x)\sin(\pi y) - \frac{4}{\pi^2} \quad , \quad u_2(x,y) = \cos(\pi x)\cos(\pi y). \tag{140}$$

We notice that in this case, g_1 *and* g_2 *are nonhomogeneous on* Γ_1. *Table 4 shows the history of convergence of the energy norm of the potential error and the flux error, when approximating the exact solution with piecewise polynomials of degree at most* $k \in \{0,1,2,3,4\}$. *In both two cases, we observe that the rate of convergence is* $k+2$, *as predicted by Theorem 5.1, with* δ_1 *and* δ_2 *close to 1. Concerning the auxiliary transmission unknown* ξ, *in Table 5 we report the corresponding histories of convergence of the projection of* $\xi - \xi_h$ *in a weighted* L^2- *norm as well as the usual* L^2-*norm, for comparison. We notice that the rate of convergence of* ξ *in the weighted norm is close to* $k+3/2$ *(which is* $1/2$ *faster than the predicted by Theorem 5.1). Also, we observe an order of convergence* $k+1$, *for* ξ *in the usual* L^2*-norm, which is in agreement with Remark 5.1. The histories of convergence of* L^2-*norm of the potential and the reconstructive potential errors, are provided in Table 6. We notice that the rates of convergence for these errors are* $k+2$, *in agreement with Theorems 5.2 and 5.3. Figure 7 shows the first two initial meshes of the domain, considered in this numerical simulation, while Figures 8, 9 and 10 resume the information given in Tables 4,5 and 6, respectively.*

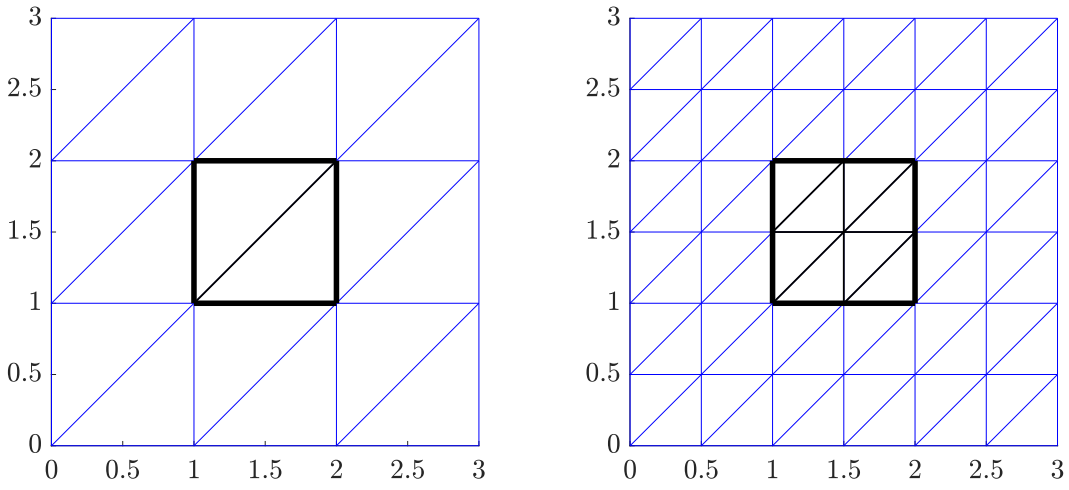

Figure 7: First two simplicial meshes for Example 2

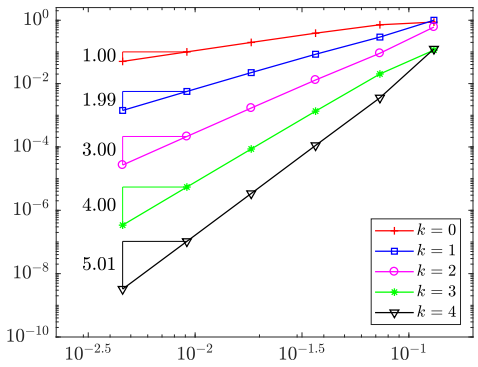

(a) Energy norm of the potential error vs. h

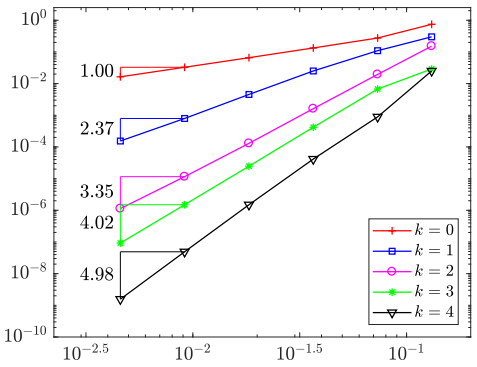

(b) L^2-norm of the flux error vs. h

Figure 8: Rates of convergence of the (a) energy norm of the potential error, and (b) flux error (Example 2)

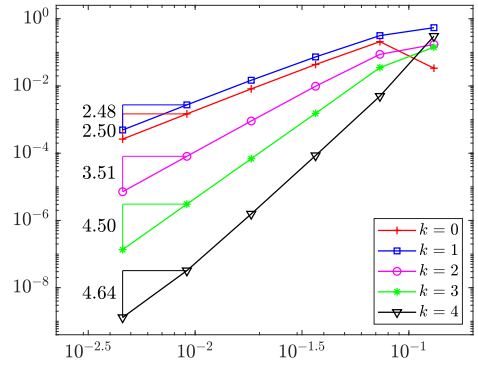

(a) $||\widehat{\xi}_h - \xi_h||_{\Gamma_{1,h}}$ vs. h

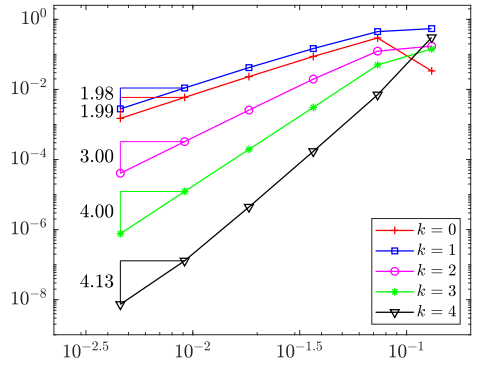

(b) $||\widehat{\xi}_h - \xi_h||_{0,\Gamma_1}$ vs. h

Figure 9: Rates of convergence of the Lagrange multiplier considering the (a) Discrete trace norm $||\cdot||_{\Gamma_{1,h}}$, and (b) Standard L^2-norm (Example 2)

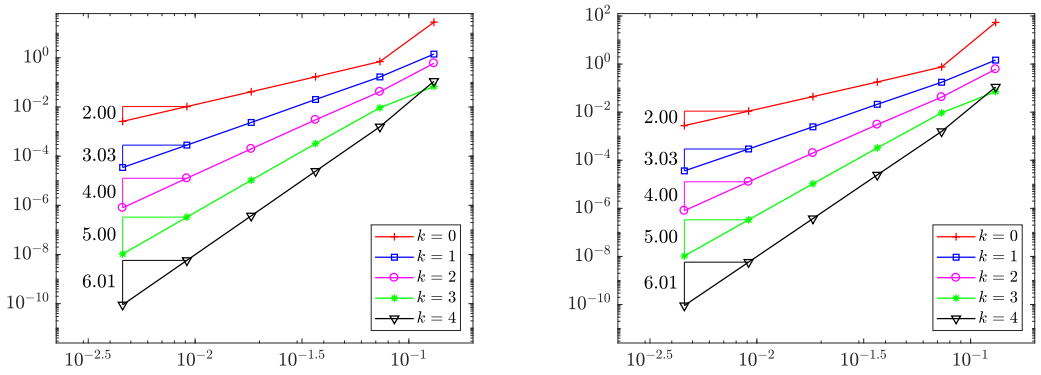

(a) L^2-norm of the potential error vs. h

(b) L^2-norm of the reconstructive potential error vs. h

Figure 10: Rates of convergence of the L^2-norm of the (a) potential error, and (b) reconstructive potential error (Example 2)

Table 4: Histories of convergence of the energy norm of the potential error and L^2-norm of the flux error, considering $k \in \{0, 1, 2, 3, 4\}$ (Example 2)

Energy norm of the potential error										
	$k = 0$		$k = 1$		$k = 2$		$k = 3$		$k = 4$	
h	error	rate	error	rate	error	rate	error	rate	error	rate
1.31e-01	8.74e-01		1.00e+00		6.11e-01		1.14e-01		1.24e-01	
7.32e-02	7.20e-01	0.334	2.94e-01	2.104	9.07e-02	3.276	2.01e-02	2.981	3.56e-03	6.102
3.66e-02	3.91e-01	0.882	8.44e-02	1.801	1.30e-02	2.803	1.35e-03	3.899	1.12e-04	4.996
1.83e-02	1.99e-01	0.970	2.22e-02	1.926	1.69e-03	2.941	8.63e-05	3.967	3.39e-06	5.039
9.15e-03	1.00e-01	0.993	5.65e-03	1.975	2.14e-04	2.982	5.43e-06	3.991	1.04e-07	5.023
4.58e-03	5.02e-02	1.000	1.42e-03	1.995	2.69e-05	2.999	3.40e-07	4.004	3.26e-09	5.010
L^2-norm of the flux error										
	$k = 0$		$k = 1$		$k = 2$		$k = 3$		$k = 4$	
h	error	rate	error	rate	error	rate	error	rate	error	rate
1.31e-01	7.45e-01		3.00e-01		1.53e-01		2.90e-02		2.51e-02	
7.32e-02	2.75e-01	1.716	1.09e-01	1.732	1.95e-02	3.532	6.73e-03	2.507	8.89e-04	5.738
3.66e-02	1.33e-01	1.042	2.50e-02	2.126	1.62e-03	3.594	4.19e-04	4.007	4.14e-05	4.424
1.83e-02	6.58e-02	1.019	4.54e-03	2.463	1.30e-04	3.637	2.47e-05	4.085	1.50e-06	4.792
9.15e-03	3.28e-02	1.006	7.92e-04	2.519	1.15e-05	3.496	1.50e-06	4.041	4.90e-08	4.931
4.58e-03	1.64e-02	1.003	1.54e-04	2.367	1.13e-06	3.354	9.26e-08	4.023	1.56e-09	4.979

Table 5: Histories of convergence of the L^2-projection of $\xi - \xi_h$ in $||\cdot||_{\Gamma_{1,h}}$ and $||\cdot||_{0,\Gamma_1}$ norms, for $k \in \{0,1,2,3,4\}$ (Example 2)

$\|\widehat{\xi_h} - \xi_h\|_{\Gamma_{1,h}}$										
	$k=0$		$k=1$		$k=2$		$k=3$		$k=4$	
h	error	rate	error	rate	error	rate	error	rate	error	rate
1.31e-01	3.38e-02		5.43e-01		1.72e-01		1.43e-01		3.04e-01	
7.32e-02	2.08e-01	-3.127	3.16e-01	0.933	8.74e-02	1.164	3.53e-02	2.399	4.99e-03	7.061
3.66e-02	4.36e-02	2.258	7.33e-02	2.107	9.84e-03	3.151	1.53e-03	4.527	8.52e-05	5.870
1.83e-02	8.21e-03	2.408	1.48e-02	2.306	9.09e-04	3.435	6.87e-05	4.478	1.56e-06	5.772
9.15e-03	1.48e-03	2.471	2.75e-03	2.432	8.09e-05	3.490	3.06e-06	4.490	3.22e-08	5.600
4.58e-03	2.63e-04	2.496	4.92e-04	2.485	7.16e-06	3.505	1.35e-07	4.504	1.30e-09	4.636
$\|\widehat{\xi_h} - \xi_h\|_{0,\Gamma_1}$										
	$k=0$		$k=1$		$k=2$		$k=3$		$k=4$	
h	error	rate	error	rate	error	rate	error	rate	error	rate
1.31e-01	3.38e-02		5.43e-01		1.72e-01		1.43e-01		3.04e-01	
7.32e-02	2.95e-01	-3.722	4.46e-01	0.337	1.24e-01	0.569	4.99e-02	1.803	7.05e-03	6.466
3.66e-02	8.71e-02	1.758	1.47e-01	1.607	1.97e-02	2.651	3.06e-03	4.027	1.70e-04	5.370
1.83e-02	2.32e-02	1.908	4.19e-02	1.806	2.57e-03	2.935	1.94e-04	3.978	4.41e-06	5.272
9.15e-03	5.92e-03	1.971	1.10e-02	1.932	3.24e-04	2.990	1.22e-05	3.990	1.29e-07	5.100
4.58e-03	1.49e-03	1.995	2.78e-03	1.984	4.05e-05	3.004	7.66e-07	4.003	7.36e-09	4.135

Table 6: Histories of convergence of L^2-norm of the potential and reconstructive potential errors, considering $k \in \{0,1,2,3,4\}$ (Example 2)

L^2-norm of the potential error										
	$k=0$		$k=1$		$k=2$		$k=3$		$k=4$	
h	error	rate	error	rate	error	rate	error	rate	error	rate
1.31e-01	2.81e+01		1.41e+00		6.02e-01		6.80e-02		1.11e-01	
7.32e-02	7.05e-01	6.331	1.67e-01	3.671	4.17e-02	4.589	9.33e-03	3.413	1.57e-03	7.321
3.66e-02	1.69e-01	2.062	2.02e-02	3.048	3.01e-03	3.792	3.25e-04	4.844	2.45e-05	6.007
1.83e-02	4.17e-02	2.015	2.35e-03	3.106	1.99e-04	3.921	1.05e-05	4.951	3.74e-07	6.033
9.15e-03	1.04e-02	2.004	2.82e-04	3.059	1.26e-05	3.975	3.32e-07	4.985	5.76e-09	6.018
4.58e-03	2.60e-03	2.004	3.46e-05	3.027	7.94e-07	3.998	1.04e-08	5.003	8.99e-11	6.012
L^2-norm of the reconstructive potential error										
	$k=0$		$k=1$		$k=2$		$k=3$		$k=4$	
h	error	rate	error	rate	error	rate	error	rate	error	rate
1.31e-01	5.39e+01		1.46e+00		6.13e-01		7.14e-02		1.12e-01	
7.32e-02	7.57e-01	7.331	1.75e-01	3.646	4.23e-02	4.595	9.37e-03	3.490	1.58e-03	7.321
3.66e-02	1.80e-01	2.075	2.12e-02	3.050	3.04e-03	3.799	3.26e-04	4.845	2.45e-05	6.006
1.83e-02	4.43e-02	2.019	2.45e-03	3.109	2.00e-04	3.923	1.05e-05	4.952	3.75e-07	6.032
9.15e-03	1.10e-02	2.005	2.94e-04	3.061	1.27e-05	3.975	3.33e-07	4.985	5.79e-09	6.018
4.58e-03	2.76e-03	2.004	3.61e-05	3.029	8.00e-07	3.999	1.04e-08	5.003	9.03e-11	6.012

7.3 Example 3: A numerical singularity

We solve transmission problem (1)*, considering* $\Omega_1 := (-1/2, 1/2)^2$ *and* $\Omega_2 := (-2, 2)^2 \setminus \overline{\Omega}_1$*, with given data such that the exact solution is*

$$u_1(x, y) = \frac{xy}{(x - 0.55)^2 + y^2}, \quad u_2(x, y) = \frac{x - y}{x^2 + y^2}\,. \tag{141}$$

We pointwise that in this case, u_1 *presents a singularity at* $(0.55, 0)$*, which is close to* Γ_1*. For this example, we consider two families of simplicial meshes: one conforming mesh and the other non-conforming, with hanging nodes just on* Γ_1*. We emphasize that the latter is not covered by the current theory, so our aim is to check the robustness of our scheme in this situation.*

7.3.1 Results when solving using conforming meshes

From Tables 7, 8 and 9, we observe that the method converges at the optimal rates of convergence, in agreement with Theorems 5.1, 5.2 and 5.3, and Remark 5.1. Figure 11 shows the first two conforming meshes, considered in this situation, while in Figure 12 we display the rates of convergence of energy norm of the potential error and L^2*-norm of the flux error. Moreover, the rates of convergence of* $\widehat{\xi}_h - \xi_h$ *in* $||\cdot||_{\Gamma_{1,h}}$ *and* $||\cdot||_{0,\Gamma_1}$ *norms, are shown in Figure 13. Information contained in Table 9 is reported in Figure 14.*

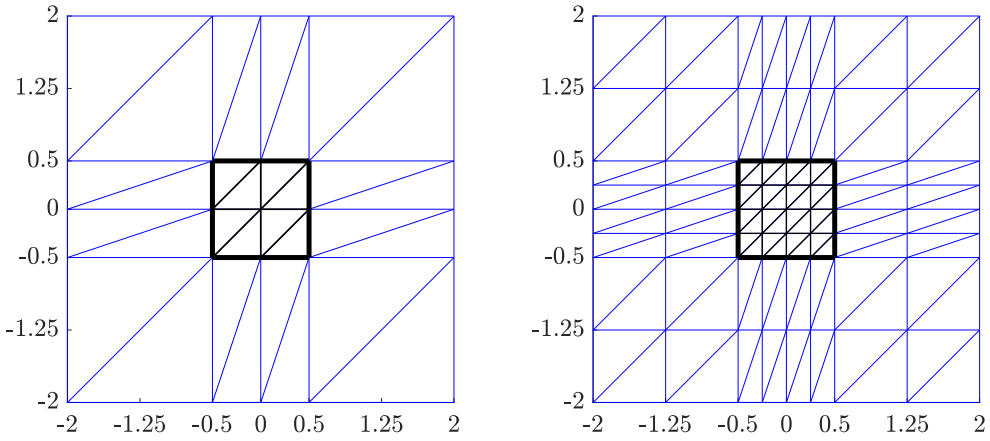

Figure 11: First two conforming meshes for Example 3.

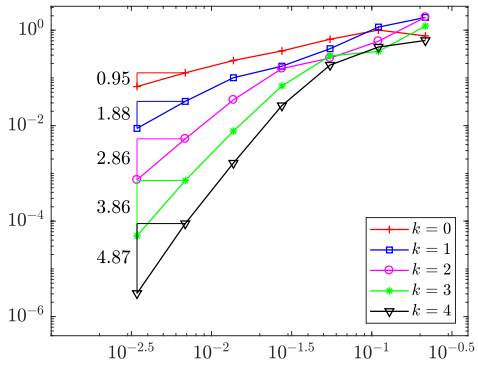

(a) Energy norm of the potential error vs. h

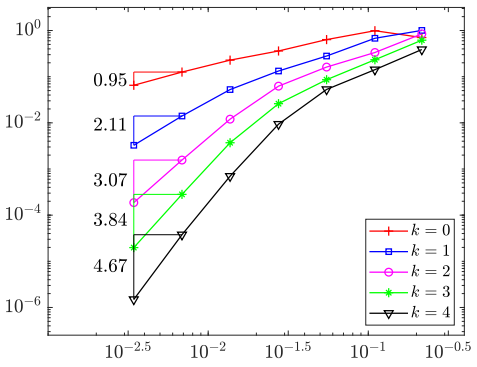

(b) L^2-norm of the flux error vs. h

Figure 12: Rates of convergence of the (a) energy norm of the potential error, and (b) flux error (Example 3, conforming meshes)

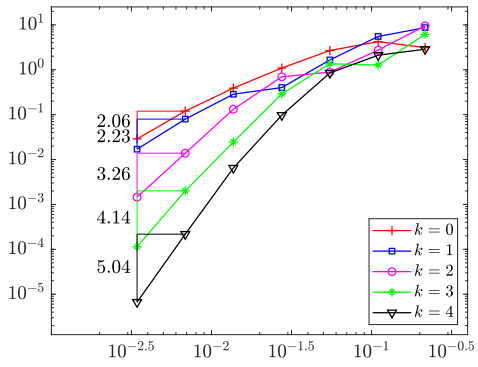

(a) $||\widehat{\xi}_h - \xi_h||_{\Gamma_{1,h}}$ vs. h

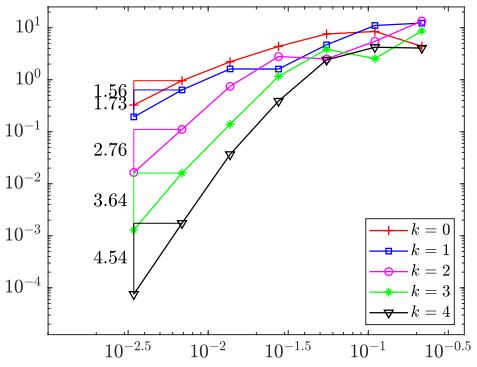

(b) $||\widehat{\xi}_h - \xi_h||_{0,\Gamma_1}$ vs. h

Figure 13: Rates of convergence of the Lagrange multiplier considering the (a) Discrete trace norm $||\cdot||_{\Gamma_{1,h}}$, and (b) Standard L^2-norm (Example 3, conforming meshes)

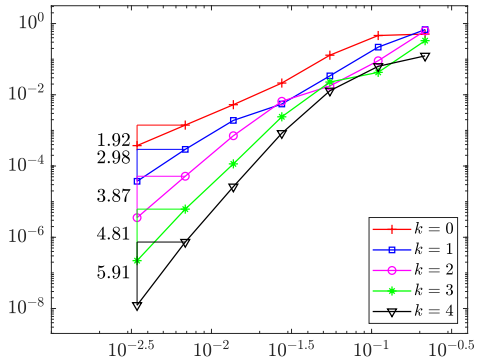

(a) L^2-norm of the potential error vs. h

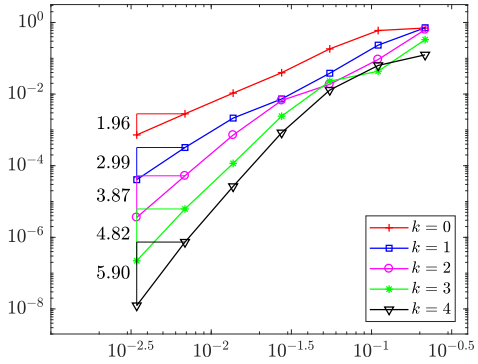

(b) L^2-norm of the reconstructive potential error vs. h

Figure 14: Rates of convergence of the L^2-norm of the (a) potential error, and (b) reconstructive potential error (Example 3, conforming meshes)

Table 7: Histories of convergence of the energy norm of the potential error and L^2-norm of the flux error, considering $k \in \{0, 1, 2, 3, 4\}$ (Example 3, conforming meshes)

Energy norm of the potential error										
	$k=0$		$k=1$		$k=2$		$k=3$		$k=4$	
h	error	rate	error	rate	error	rate	error	rate	error	rate
2.16e-01	7.57e-01		1.85e+00		1.87e+00		1.22e+00		6.09e-01	
1.10e-01	1.01e+00	-0.419	1.16e+00	0.689	5.87e-01	1.718	3.59e-01	1.814	4.43e-01	0.472
5.49e-02	6.46e-01	0.635	4.09e-01	1.500	2.60e-01	1.170	2.89e-01	0.311	1.86e-01	1.249
2.75e-02	3.68e-01	0.816	1.76e-01	1.221	1.57e-01	0.730	6.79e-02	2.095	2.63e-02	2.828
1.37e-02	2.32e-01	0.662	1.01e-01	0.798	3.47e-02	2.166	7.69e-03	3.127	1.65e-03	3.978
6.86e-03	1.28e-01	0.861	3.22e-02	1.650	5.29e-03	2.721	7.10e-04	3.444	8.89e-05	4.220
3.43e-03	6.60e-02	0.952	8.77e-03	1.878	7.32e-04	2.854	4.91e-05	3.854	3.07e-06	4.856
L^2-norm of the flux error										
	$k=0$		$k=1$		$k=2$		$k=3$		$k=4$	
h	error	rate	error	rate	error	rate	error	rate	error	rate
2.16e-01	7.04e-01		1.01e+00		8.45e-01		6.18e-01		3.88e-01	
1.10e-01	9.90e-01	-0.505	6.79e-01	0.582	3.34e-01	1.375	2.33e-01	1.446	1.42e-01	1.490
5.49e-02	6.36e-01	0.637	2.80e-01	1.274	1.62e-01	1.046	8.60e-02	1.433	5.29e-02	1.419
2.75e-02	3.61e-01	0.821	1.33e-01	1.081	6.23e-02	1.378	2.60e-02	1.729	9.36e-03	2.505
1.37e-02	2.28e-01	0.656	5.26e-02	1.328	1.20e-02	2.364	3.71e-03	2.797	6.98e-04	3.725
6.86e-03	1.26e-01	0.859	1.41e-02	1.907	1.56e-03	2.949	2.82e-04	3.724	3.77e-05	4.221
3.43e-03	6.51e-02	0.951	3.27e-03	2.107	1.87e-04	3.062	1.98e-05	3.830	1.49e-06	4.659

Table 8: Histories of convergence of the L^2-projection of $\xi - \xi_h$ in $||\cdot||_{\Gamma_{1,h}}$ and $||\cdot||_{0,\Gamma_1}$ norms, for $k \in \{0,1,2,3,4\}$ (Example 3, conforming meshes)

$\|\widehat{\xi_h} - \xi_h\|_{\Gamma_{1,h}}$										
	$k=0$		$k=1$		$k=2$		$k=3$		$k=4$	
h	error	rate	error	rate	error	rate	error	rate	error	rate
2.16e-01	3.11e+00		8.67e+00		9.49e+00		6.14e+00		2.87e+00	
1.10e-01	4.23e+00	-0.457	5.52e+00	0.668	2.74e+00	1.842	1.27e+00	2.330	2.11e+00	0.457
5.49e-02	2.68e+00	0.658	1.66e+00	1.732	8.86e-01	1.623	1.36e+00	-0.097	8.49e-01	1.309
2.75e-02	1.09e+00	1.299	4.01e-01	2.052	6.98e-01	0.346	2.90e-01	2.239	9.73e-02	3.134
1.37e-02	3.91e-01	1.476	2.85e-01	0.489	1.32e-01	2.391	2.46e-02	3.539	6.48e-03	3.888
6.86e-03	1.20e-01	1.708	7.96e-02	1.845	1.38e-02	3.258	2.01e-03	3.622	2.18e-04	4.906
3.43e-03	2.89e-02	2.054	1.70e-02	2.225	1.45e-03	3.253	1.14e-04	4.135	6.66e-06	5.030
$\|\widehat{\xi_h} - \xi_h\|_{0,\Gamma_1}$										
	$k=0$		$k=1$		$k=2$		$k=3$		$k=4$	
h	error	rate	error	rate	error	rate	error	rate	error	rate
2.16e-01	4.40e+00		1.23e+01		1.34e+01		8.68e+00		4.06e+00	
1.10e-01	8.47e+00	-0.970	1.10e+01	0.154	5.47e+00	1.328	2.55e+00	1.817	4.22e+00	-0.056
5.49e-02	7.58e+00	0.159	4.69e+00	1.234	2.51e+00	1.124	3.85e+00	-0.595	2.40e+00	0.810
2.75e-02	4.37e+00	0.797	1.60e+00	1.551	2.79e+00	-0.156	1.16e+00	1.738	3.89e-01	2.633
1.37e-02	2.21e+00	0.979	1.61e+00	-0.008	7.46e-01	1.894	1.39e-01	3.042	3.67e-02	3.391
6.86e-03	9.59e-01	1.207	6.37e-01	1.344	1.11e-01	2.757	1.61e-02	3.121	1.74e-03	4.405
3.43e-03	3.27e-01	1.554	1.93e-01	1.725	1.64e-02	2.753	1.29e-03	3.635	7.54e-05	4.530

Table 9: Histories of convergence of L^2-norm of the potential and reconstructive potential errors, considering $k \in \{0, 1, 2, 3, 4\}$ (Example 3, conforming meshes)

L^2-norm of the potential error										
	$k=0$		$k=1$		$k=2$		$k=3$		$k=4$	
h	error	rate	error	rate	error	rate	error	rate	error	rate
2.16e-01	5.06e-01		6.75e-01		6.25e-01		3.30e-01		1.24e-01	
1.10e-01	4.61e-01	0.138	2.17e-01	1.679	9.01e-02	2.870	4.26e-02	3.036	6.30e-02	1.001
5.49e-02	1.29e-01	1.830	3.40e-02	2.672	1.76e-02	2.348	2.28e-02	0.900	1.29e-02	2.276
2.75e-02	2.13e-02	2.605	5.51e-03	2.631	6.56e-03	1.430	2.41e-03	3.250	8.32e-04	3.970
1.37e-02	5.27e-03	2.008	1.91e-03	1.521	7.08e-04	3.195	1.15e-04	4.367	2.63e-05	4.959
6.86e-03	1.41e-03	1.907	2.94e-04	2.706	5.16e-05	3.786	6.16e-06	4.229	7.34e-07	5.172
3.43e-03	3.74e-04	1.912	3.73e-05	2.978	3.55e-06	3.861	2.21e-07	4.804	1.24e-08	5.893
L^2-norm of the reconstructive potential error										
	$k=0$		$k=1$		$k=2$		$k=3$		$k=4$	
h	error	rate	error	rate	error	rate	error	rate	error	rate
2.16e-01	7.01e-01		7.13e-01		6.30e-01		3.32e-01		1.25e-01	
1.10e-01	5.96e-01	0.238	2.33e-01	1.659	9.24e-02	2.846	4.35e-02	3.013	6.31e-02	1.011
5.49e-02	1.83e-01	1.699	3.83e-02	2.598	1.88e-02	2.292	2.29e-02	0.924	1.30e-02	2.277
2.75e-02	3.96e-02	2.217	7.31e-03	2.394	6.65e-03	1.502	2.42e-03	3.248	8.35e-04	3.969
1.37e-02	1.06e-02	1.884	2.14e-03	1.766	7.16e-04	3.197	1.16e-04	4.359	2.64e-05	4.957
6.86e-03	2.81e-03	1.924	3.22e-04	2.735	5.22e-05	3.786	6.20e-06	4.237	7.37e-07	5.173
3.43e-03	7.23e-04	1.959	4.07e-05	2.985	3.59e-06	3.864	2.22e-07	4.805	1.24e-08	5.892

7.3.2 Results when solving with meshes having hanging nodes only on Γ_1

The purpose here is to exhibit the robustness of the method when a family of meshes with hanging nodes only on Γ_1 is considered. We emphasize that this case is not covered by the current analysis. From Tables 10, 11 and 12, we observe that the different errors we have considered, go to zero at the optimal rates of convergence as indicated in Theorems 5.1, 5.2 and 5.3, as well as in Remark 5.1. Figure 7 shows the first two initial meshes (with hanging nodes on Γ_1) of the domain, to perform this numerical simulation., In addition, Figures 16, 17 and 18, resume the information given in Tables 10, 11 and 12, respectively. This gives us numerical evidence that the approach can be extended to deal, at least, with hanging nodes on Γ_1. This could be the subject of future work.

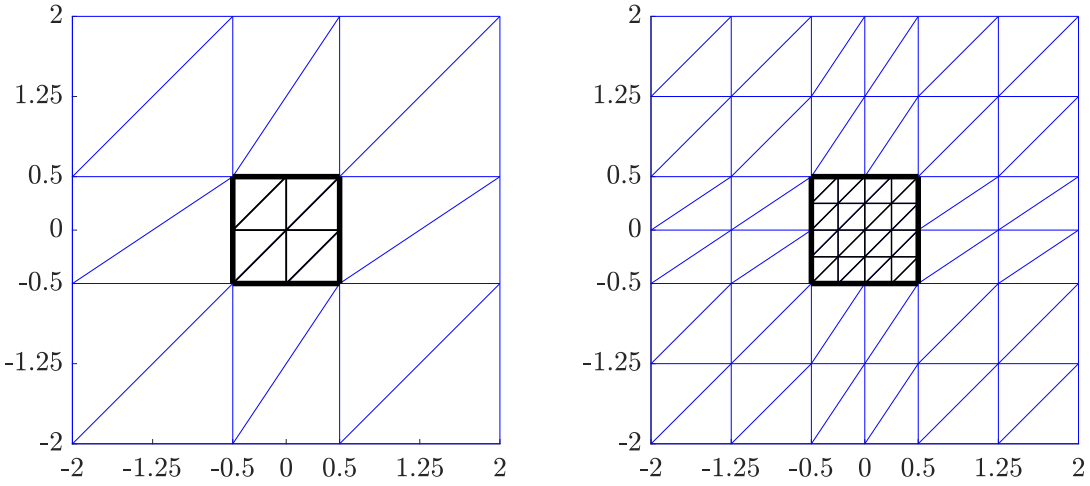

Figure 15: First two meshes with hanging nodes on Γ_1

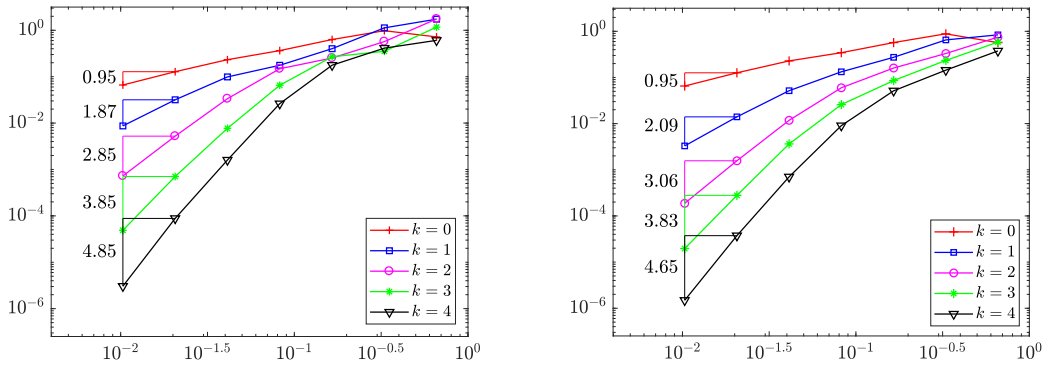

(a) Energy norm of the potential error vs. h

(b) L^2-norm of the flux error vs. h

Figure 16: Rates of convergence of the (a) energy norm of the potential error, and (b) flux error (Example 3, nonconforming meshes)

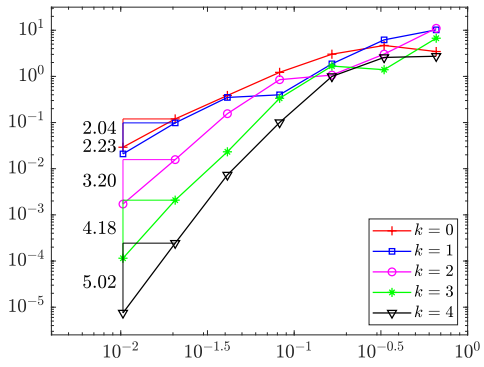

(a) $||\widehat{\xi}_h - \xi_h||_{\Gamma_{1,h}}$ vs. h

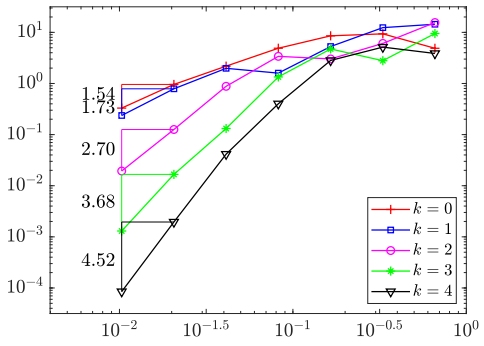

(b) $||\widehat{\xi}_h - \xi_h||_{0,\Gamma_1}$ vs. h

Figure 17: Rates of convergence of the Lagrange multiplier considering the (a) Discrete trace norm $||\cdot||_{\Gamma_{1,h}}$, and (b) Standard L^2-norm (Example 3, nonconforming meshes)

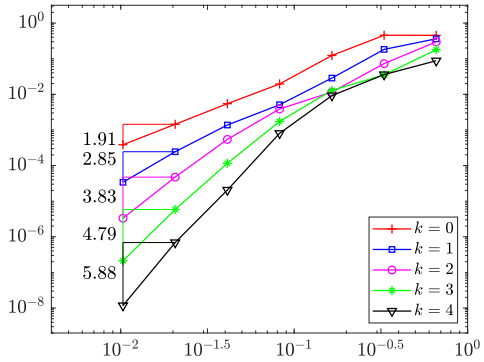

(a) L^2-norm of the potential error vs. h

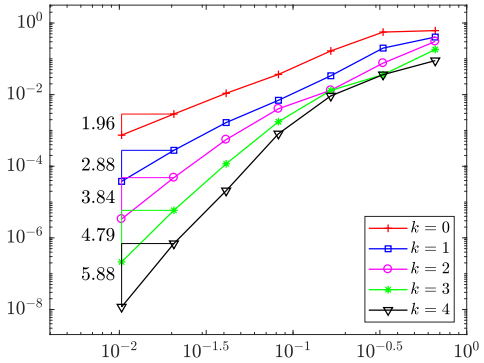

(b) L^2-norm of the reconstructive potential error vs. h

Figure 18: Rates of convergence of the L^2-norm of the (a) potential error, and (b) reconstructive potential error (Example 3, nonconforming meshes)

Table 10: Histories of convergence of the energy norm of the potential error and L^2-norm of the flux error, considering $k \in \{0, 1, 2, 3, 4\}$ using meshes with hanging nodes on Γ_1 (Example 3)

Energy norm of the potential error										
	$k=0$		$k=1$		$k=2$		$k=3$		$k=4$	
h	error	rate	error	rate	error	rate	error	rate	error	rate
2.16e-01	7.19e-01		1.73e+00		1.75e+00		1.17e+00		6.06e-01	
1.10e-01	9.78e-01	-0.456	1.13e+00	0.639	5.70e-01	1.661	3.52e-01	1.779	4.12e-01	0.574
5.49e-02	6.31e-01	0.630	4.01e-01	1.486	2.53e-01	1.172	2.69e-01	0.390	1.77e-01	1.217
2.75e-02	3.64e-01	0.795	1.76e-01	1.193	1.48e-01	0.771	6.52e-02	2.048	2.62e-02	2.762
1.37e-02	2.32e-01	0.646	9.87e-02	0.829	3.35e-02	2.133	7.70e-03	3.066	1.60e-03	4.013
6.86e-03	1.28e-01	0.862	3.17e-02	1.642	5.23e-03	2.687	7.04e-04	3.458	8.81e-05	4.189
3.43e-03	6.61e-02	0.952	8.69e-03	1.868	7.25e-04	2.849	4.89e-05	3.850	3.05e-06	4.853
L^2-norm of the flux error										
	$k=0$		$k=1$		$k=2$		$k=3$		$k=4$	
h	error	rate	error	rate	error	rate	error	rate	error	rate
6.59e-01	5.68e-01		8.38e-01		7.48e-01		5.84e-01		3.76e-01	
3.30e-01	8.82e-01	-0.637	6.51e-01	0.365	3.30e-01	1.183	2.34e-01	1.322	1.44e-01	1.386
1.65e-01	5.70e-01	0.630	2.73e-01	1.252	1.60e-01	1.044	8.57e-02	1.449	5.14e-02	1.487
8.24e-02	3.44e-01	0.728	1.33e-01	1.042	5.97e-02	1.420	2.58e-02	1.728	9.04e-03	2.502
4.12e-02	2.28e-01	0.591	5.16e-02	1.360	1.18e-02	2.340	3.63e-03	2.830	7.03e-04	3.684
2.06e-02	1.26e-01	0.857	1.40e-02	1.882	1.57e-03	2.912	2.79e-04	3.702	3.74e-05	4.233
1.03e-02	6.52e-02	0.951	3.29e-03	2.090	1.87e-04	3.064	1.96e-05	3.827	1.49e-06	4.652

Table 11: Histories of convergence of the L^2-projection of $\xi - \xi_h$ in $||\cdot||_{\Gamma_{1,h}}$ and $||\cdot||_{0,\Gamma_1}$ norms, for $k \in \{0,1,2,3,4\}$ using meshes with hanging nodes (Example 3)

$\|\widehat{\xi_h} - \xi_h\|_{\Gamma_{1,h}}$										
	$k=0$		$k=1$		$k=2$		$k=3$		$k=4$	
h	error	rate	error	rate	error	rate	error	rate	error	rate
6.59e-01	3.45e+00		1.02e+01		1.10e+01		6.71e+00		2.73e+00	
3.30e-01	4.68e+00	-0.439	6.19e+00	0.722	3.04e+00	1.860	1.40e+00	2.271	2.57e+00	0.088
1.65e-01	3.03e+00	0.629	1.87e+00	1.728	1.07e+00	1.509	1.67e+00	-0.262	9.98e-01	1.366
8.24e-02	1.22e+00	1.304	3.99e-01	2.224	8.49e-01	0.331	3.36e-01	2.315	1.00e-01	3.310
4.12e-02	3.86e-01	1.664	3.50e-01	0.188	1.56e-01	2.448	2.32e-02	3.851	7.33e-03	3.774
2.06e-02	1.20e-01	1.688	9.84e-02	1.831	1.57e-02	3.306	2.08e-03	3.481	2.44e-04	4.909
1.03e-02	2.92e-02	2.037	2.09e-02	2.234	1.71e-03	3.199	1.15e-04	4.178	7.50e-06	5.023
$\|\widehat{\xi_h} - \xi_h\|_{0,\Gamma_1}$										
	$k=0$		$k=1$		$k=2$		$k=3$		$k=4$	
h	error	rate	error	rate	error	rate	error	rate	error	rate
6.59e-01	4.88e+00		1.44e+01		1.56e+01		9.49e+00		3.87e+00	
3.30e-01	9.36e+00	-0.940	1.24e+01	0.221	6.08e+00	1.359	2.79e+00	1.770	5.15e+00	-0.413
1.65e-01	8.56e+00	0.129	5.28e+00	1.228	3.02e+00	1.009	4.74e+00	-0.762	2.82e+00	0.866
8.24e-02	4.89e+00	0.805	1.59e+00	1.725	3.40e+00	-0.168	1.34e+00	1.816	4.01e-01	2.811
4.12e-02	2.18e+00	1.164	1.98e+00	-0.312	8.80e-01	1.948	1.31e-01	3.351	4.15e-02	3.274
2.06e-02	9.58e-01	1.188	7.87e-01	1.331	1.26e-01	2.806	1.67e-02	2.981	1.95e-03	4.409
1.03e-02	3.30e-01	1.537	2.37e-01	1.734	1.94e-02	2.699	1.30e-03	3.678	8.48e-05	4.523

Table 12: Histories of convergence of L^2-norm of the potential and reconstructive potential errors, considering $k \in \{0, 1, 2, 3, 4\}$ using meshes with hanging nodes (Example 3)

L^2-norm of the potential error										
	$k=0$		$k=1$		$k=2$		$k=3$		$k=4$	
h	error	rate	error	rate	error	rate	error	rate	error	rate
6.59e-01	4.53e-01		3.62e-01		2.97e-01		1.79e-01		8.76e-02	
3.30e-01	4.56e-01	-0.009	1.83e-01	0.990	7.28e-02	2.030	3.50e-02	2.362	3.59e-02	1.291
1.65e-01	1.23e-01	1.886	2.86e-02	2.676	1.16e-02	2.656	1.29e-02	1.439	9.20e-03	1.964
8.24e-02	1.95e-02	2.654	5.10e-03	2.483	3.88e-03	1.572	1.73e-03	2.891	8.05e-04	3.508
4.12e-02	5.46e-03	1.837	1.37e-03	1.890	5.43e-04	2.837	1.16e-04	3.907	2.06e-05	5.288
2.06e-02	1.44e-03	1.923	2.45e-04	2.490	4.74e-05	3.519	5.84e-06	4.308	6.90e-07	4.900
1.03e-02	3.83e-04	1.910	3.40e-05	2.848	3.32e-06	3.834	2.12e-07	4.785	1.17e-08	5.881
L^2-norm of the reconstructive potential error										
	$k=0$		$k=1$		$k=2$		$k=3$		$k=4$	
h	error	rate	error	rate	error	rate	error	rate	error	rate
2.16e-01	6.14e-01		4.05e-01		3.06e-01		1.82e-01		8.93e-02	
1.10e-01	5.59e-01	0.139	1.99e-01	1.051	7.58e-02	2.068	3.61e-02	2.397	3.62e-02	1.338
5.49e-02	1.66e-01	1.745	3.36e-02	2.561	1.32e-02	2.512	1.31e-02	1.461	9.23e-03	1.965
2.75e-02	3.67e-02	2.186	6.95e-03	2.282	4.03e-03	1.720	1.76e-03	2.907	8.07e-04	3.525
1.37e-02	1.09e-02	1.741	1.66e-03	2.056	5.54e-04	2.847	1.17e-04	3.888	2.08e-05	5.253
6.86e-03	2.87e-03	1.930	2.79e-04	2.579	4.81e-05	3.535	5.87e-06	4.323	6.93e-07	4.916
3.43e-03	7.38e-04	1.958	3.78e-05	2.882	3.36e-06	3.838	2.13e-07	4.787	1.18e-08	5.879

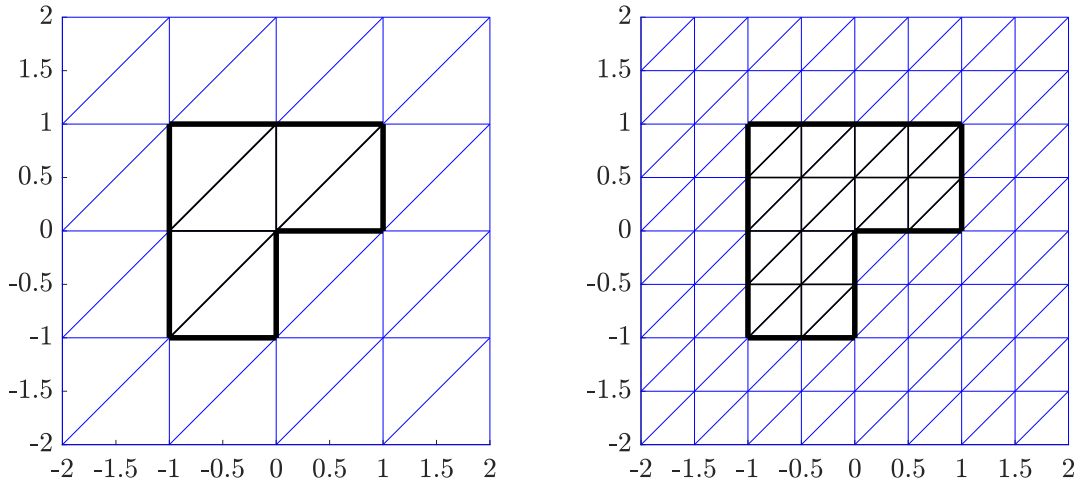

Figure 19: First two simplicial meshes for Example 4

7.4 Example 4: A non regular exact solution

We solve transmission problem (1)*, considering* $\Omega_1 = (-1,1)^2 \setminus [0,1] \times [-1,0]$ *and* $\Omega_2 := (-2,2)^2 \setminus \overline{\Omega}_1$ *(see Figure 19), while the data are such that the exact solution is* (u_1, u_2)*, where*

$$u_1(r,\theta) = r^{2/3}\sin(2\theta/3) \; - \; c_1 \quad (\textit{in polar coordinates})\,,$$

$$u_2(x,y) = \sin(\pi x)\sin(\pi y) \; - \; c_2\,,$$

and c_1 *and* c_2 *are real constants such that* $u_j \in L^2_0(\Omega_j)$*,* $j \in \{1,2\}$*. We point out that* $u_1 \in H^{1+\frac{2}{3}-s}(\Omega_1)$*, for an arbitrary small number* $s > 0$*, and* u_2 *is a smooth function. Figure 19 shows the first two conforming meshes that we consider for our simulations, while Figure 20 exhibits the behavior of the energy norm of the potential error (left) and the flux error (right), with respect to the meshsize* h*. Their corresponding histories of convergence are given in Table 13, and do not contradict Theorem 5.1, since in this case the function* u_1 *is non regular. Similar behavior is noticed in Table 14 for the error of* $\widehat{\xi}_h - \xi_h$ *in the weighted and usual* L^2-*norms, with rates of convergence* $2/3$ *and* $1/6$*, respectively. These are also displayed in Figure 21. In addition, Table 15 (see also Figure 14) reports the histories of convergence of the* L^2-*norm of the potential and the reconstructive potential errors, which are not the optimal ones, as prescribed by Theorems 5.2 and* (5.3)*, and by Remark 5.1, due to the lack of smoothness of function* u_1*.*

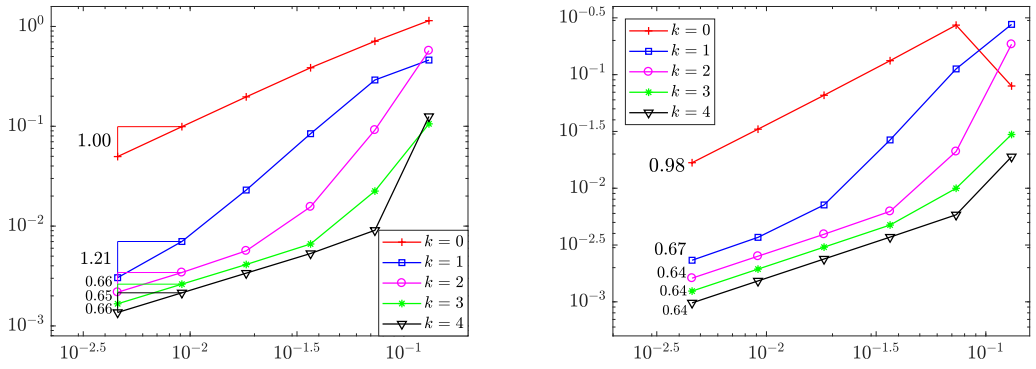

(a) Energy norm of the potential error vs. h

(b) L^2-norm of the flux error vs. h

Figure 20: Rates of convergence of the (a) energy norm of the potential error, and (b) flux error (Example 4)

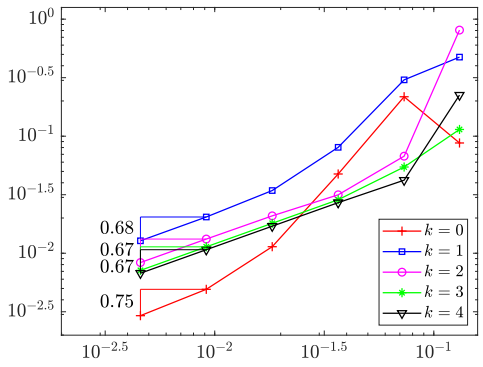

(a) $||\widehat{\xi}_h - \xi_h||_{\Gamma_{1,h}}$ vs. h

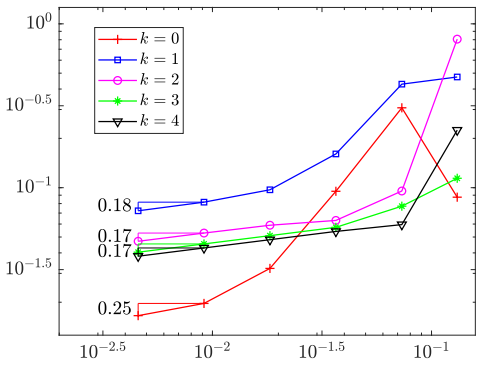

(b) $||\widehat{\xi}_h - \xi_h||_{0,\Gamma_1}$ vs. h

Figure 21: Rates of convergence of the Lagrange multiplier considering the (a) Discrete trace norm $||\cdot||_{\Gamma_{1,h}}$, and (b) Standard L^2-norm (Example 4)

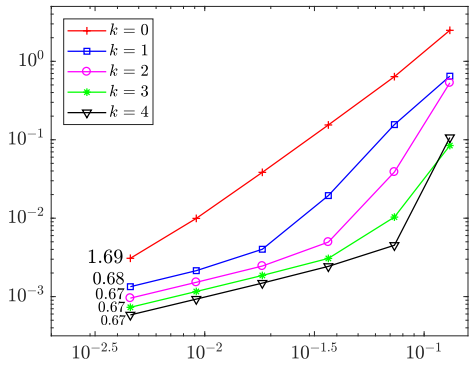

(a) L^2-norm of the potential error vs. h

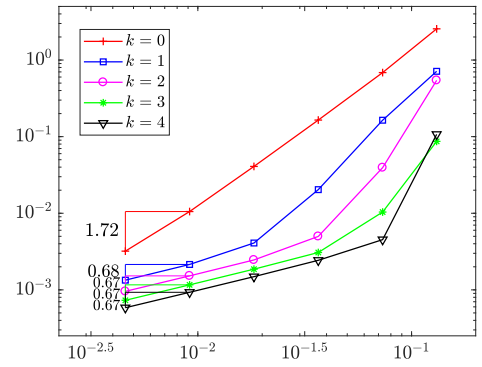

(b) L^2-norm of the reconstructive potential error vs. h

Figure 22: Rates of convergence of the L^2-norm of the (a) potential error, and (b) reconstructive potential error (Example 4)

Table 13: Histories of convergence of the energy norm of the potential error and L^2-norm of the flux error, considering $k \in \{0, 1, 2, 3, 4\}$ (Example 4)

Energy norm of the potential error										
	$k=0$		$k=1$		$k=2$		$k=3$		$k=4$	
h	error	rate	error	rate	error	rate	error	rate	error	rate
1.31e-01	1.14e+00		4.61e-01		5.72e-01		1.06e-01		1.25e-01	
7.32e-02	7.11e-01	0.817	2.91e-01	0.790	9.17e-02	3.145	2.24e-02	2.664	9.08e-03	4.511
3.66e-02	3.86e-01	0.882	8.43e-02	1.787	1.56e-02	2.554	6.62e-03	1.760	5.31e-03	0.772
1.83e-02	1.97e-01	0.969	2.30e-02	1.875	5.65e-03	1.465	4.12e-03	0.683	3.38e-03	0.654
9.15e-03	9.91e-02	0.991	7.01e-03	1.712	3.43e-03	0.722	2.62e-03	0.654	2.15e-03	0.654
4.58e-03	4.97e-02	0.997	3.04e-03	1.206	2.17e-03	0.658	1.67e-03	0.655	1.36e-03	0.655
L^2-norm of the flux error										
	$k=0$		$k=1$		$k=2$		$k=3$		$k=4$	
h	error	rate	error	rate	error	rate	error	rate	error	rate
1.31e-01	7.94e-02		2.77e-01		1.85e-01		2.97e-02		1.89e-02	
7.32e-02	2.73e-01	–	1.12e-01	1.551	2.11e-02	3.734	9.99e-03	1.873	5.84e-03	2.023
3.66e-02	1.33e-01	1.040	2.66e-02	2.077	6.26e-03	1.751	4.74e-03	1.075	3.71e-03	0.652
1.83e-02	6.58e-02	1.012	7.13e-03	1.901	3.93e-03	0.670	3.03e-03	0.647	2.38e-03	0.640
9.15e-03	3.31e-02	0.992	3.70e-03	0.947	2.52e-03	0.641	1.94e-03	0.642	1.53e-03	0.641
4.58e-03	1.68e-02	0.981	2.32e-03	0.671	1.62e-03	0.643	1.24e-03	0.644	9.79e-04	0.643

Table 14: Histories of convergence of the L^2- projection of $\xi - \xi_h$ in $||\cdot||_{\Gamma_{1,h}}$ and $||\cdot||_{0,\Gamma_1}$ norms, for $k \in \{0, 1, 2, 3, 4\}$ (Example 4)

$\|\widehat{\xi_h} - \xi_h\|_{\Gamma_{1,h}}$										
	$k=0$		$k=1$		$k=2$		$k=3$		$k=4$	
h	error	rate	error	rate	error	rate	error	rate	error	rate
1.31e-01	8.75e-02		4.74e-01		8.06e-01		1.14e-01		2.25e-01	
7.32e-02	2.17e-01	-1.562	3.03e-01	0.769	6.75e-02	4.262	5.45e-02	1.269	4.21e-02	2.877
3.66e-02	4.75e-02	2.192	8.03e-02	1.915	3.16e-02	1.096	2.86e-02	0.929	2.70e-02	0.638
1.83e-02	1.14e-02	2.064	3.43e-02	1.227	2.09e-02	0.597	1.80e-02	0.669	1.70e-02	0.668
9.15e-03	4.92e-03	1.210	2.04e-02	0.751	1.32e-02	0.659	1.13e-02	0.668	1.07e-02	0.668
4.58e-03	2.93e-03	0.749	1.28e-02	0.676	8.33e-03	0.668	7.14e-03	0.668	6.75e-03	0.668
$\|\widehat{\xi_h} - \xi_h\|_{0,\Gamma_1}$										
	$k=0$		$k=1$		$k=2$		$k=3$		$k=4$	
h	error	rate	error	rate	error	rate	error	rate	error	rate
1.31e-01	8.75e-02		4.74e-01		8.06e-01		1.14e-01		2.25e-01	
7.32e-02	3.07e-01	-2.158	4.28e-01	0.173	9.54e-02	3.667	7.71e-02	0.674	5.95e-02	2.281
3.66e-02	9.51e-02	1.692	1.61e-01	1.415	6.31e-02	0.596	5.73e-02	0.429	5.41e-02	0.138
1.83e-02	3.22e-02	1.564	9.71e-02	0.727	5.90e-02	0.097	5.10e-02	0.169	4.82e-02	0.168
9.15e-03	1.97e-02	0.710	8.16e-02	0.251	5.29e-02	0.158	4.54e-02	0.168	4.29e-02	0.168
4.58e-03	1.66e-02	0.248	7.23e-02	0.175	4.71e-02	0.167	4.04e-02	0.168	3.82e-02	0.167

Table 15: Histories of convergence of L^2-norm of the potential and reconstructive potential errors, considering $k \in \{0, 1, 2, 3, 4\}$ (Example 4)

L^2-norm of the potential error										
	$k=0$		$k=1$		$k=2$		$k=3$		$k=4$	
h	error	rate	error	rate	error	rate	error	rate	error	rate
1.31e-01	2.48e+00		6.46e-01		5.31e-01		8.44e-02		1.07e-01	
7.32e-02	6.37e-01	2.338	1.56e-01	2.443	3.88e-02	4.498	1.03e-02	3.609	4.51e-03	5.435
3.66e-02	1.54e-01	2.046	1.94e-02	3.006	4.96e-03	2.967	3.07e-03	1.750	2.43e-03	0.893
1.83e-02	3.84e-02	2.007	4.02e-03	2.273	2.45e-03	1.014	1.86e-03	0.722	1.49e-03	0.709
9.15e-03	9.94e-03	1.950	2.14e-03	0.907	1.52e-03	0.689	1.16e-03	0.679	9.30e-04	0.678
4.58e-03	3.08e-03	1.693	1.34e-03	0.679	9.56e-04	0.672	7.31e-04	0.671	5.84e-04	0.670
L^2-norm of the reconstructive potential error										
	$k=0$		$k=1$		$k=2$		$k=3$		$k=4$	
h	error	rate	error	rate	error	rate	error	rate	error	rate
1.31e-01	2.55e+00		7.12e-01		5.43e-01		8.67e-02		1.07e-01	
7.32e-02	6.86e-01	2.259	1.64e-01	2.525	3.94e-02	4.508	1.04e-02	3.649	4.52e-03	5.436
3.66e-02	1.65e-01	2.059	2.03e-02	3.010	4.99e-03	2.981	3.07e-03	1.754	2.43e-03	0.896
1.83e-02	4.09e-02	2.011	4.09e-03	2.315	2.46e-03	1.021	1.86e-03	0.723	1.49e-03	0.710
9.15e-03	1.05e-02	1.956	2.15e-03	0.929	1.52e-03	0.690	1.16e-03	0.680	9.30e-04	0.678
4.58e-03	3.20e-03	1.720	1.34e-03	0.682	9.56e-04	0.673	7.31e-04	0.671	5.84e-04	0.671

7.5 Example 5: A non smooth enough exact solution

Here, we solve the linear transmission problem (1)*, considering the same domain as in Example 4, whose data are such that its exact solution is given by*

$$u_1(x,y) = \cos\left(\frac{\pi}{2}y\right) + \chi(x)x^{3.5} \; - \; c_1 \, ,$$

where $\chi(x)$ is the characteristic function on $[0,1]$ with respect to x, and

$$u_2(x,y) = \sin(\pi x)\sin(\pi y) \; - \; c_2 \, ,$$

with c_1 and c_2 being real constants, such that u_1 and u_2 have zero mean value in Ω_1 and Ω_2, respectively. It is known that $u_1 \in H^4(\Omega_1)$, but does not belong to $H^{4+\epsilon}(\Omega_1)$, for an arbitrary small number $\epsilon > 0$. Table 16 reports the histories of convergence of the energy norm of the potential error and the flux error, considering $k \in \{0,1,2,3,4\}$. We observe that the rates of convergence are the expected optimal ones: $k+1$, when the solution is approximated by piecewise polynomials of degree at most $k \in \{0,1,2,3\}$. These are in agreement with Theorems 5.1. For $k = 4$, we still notice convergence, but not at the optimal rate of convergence, since the exact solution is not smooth enough. We display these results also in Figure 23. On the other hand, in Figure 24, we show the behavior of the weighted and usual L^2-norms of $\widehat{\xi}_h - \xi_h$, with respect to the meshsize h. Their corresponding histories of convergence are displayed in Table 17, and they are the optimal ones, as predicted by Theorem 5.1 and Remark 5.1. In Table 18 we provide the histories of convergence in the L^2-norm of the potential and the reconstructive potential errors. The behavior of the rates of convergence, for $k \in \{0,1,2,3\}$ are in agreement

with the ones predicted by Theorems 5.2 and 5.3 for smooth functions, and are resumed in Figure 25. We notice again a lost in the order of convergence for $k = 4$, due to the small smoothness of u_1.

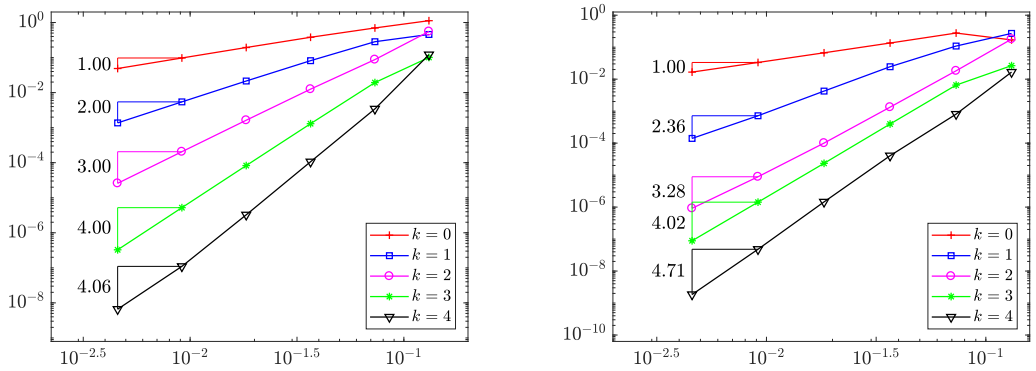

(a) Energy norm of the potential error vs. h

(b) L^2-norm of the flux error vs. h

Figure 23: Rates of convergence of the (a) energy norm of the potential error, and (b) flux error (Example 5)

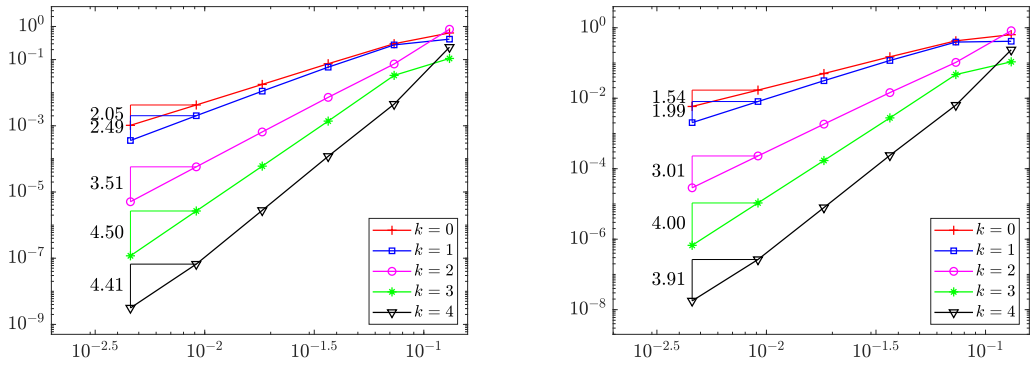

(a) $||\widehat{\xi}_h - \xi_h||_{\Gamma_{1,h}}$ vs. h

(b) $||\widehat{\xi}_h - \xi_h||_{0,\Gamma_1}$ vs. h

Figure 24: Rates of convergence of the Lagrange multiplier considering the (a) Discrete trace norm $||\cdot||_{\Gamma_{1,h}}$, and (b) Standard L^2-norm (Example 5)

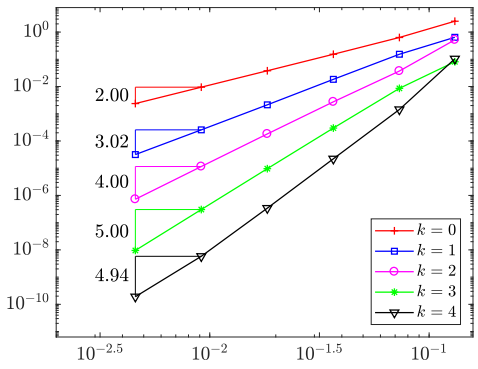

(a) L^2-norm of the potential error vs. h

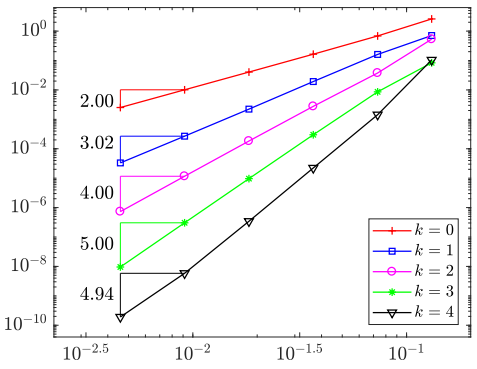

(b) L^2-norm of the reconstructive potential error vs. h

Figure 25: Rates of convergence of the L^2-norm of the (a) potential error, and (b) reconstructive potential error (Example 5)

Table 16: Histories of convergence of the energy norm of the potential error and L^2-norm of the flux error, considering $k \in \{0, 1, 2, 3, 4\}$ (Example 5)

Energy norm of the potential error										
	$k = 0$		$k = 1$		$k = 2$		$k = 3$		$k = 4$	
h	error	rate	error	rate	error	rate	error	rate	error	rate
1.31e-01	1.13e+00		4.56e-01		5.54e-01		1.01e-01		1.21e-01	
7.32e-02	7.00e-01	0.820	2.83e-01	0.817	8.75e-02	3.171	1.93e-02	2.834	3.43e-03	6.124
3.66e-02	3.79e-01	0.884	8.15e-02	1.798	1.25e-02	2.802	1.30e-03	3.899	1.06e-04	5.010
1.83e-02	1.93e-01	0.970	2.14e-02	1.928	1.63e-03	2.946	8.28e-05	3.969	3.26e-06	5.030
9.15e-03	9.72e-02	0.993	5.44e-03	1.978	2.06e-04	2.985	5.21e-06	3.991	1.10e-07	4.887
4.58e-03	4.87e-02	1.000	1.37e-03	1.997	2.58e-05	3.001	3.27e-07	4.001	6.60e-09	4.065
L^2-norm of the flux error										
	$k = 0$		$k = 1$		$k = 2$		$k = 3$		$k = 4$	
h	error	rate	error	rate	error	rate	error	rate	error	rate
1.31e-01	1.69e-01		2.70e-01		1.79e-01		2.65e-02		1.66e-02	
7.32e-02	2.76e-01	–	1.09e-01	1.564	1.83e-02	3.921	6.53e-03	2.408	8.07e-04	5.198
3.66e-02	1.35e-01	1.035	2.45e-02	2.149	1.33e-03	3.775	3.96e-04	4.044	4.04e-05	4.320
1.83e-02	6.67e-02	1.016	4.24e-03	2.530	1.00e-04	3.733	2.34e-05	4.082	1.45e-06	4.799
9.15e-03	3.33e-02	1.004	7.18e-04	2.562	8.88e-06	3.498	1.43e-06	4.033	4.80e-08	4.918
4.58e-03	1.66e-02	1.003	1.40e-04	2.359	9.17e-07	3.281	8.85e-08	4.017	1.85e-09	4.706

Table 17: Histories of convergence of the L^2-projection of $\xi - \xi_h$ in $||\cdot||_{\Gamma_{1,h}}$ and $||\cdot||_{0,\Gamma_1}$ norms, for $k \in \{0,1,2,3,4\}$ (Example 5)

$\|\widehat{\xi_h} - \xi_h\|_{\Gamma_{1,h}}$										
	$k=0$		$k=1$		$k=2$		$k=3$		$k=4$	
h	error	rate	error	rate	error	rate	error	rate	error	rate
1.31e-01	6.37e-01		4.14e-01		8.23e-01		1.08e-01		2.37e-01	
7.32e-02	3.01e-01	1.287	2.78e-01	0.685	7.36e-02	4.148	3.33e-02	2.023	4.50e-03	6.808
3.66e-02	7.49e-02	2.009	5.89e-02	2.237	7.23e-03	3.348	1.39e-03	4.586	1.20e-04	5.234
1.83e-02	1.78e-02	2.075	1.11e-02	2.406	6.51e-04	3.473	6.04e-05	4.520	2.79e-06	5.424
9.15e-03	4.25e-03	2.064	2.02e-03	2.463	5.75e-05	3.500	2.67e-06	4.501	6.63e-08	5.394
4.58e-03	1.03e-03	2.045	3.59e-04	2.491	5.08e-06	3.508	1.18e-07	4.504	3.14e-09	4.408
$\|\widehat{\xi_h} - \xi_h\|_{0,\Gamma_1}$										
	$k=0$		$k=1$		$k=2$		$k=3$		$k=4$	
h	error	rate	error	rate	error	rate	error	rate	error	rate
1.31e-01	6.37e-01		4.14e-01		8.23e-01		1.08e-01		2.37e-01	
7.32e-02	4.26e-01	0.692	3.93e-01	0.089	1.04e-01	3.553	4.71e-02	1.428	6.37e-03	6.212
3.66e-02	1.50e-01	1.509	1.18e-01	1.737	1.45e-02	2.848	2.77e-03	4.086	2.39e-04	4.734
1.83e-02	5.03e-02	1.575	3.14e-02	1.906	1.84e-03	2.973	1.71e-04	4.020	7.88e-06	4.924
9.15e-03	1.70e-02	1.564	8.06e-03	1.963	2.30e-04	3.000	1.07e-05	4.001	2.65e-07	4.894
4.58e-03	5.84e-03	1.544	2.03e-03	1.990	2.87e-05	3.007	6.69e-07	4.003	1.77e-08	3.907

Table 18: Histories of convergence of L^2-norm of the potential and reconstructive potential errors, considering $k \in \{0,1,2,3,4\}$ (Example 5)

L^2-norm of the potential error										
	$k=0$		$k=1$		$k=2$		$k=3$		$k=4$	
h	error	rate	error	rate	error	rate	error	rate	error	rate
1.31e-01	2.50e+00		6.43e-01		5.20e-01		8.12e-02		1.04e-01	
7.32e-02	6.33e-01	2.362	1.53e-01	2.463	3.70e-02	4.538	8.57e-03	3.863	1.43e-03	7.367
3.66e-02	1.53e-01	2.049	1.84e-02	3.062	2.74e-03	3.756	2.98e-04	4.845	2.21e-05	6.015
1.83e-02	3.80e-02	2.012	2.13e-03	3.110	1.81e-04	3.917	9.61e-06	4.955	3.41e-07	6.021
9.15e-03	9.47e-03	2.003	2.56e-04	3.053	1.15e-05	3.976	3.03e-07	4.987	5.81e-09	5.876
4.58e-03	2.37e-03	2.004	3.17e-05	3.022	7.24e-07	3.999	9.52e-09	5.000	1.90e-10	4.940
L^2-norm of the reconstructive potential error										
	$k=0$		$k=1$		$k=2$		$k=3$		$k=4$	
h	error	rate	error	rate	error	rate	error	rate	error	rate
1.31e-01	2.59e+00		7.07e-01		5.31e-01		8.35e-02		1.04e-01	
7.32e-02	6.84e-01	2.287	1.61e-01	2.542	3.76e-02	4.548	8.60e-03	3.905	1.44e-03	7.366
3.66e-02	1.64e-01	2.062	1.93e-02	3.063	2.77e-03	3.765	2.99e-04	4.846	2.22e-05	6.014
1.83e-02	4.05e-02	2.016	2.23e-03	3.114	1.83e-04	3.919	9.64e-06	4.956	3.42e-07	6.020
9.15e-03	1.01e-02	2.004	2.68e-04	3.056	1.16e-05	3.977	3.04e-07	4.987	5.83e-09	5.876
4.58e-03	2.52e-03	2.004	3.30e-05	3.023	7.29e-07	4.000	9.55e-09	5.000	1.90e-10	4.944

The purpose of the next two examples, is to study the robustness of our implementation when

the domain $\Omega := \Omega_1 \cup \Gamma_1 \cup \Omega_2$ *is non convex. We remark that in this situation, we can not ensure the validity of* (90)*, and then Theorems 5.2 and 5.3 do not hold, necessarily.*

7.6 Example 6: A regular solution in a non convex Ω

In this example, we approximate the solution of (1)*, with subdomains* $\Omega_1 = (-2,2)^2 \setminus [-1,2] \times [-2,1]$ *and* $\Omega_2 := (-3,3)^2 \setminus (\overline{\Omega}_1 \cup [0,3] \times [-3,0])$*, and the data are such that the exact solution is given by the smoothness functions*

$$u_1(x,y) = \frac{xy}{x^2+y^2} - \frac{13\ln(2) - 5\ln(5)}{14} \quad , \quad u_2(x,y) = \cos(\pi x)\cos(\pi y)\,. \tag{142}$$

We consider a family of simplicial meshes, whose coarse/first mesh is displayed in Figure 26. In Tables 19 and 20 we report the rates of convergence of the method, when the solution is approximated by piecewise polynomials of degree at most $k\{0,1,2,3,4\}$*. We notice that the results are in agreement with Theorem 5.1 and Remark 5.1. On the other hand, from Table 21, we notice that the convergence of the potential and the reconstructive potential errors behave as* $\mathcal{O}(h^{k+2})$*, the optimal rate predicted by Theorems 5.2 and 5.3, despite the fact that this situation is not covered by the current theory. We can also see these behaviors in Figures 27, 28 and 29.*

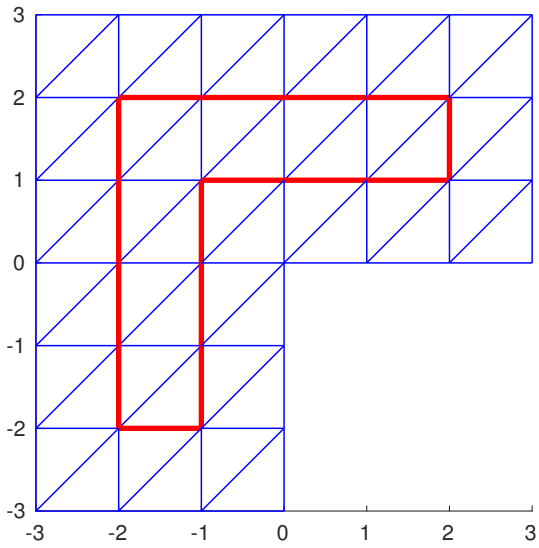

Figure 26: Initial mesh for Examples 6 and 7

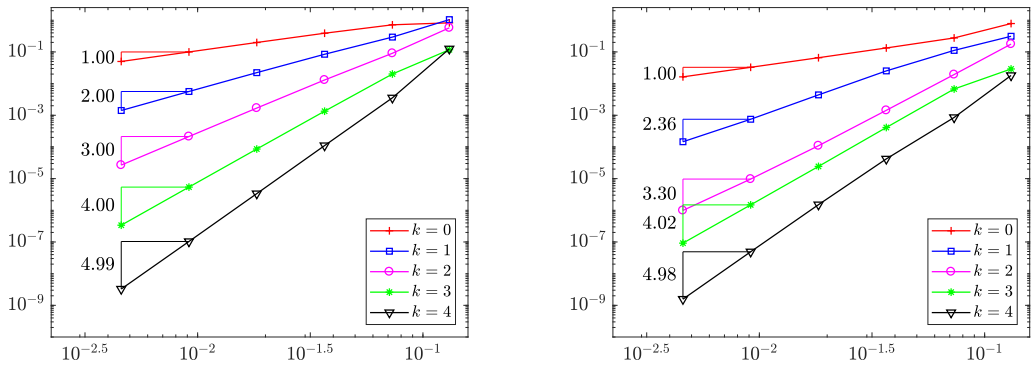

(a) Energy norm of the potential error vs. h (b) L^2-norm of the flux error vs. h

Figure 27: Rates of convergence of the (a) energy norm of the potential error, and (b) flux error (Example 6)

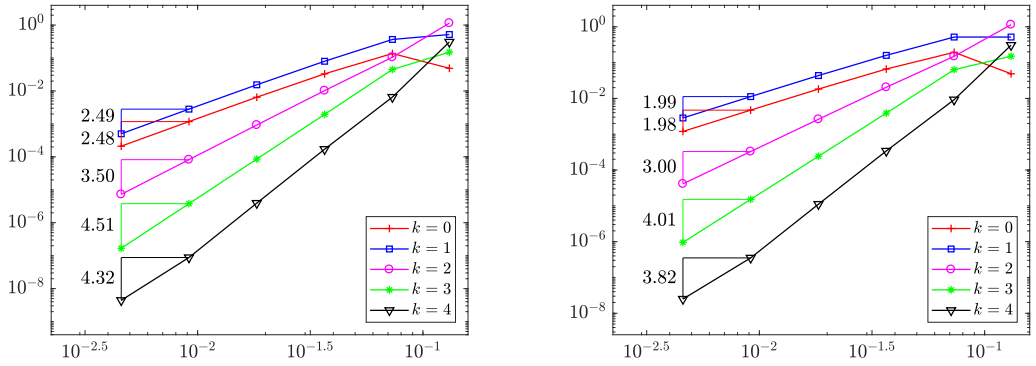

(a) $||\widehat{\xi}_h - \xi_h||_{\Gamma_{1,h}}$ vs. h (b) $||\widehat{\xi}_h - \xi_h||_{0,\Gamma_1}$ vs. h

Figure 28: Rates of convergence of the Lagrange multiplier considering the (a) Discrete trace norm $||\cdot||_{\Gamma_{1,h}}$, and (b) Standard L^2-norm (Example 6)

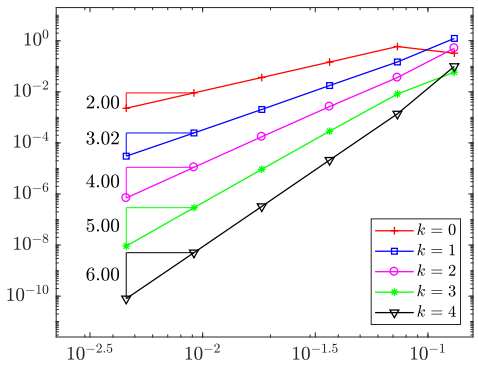

(a) L^2-norm of the potential error vs. h

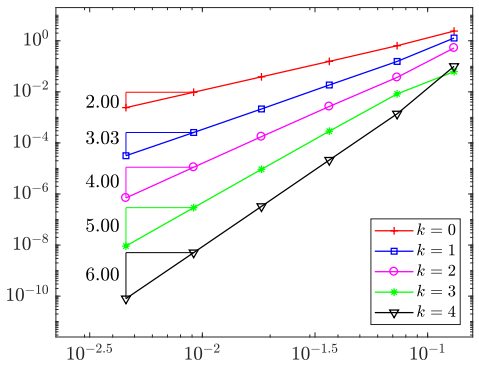

(b) L^2-norm of the reconstructive potential error vs. h

Figure 29: Rates of convergence of the L^2-norm of the (a) potential error, and (b) reconstructive potential error (Example 6)

Table 19: Histories of convergence of energy norm of the potential error and L^2-norm of the flux error, considering $k \in \{0, 1, 2, 3, 4\}$ (Example 6)

Energy norm of the potential error										
	$k = 0$		$k = 1$		$k = 2$		$k = 3$		$k = 4$	
h	error	rate	error	rate	error	rate	error	rate	error	rate
1.31e-01	8.29e-01		1.05e+00		5.77e-01		1.17e-01		1.25e-01	
7.32e-02	7.18e-01	0.248	2.94e-01	2.182	9.07e-02	3.178	2.01e-02	3.032	3.55e-03	6.123
3.66e-02	3.89e-01	0.883	8.44e-02	1.800	1.30e-02	2.802	1.34e-03	3.899	1.10e-04	5.008
1.83e-02	1.99e-01	0.970	2.22e-02	1.928	1.69e-03	2.945	8.59e-05	3.968	3.36e-06	5.039
9.15e-03	9.98e-02	0.993	5.63e-03	1.977	2.13e-04	2.985	5.40e-06	3.992	1.04e-07	5.020
4.58e-03	4.99e-02	1.000	1.41e-03	1.996	2.68e-05	3.000	3.38e-07	4.004	3.27e-09	4.992
L^2-norm of the flux error										
	$k = 0$		$k = 1$		$k = 2$		$k = 3$		$k = 4$	
h	error	rate	error	rate	error	rate	error	rate	error	rate
1.31e-01	7.86e-01		3.12e-01		1.77e-01		2.90e-02		1.81e-02	
7.32e-02	2.76e-01	1.797	1.12e-01	1.763	1.93e-02	3.805	6.74e-03	2.505	8.53e-04	5.248
3.66e-02	1.33e-01	1.051	2.52e-02	2.150	1.43e-03	3.752	4.11e-04	4.036	4.19e-05	4.346
1.83e-02	6.56e-02	1.022	4.40e-03	2.517	1.09e-04	3.713	2.43e-05	4.081	1.50e-06	4.801
9.15e-03	3.27e-02	1.006	7.49e-04	2.555	9.68e-06	3.497	1.48e-06	4.034	4.90e-08	4.939
4.58e-03	1.63e-02	1.003	1.46e-04	2.362	9.89e-07	3.296	9.18e-08	4.019	1.57e-09	4.975

Table 20: Histories of convergence of the L^2-projection of $\xi - \xi_h$ in $||\cdot||_{\Gamma_{1,h}}$ and $||\cdot||_{0,\Gamma_1}$ norms, for $k \in \{0, 1, 2, 3, 4\}$ (Example 6)

$\|\widehat{\xi_h} - \xi_h\|_{\Gamma_{1,h}}$										
	$k=0$		$k=1$		$k=2$		$k=3$		$k=4$	
h	error	rate	error	rate	error	rate	error	rate	error	rate
1.31e-01	4.88e-02		5.18e-01		1.15e+00		1.51e-01		3.07e-01	
7.32e-02	1.37e-01	-1.774	3.66e-01	0.595	1.06e-01	4.096	4.49e-02	2.080	6.51e-03	6.620
3.66e-02	3.31e-02	2.050	7.97e-02	2.199	1.03e-02	3.369	1.94e-03	4.531	1.70e-04	5.255
1.83e-02	6.45e-03	2.359	1.54e-02	2.372	9.26e-04	3.469	8.57e-05	4.503	3.94e-06	5.436
9.15e-03	1.18e-03	2.455	2.81e-03	2.453	8.22e-05	3.494	3.79e-06	4.498	8.79e-08	5.486
4.58e-03	2.11e-04	2.482	5.02e-04	2.488	7.27e-06	3.504	1.68e-07	4.506	4.41e-09	4.324
$\|\widehat{\xi_h} - \xi_h\|_{0,\Gamma_1}$										
	$k=0$		$k=1$		$k=2$		$k=3$		$k=4$	
h	error	rate	error	rate	error	rate	error	rate	error	rate
1.31e-01	4.88e-02		5.18e-01		1.15e+00		1.51e-01		3.07e-01	
7.32e-02	1.94e-01	-2.369	5.18e-01	-0.000	1.50e-01	3.501	6.35e-02	1.485	9.20e-03	6.025
3.66e-02	6.62e-02	1.550	1.59e-01	1.699	2.05e-02	2.869	3.88e-03	4.031	3.41e-04	4.755
1.83e-02	1.83e-02	1.859	4.35e-02	1.872	2.62e-03	2.969	2.42e-04	4.003	1.11e-05	4.936
9.15e-03	4.71e-03	1.955	1.12e-02	1.953	3.29e-04	2.994	1.52e-05	3.998	3.51e-07	4.986
4.58e-03	1.19e-03	1.981	2.84e-03	1.987	4.11e-05	3.004	9.48e-07	4.005	2.49e-08	3.823

Table 21: Histories of convergence of L^2-norm of the potential and reconstructive potential errors, considering $k \in \{0, 1, 2, 3, 4\}$ (Example 6)

L^2-norm of the potential error										
	$k=0$		$k=1$		$k=2$		$k=3$		$k=4$	
h	error	rate	error	rate	error	rate	error	rate	error	rate
1.31e-01	3.25e-01		1.24e+00		5.13e-01		5.88e-02		9.96e-02	
7.32e-02	5.95e-01	-1.041	1.48e-01	3.650	3.63e-02	4.553	8.26e-03	3.374	1.38e-03	7.358
3.66e-02	1.46e-01	2.024	1.77e-02	3.064	2.65e-03	3.776	2.87e-04	4.848	2.13e-05	6.014
1.83e-02	3.64e-02	2.006	2.04e-03	3.113	1.75e-04	3.922	9.23e-06	4.957	3.26e-07	6.030
9.15e-03	9.10e-03	2.002	2.45e-04	3.057	1.11e-05	3.978	2.91e-07	4.988	5.03e-09	6.015
4.58e-03	2.27e-03	2.004	3.02e-05	3.025	6.96e-07	4.000	9.11e-09	5.005	7.94e-11	5.996
L^2-norm of the reconstructive potential error										
	$k=0$		$k=1$		$k=2$		$k=3$		$k=4$	
h	error	rate	error	rate	error	rate	error	rate	error	rate
1.31e-01	2.40e+00		1.28e+00		5.24e-01		6.19e-02		9.99e-02	
7.32e-02	6.40e-01	2.269	1.55e-01	3.624	3.68e-02	4.563	8.29e-03	3.454	1.38e-03	7.358
3.66e-02	1.56e-01	2.038	1.85e-02	3.065	2.67e-03	3.784	2.88e-04	4.849	2.13e-05	6.013
1.83e-02	3.87e-02	2.010	2.14e-03	3.117	1.76e-04	3.924	9.26e-06	4.957	3.27e-07	6.029
9.15e-03	9.66e-03	2.003	2.56e-04	3.060	1.12e-05	3.978	2.92e-07	4.988	5.05e-09	6.015
4.58e-03	2.41e-03	2.004	3.16e-05	3.026	7.01e-07	4.000	9.14e-09	5.005	7.97e-11	5.996

7.7 Example 7: Non smooth solution in non convex Ω

Given $\Omega_1 = (-2,2)^2 \setminus [-1,2] \times [-2,1]$ *and* $\Omega_2 := (-3,3)^2 \setminus (\overline{\Omega}_1 \cup [0,3] \times [-3,0])$*, we solve* (38)*, with* f_1*,* f_2*,* g_1*,* g_2 *and* g *given so that the exact solution is*

$$u_1(x,y) = \frac{xy}{x^2+y^2} - \frac{13\ln(2) - 5\ln(5)}{14} \quad , \quad u_2(r,\theta) = r^{2/3}\sin(2\theta/3) - c\,, \tag{143}$$

where u_2 *is given in polar coordinates, and* c *is a real constant such that* u_2 *has zero mean value in* Ω_2*. We pointwise that* $u_2 \in H^{1+2/3-\epsilon}(\Omega_2)$*, for an arbitrary small number* $\epsilon > 0$*, since its gradient has a singularity at origin. The family of simplicial meshes we consider here, is the same as in Example 7.6, and we approximate also the exact solution of* (1) *with polynomials of degree at most* $k \in \{0,1,2,3,4\}$*. The numerical results, obtained by the HHO method, can be seen in Tables 22, 23 and 24. They are also displayed in Figures 30, 31 and 32, respectively. We notice here that the non smoothness of* u_2 *affects the rates of convergence of the energy norm of the potential error, the flux error, the discrete norm of trace error, in the sense that they are not the optimal ones established in Theorem 5.1. On the other hand, we notice also that the potential and reconstructive potential errors decay to zero as* $\mathcal{O}(h^{2/3})$*, for any of the values of* k *we have considered in this simulation. This situation is not covered by our current analysis, and motivate us to obtain an a posteriori error estimator that could help us to improve the quality of the approximation. This could be the subject of future work.*

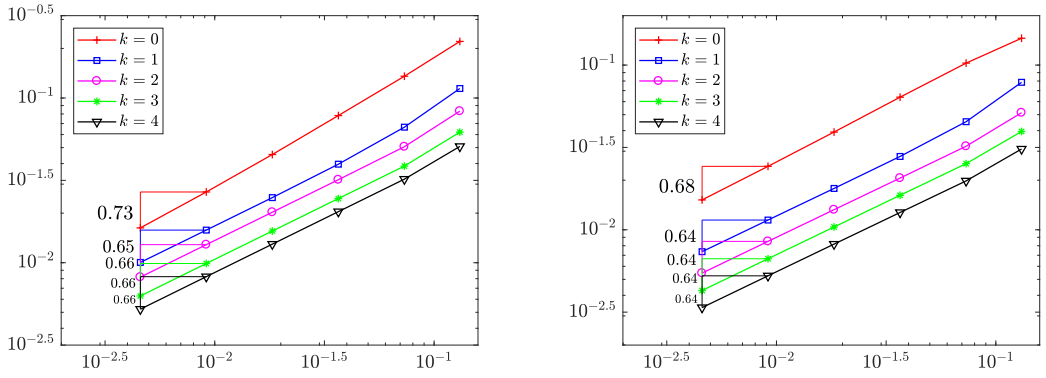

(a) Energy norm of the potential error vs. h

(b) L^2-norm of the flux error vs. h

Figure 30: Rates of convergence of the (a) energy norm of the potential error, and (b) flux error (Example 7)

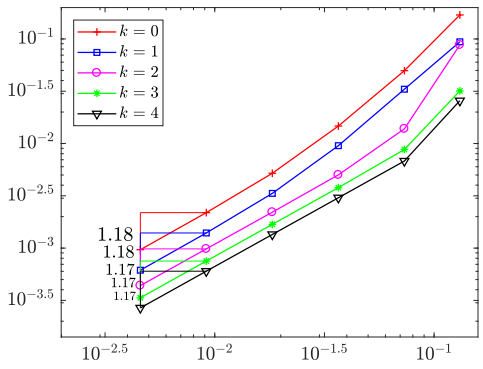

(a) $||\widehat{\xi}_h - \xi_h||_{\Gamma_{1,h}}$ vs. h

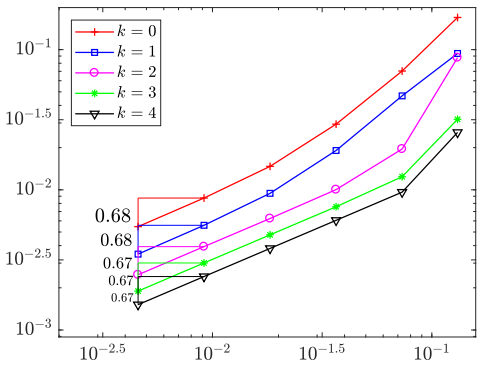

(b) $||\widehat{\xi}_h - \xi_h||_{0,\Gamma_1}$ vs. h

Figure 31: Rates of convergence of the Lagrange multiplier considering the (a) Discrete trace norm $||\cdot||_{\Gamma_{1,h}}$, and (b) Standard L^2-norm (Example 7)

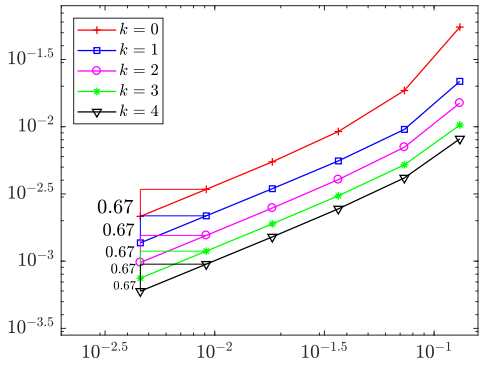

(a) L^2-norm of the potential error vs. h

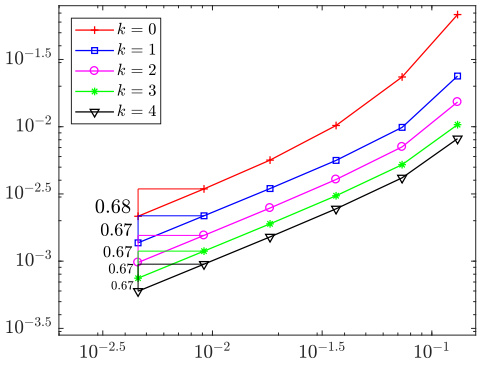

(b) L^2-norm of the reconstructive potential error vs. h

Figure 32: Rates of convergence of the L^2-norm of the (a) potential error, and (b) reconstructive potential error (Example 7)

Table 22: Histories of convergence of the energy norm of the potential error and L^2-norm of the flux error, considering $k \in \{0, 1, 2, 3, 4\}$ (Example 7)

Energy norm of the potential error										
	$k=0$		$k=1$		$k=2$		$k=3$		$k=4$	
h	error	rate	error	rate	error	rate	error	rate	error	rate
1.31e-01	2.21e-01		1.14e-01		8.32e-02		6.21e-02		5.08e-02	
7.32e-02	1.36e-01	0.836	6.65e-02	0.928	5.06e-02	0.855	3.86e-02	0.816	3.22e-02	0.786
3.66e-02	7.83e-02	0.793	3.97e-02	0.747	3.19e-02	0.665	2.45e-02	0.655	2.04e-02	0.655
1.83e-02	4.54e-02	0.786	2.49e-02	0.674	2.03e-02	0.655	1.56e-02	0.655	1.30e-02	0.655
9.15e-03	2.69e-02	0.755	1.58e-02	0.655	1.29e-02	0.655	9.89e-03	0.655	8.23e-03	0.656
4.58e-03	1.63e-02	0.726	1.00e-02	0.653	8.18e-03	0.656	6.28e-03	0.656	5.22e-03	0.657
L^2-norm of the flux error										
	$k=0$		$k=1$		$k=2$		$k=3$		$k=4$	
h	error	rate	error	rate	error	rate	error	rate	error	rate
1.31e-01	1.45e-01		7.86e-02		5.14e-02		3.95e-02		3.09e-02	
7.32e-02	1.03e-01	0.597	4.53e-02	0.946	3.22e-02	0.805	2.52e-02	0.773	1.98e-02	0.766
3.66e-02	6.38e-02	0.687	2.79e-02	0.701	2.06e-02	0.642	1.62e-02	0.639	1.27e-02	0.637
1.83e-02	3.92e-02	0.703	1.78e-02	0.645	1.32e-02	0.638	1.04e-02	0.639	8.18e-03	0.638
9.15e-03	2.43e-02	0.691	1.15e-02	0.638	8.50e-03	0.639	6.67e-03	0.640	5.25e-03	0.639
4.58e-03	1.52e-02	0.678	7.36e-03	0.639	5.46e-03	0.641	4.28e-03	0.642	3.37e-03	0.641

Table 23: Histories of convergence of the L^2-projection of $\xi - \xi_h$ in $||\cdot||_{\Gamma_{1,h}}$ and $||\cdot||_{0,\Gamma_1}$ norms, for $k \in \{0, 1, 2, 3, 4\}$ (Example 7)

$\|\widehat{\xi_h} - \xi_h\|_{\Gamma_{1,h}}$										
	$k=0$		$k=1$		$k=2$		$k=3$		$k=4$	
h	error	rate	error	rate	error	rate	error	rate	error	rate
1.31e-01	1.70e-01		9.39e-02		8.77e-02		3.18e-02		2.57e-02	
7.32e-02	4.97e-02	2.107	3.31e-02	1.792	1.38e-02	3.174	8.77e-03	2.216	6.80e-03	2.281
3.66e-02	1.47e-02	1.759	9.54e-03	1.795	5.01e-03	1.463	3.79e-03	1.212	3.03e-03	1.168
1.83e-02	5.20e-03	1.500	3.34e-03	1.515	2.21e-03	1.185	1.69e-03	1.166	1.35e-03	1.166
9.15e-03	2.18e-03	1.251	1.40e-03	1.257	9.83e-04	1.166	7.52e-04	1.166	6.01e-04	1.166
4.58e-03	9.65e-04	1.179	6.15e-04	1.185	4.38e-04	1.168	3.35e-04	1.168	2.68e-04	1.168
$\|\widehat{\xi_h} - \xi_h\|_{0,\Gamma_1}$										
	$k=0$		$k=1$		$k=2$		$k=3$		$k=4$	
h	error	rate	error	rate	error	rate	error	rate	error	rate
1.31e-01	1.70e-01		9.39e-02		8.77e-02		3.18e-02		2.57e-02	
7.32e-02	7.03e-02	1.512	4.68e-02	1.197	1.95e-02	2.578	1.24e-02	1.621	9.62e-03	1.685
3.66e-02	2.94e-02	1.259	1.91e-02	1.295	1.00e-02	0.963	7.57e-03	0.712	6.06e-03	0.668
1.83e-02	1.47e-02	1.000	9.44e-03	1.015	6.24e-03	0.685	4.77e-03	0.666	3.82e-03	0.666
9.15e-03	8.73e-03	0.751	5.58e-03	0.757	3.93e-03	0.666	3.01e-03	0.666	2.41e-03	0.666
4.58e-03	5.46e-03	0.678	3.48e-03	0.684	2.48e-03	0.667	1.89e-03	0.667	1.52e-03	0.668

Table 24: Histories of convergence of L^2-norm of the potential and reconstructive potential errors, considering $k \in \{0, 1, 2, 3, 4\}$ (Example 7)

L^2-norm of the potential error										
	$k=0$		$k=1$		$k=2$		$k=3$		$k=4$	
h	error	rate	error	rate	error	rate	error	rate	error	rate
1.31e-01	5.51e-02		2.17e-02		1.50e-02		1.03e-02		8.12e-03	
7.32e-02	1.86e-02	1.866	9.55e-03	1.414	7.04e-03	1.300	5.20e-03	1.170	4.16e-03	1.149
3.66e-02	9.21e-03	1.014	5.56e-03	0.779	4.04e-03	0.800	3.06e-03	0.765	2.45e-03	0.764
1.83e-02	5.48e-03	0.748	3.46e-03	0.686	2.48e-03	0.703	1.89e-03	0.693	1.52e-03	0.693
9.15e-03	3.42e-03	0.680	2.17e-03	0.670	1.55e-03	0.676	1.19e-03	0.674	9.50e-04	0.673
4.58e-03	2.15e-03	0.669	1.37e-03	0.668	9.77e-04	0.670	7.47e-04	0.669	5.98e-04	0.669
L^2-norm of the reconstructive potential error										
	$k=0$		$k=1$		$k=2$		$k=3$		$k=4$	
h	error	rate	error	rate	error	rate	error	rate	error	rate
1.31e-01	6.82e-02		2.38e-02		1.53e-02		1.04e-02		8.15e-03	
7.32e-02	2.34e-02	1.836	9.89e-03	1.510	7.08e-03	1.319	5.22e-03	1.177	4.17e-03	1.152
3.66e-02	1.02e-02	1.199	5.62e-03	0.816	4.05e-03	0.806	3.07e-03	0.768	2.45e-03	0.766
1.83e-02	5.64e-03	0.855	3.47e-03	0.696	2.48e-03	0.705	1.89e-03	0.694	1.52e-03	0.694
9.15e-03	3.45e-03	0.711	2.17e-03	0.673	1.55e-03	0.677	1.19e-03	0.674	9.50e-04	0.674
4.58e-03	2.16e-03	0.677	1.37e-03	0.669	9.77e-04	0.670	7.47e-04	0.669	5.98e-04	0.669

Conclusions

In this paper we have proposed a new mixed HHO formulation to approximate the solution of a transmission interior elliptic problem, with non homogeneous transmission boundary conditions. First, we derive the variational formulation, at continuous level, introducing the normal trace on the transmission boundary, of the solution living in inner subdomain, as an auxiliary unknown. In practice, this unknown acts as a Lagrange multiplier. Then, we propose a discrete variational scheme, applying the HHO approach. Although we have considered, for simplicity, a family of uniform simplicial meshes for the current analysis, it is possible to extend it to deal with polytopal meshes, as in [19].

We have proven that our discrete mixed HHO scheme is well-posed and convergent in the energy-norm, as well as in the usual L^2-norm. Our a priori error estimates establish that when we approximate the solution with piecewise polynomial of degree at most $k \geq 0$, the flux and energy norm of the potential error go to zero with optimal order of convergence $k + \delta$, while the L^2-norm of potential and reconstructive potential errors' orders behave as $\mathcal{O}^{k+1+\delta}$, for some $\delta \in (1/2, 1]$ (cf. Theorems 5.1, 5.2 and 5.3). The L^2-projection of the error of Lagrange multiplier is measured in a suitable weighted L^2-norm (cf. (29)*), and converges, at least, with order $k+\delta$ (cf. Theorem 5.1). We also have computed the classical L^2-norm of this projection, noticing a convergence that decays to* 0 *as* $\mathcal{O}(h^{k+\delta-1/2})$.

Numerical examples, provided in this work, are in agreement with our theoretical results. In particular, results from Examples 7.1, 7.2, and 7.3.1, show us that our theoretical rates of convergence are achieved. In Example 7.5, we consider as exact solution a function that lives in

$H^4(\Omega_1)$ but not in $H^5(\Omega_1)$. According to Theorems 5.1, 5.2 and 5.3, we should expect optimal order of convergence for the energy norm of the potential error, the flux error in the L^2-norm, the weighted L^2- norm of the error of the Lagrange multiplier, the potential and the reconstructive potential errors in the L^2-norm, when the solution is approximated by piecewise polynomials of degree at most $k \leq 3$, which is what we observe in Tables 16, 17, and 18, whose results are also displayed in Figures 23, 24 and 25, respectively.

On the other hand, since the exact solution in Example 7.4 is non regular, we do not expect to obtain optimal rates of convergence. The results are displayed in Figures 20, 21 and 22, and reported in Tables 13, 14 and 15. Then, we just confirm that results from these tables are in agreement with Theorems 5.1, 5.2 and 5.3, for $q = 0$ and $k \in \{1, 2, 3, 4\}$. Surprisingly, we notice an unexpected (better) behavior of the errors for $k = 0$. As a consequence, this motivates us to develop, an a posteriori error analysis, in order to improve the quality of approximation and recover the optimal rate of convergence, if possible. This would be the subject of a future work.

We recall that in Example 7.3.2, we have performed our HHO approach, considering a family of simplicial meshes having hanging nodes only on the transmission boundary Γ_1. We observe that the convergence of the method behaves similarly as when we solve the same problem considering a family of conforming meshes (see Example 7.3.1), despite the fact that our analysis, in its current form, does not covered the use of family of meshes with hanging nodes on Γ_1. This could also be the subject of future work, taking the analysis developed in [50] as reference.

It is important to emphasize that the proofs of Theorems 5.2 and 5.3 rely on the well known elliptic regularity property (90)*, which can be established if we assume that $\Omega := \Omega_1 \cup \Gamma_1 \cup \Omega_2$ is a convex domain. In this sense, and with the aim of testing the robustness of our computational implementation to deal with non-convex domain Ω (cf. Figure 26), we consider Examples 7.6 and 7.7. We consider an smooth solution in Example 7.6, and the numerical results we obtain are surprisingly in agreement with Theorems 5.2 and 5.3 (and of course with Theorem 5.1, too), despite the our current theory does not support them. In Example 7.7, the solution is non smooth, and then, we do not expect optimal rates of convergence. The results have been reported in Tables 22, 23 and 24, and confirm our suspicious. As in Example 7.4, it would be desirable to find an a posteriori error estimator for this problem, that let us to improve our approximation and get the optimal convergence's behaviour.*

Finally, we point out that the analysis described in this paper, can be applied and/or extended to deal with linear transmission problems with variable diffusion, and / or with other type of boundary conditions on the external boundary of Ω_2. In addition, taking into account [26] and [20], we are motivated to extend this approach to deal with certain class of nonlinear transmission problems.

Appendix

In what follows, we write down the proof of Lemma 4.2, for a general $\Omega := \Omega_1 \cup \Gamma_1 \cup \Omega_2$ (convex or non convex domain).

To this aim, given $\underline{\mathbf{v}}_h := \left(\underline{\mathbf{v}}_{\mathcal{T}_{1,h}}, \underline{\mathbf{v}}_{\mathcal{T}_{2,h}}\right) \in \underline{\mathbf{U}}_{\mathcal{T}_h}^{k,0}$, where we recall $\mathcal{T}_h := \mathcal{T}_{1,h} \cup \mathcal{T}_{2,h}$, we

introduce $w_h \in \mathbb{P}_h^k(\mathcal{T}_h)$*, such that*

$$w_h\Big|_T := w_T := \begin{cases} v_{1,T}\ ,\ T \in \mathcal{T}_{1,h}\,, \\ v_{2,T}\ ,\ T \in \mathcal{T}_{2,h}\,. \end{cases}$$

We notice that $(w_h,1)_\Omega = (v_{1,h},1)_{\Omega_1} + (v_{2,h},1)_{\Omega_2} = 0$*, since* $\underline{\mathbf{U}}_h^{k,0}$*. Then, we define* $\underline{\mathbf{w}}_h := \Big((w_T)_{T\in\mathcal{T}_h},(w_F)_{F\in\mathcal{F}_h}\Big) \in \underline{\mathbf{W}}_h^{k,0} := \big\{\underline{\mathbf{z}}_h \in \underline{\mathbf{W}}_h^k \,|\, (z_h,1)_\Omega = 0\big\}$*, where* $\underline{\mathbf{W}}_h^k$ *collects the DOF's on* Ω*, such that*

$w_F := \begin{cases} v_{F,1}\ ,\ F \in \mathcal{F}_{1,h}\backslash\Gamma_{1,h} \\ v_{F,2}\ ,\ F \in \mathcal{F}_{2,h} \end{cases}$ *. Then, applying Theorem 6.5 in [33], we infer that*

$$||v_{1,h}||_{0,\Omega_1}^2 + ||v_{2,h}||_{0,\Omega_2}^2 = ||w_h||_{0,\Omega}^2 \lesssim ||\underline{\mathbf{w}}_h||_{1,h}^2\,. \tag{144}$$

Using the definition of $\|\cdot\|_{1,h}$*, and that* $\displaystyle\sum_{T\in\mathcal{T}_h}\|\nabla w_T\|_{0,T}^2 = \sum_{T\in\mathcal{T}_{1,h}}\|\nabla v_{1,T}\|_{0,T}^2 + \sum_{T\in\mathcal{T}_{2,h}}\|\nabla v_{2,T}\|_{0,T}^2$*, we obtain*

$$\|\underline{\mathbf{w}}_h\|_{1,h}^2 = \sum_{T\in\mathcal{T}_{1,h}}\|\nabla v_{1,T}\|_{0,T}^2 + \sum_{T\in\mathcal{T}_{2,h}}\|\nabla v_{2,T}\|_{0,T}^2 + \sum_{T\in\mathcal{T}_h}\sum_{F\in\mathcal{F}_T} h_F^{-1}\|w_F - w_T\|_{0,F}^2, \tag{145}$$

Then, given $F \in \Gamma_{1,h}$ *(transmission face), there exist* $T \in \mathcal{T}_{1,h}$ *and* $S \in \mathcal{T}_{2,h}$*, such that* $F \subset \partial T \cap \partial S$*, and using definition of* $\underline{\mathbf{w}}_h$*, we obtain*

$$\|w_F - w_T\|_{0,F}^2 + \|w_F - w_S\|_{0,F}^2 = \|v_{2,F} - v_{1,T}\|_{0,F}^2 + \|v_{2,F} - v_{2,S}\|_{0,F}^2\,, \tag{146}$$

and by triangle inequality on the first term on the right hand side, we obtain

$$\|w_F - w_T\|_{0,F}^2 + \|w_F - w_S\|_{0,F}^2 \lesssim \|v_{2,F} - v_{1,F}\|_{0,F}^2 + \|v_{1,F} - v_{1,T}\|_{0,F}^2 + \|v_{2,F} - v_{2,S}\|_{0,F}^2\,. \tag{147}$$

Thus, we can write the third term on the right hand of (145), as

$$\begin{aligned}\sum_{T\in\mathcal{T}_h}\sum_{F\in\mathcal{F}_T} h_F^{-1}\|w_F - w_T\|_{0,F}^2 \lesssim \sum_{T\in\mathcal{T}_{1,h}}\sum_{F\in\mathcal{F}_T} h_F^{-1}\|v_{1,F} - v_{1,T}\|_{0,F}^2 + \\ + \sum_{S\in\mathcal{T}_{2,h}}\sum_{F\in\mathcal{F}_T} h_F^{-1}\|v_{2,F} - v_{2,S}\|_{0,F}^2 + \sum_{F\in\Gamma_{1,h}} h_F^{-1}\|v_{2,F} - v_{1,F}\|_{0,F}^2\,.\end{aligned} \tag{148}$$

Replacing (148) in (145), we have that

$$\|\underline{\boldsymbol{w}}_h\|_{1,h}^2 \lesssim \|\underline{\mathbf{v}}_{1,h}\|_{1,h}^2 + \|\underline{\mathbf{v}}_{2,h}\|_{1,h}^2 + \sum_{F\in\Gamma_{1,h}} h_F^{-1}\|v_{2,F} - v_{1,F}\|_{0,F}^2\,. \tag{149}$$

Finally, from (144) *and* (149)*, we conclude the proof.*

References

[1] ABBAS, M., ERN, A., AND PIGNET, N. *Hybrid high-order methods for finite deformations of hyperelastic materials.* Computational Mechanics 62*, 4 (2018), 909–928.

[2] AGHILI, J., BOYAVAL, S., AND DI PIETRO, D. *Hybridization of mixed high-order methods on general meshes and application to the Stokes equations.* Computational Methods in Applied Mathematics 15*, 2 (2015), 111–134.*

[3] AYUSO DE DIOS, B., LIPNIKOV, K., AND MANZINI, G. *The nonconforming virtual element method.* ESAIM: Mathematical Modelling and Numerical Analysis 50*, 3 (2016), 879–904.*

[4] BABUŠKA, I. *The finite element method for elliptic equations with discontinuous coefficients.* Computing 5*, 3 (1970), 207–213.*

[5] BABUŠKA, I., AND MELENK, J. *The partition of unity finite element method: basic theory and applications.* Computer methods in applied mechanics and engineering 139*, 1 (1996), 289–314.*

[6] BALAY, S., BROWN, J., BUSCHELMAN, K., GROPP, W., KAUSHIK, D., KNEPLEY, M., CURFMAN MCINNES, L., SMITH, B., AND ZHANG, H. *Petsc.* `http://www.mcs.anl.gov/petsc`*, 2011.*

[7] BARRENECHEA, G., GATICA, G. N., AND THOMAS, J.-M. *Primal mixed formulations for the coupling of FEM and BEM. Part I: Linear problems.* Numerical Functional Analysis and Optimization 19 *(1998), 7–32.*

[8] BARRETT, J., AND ELLIOT, C. *Fitted and unfitted finite-element methods for elliptic equations with smooth interfaces.* IMA Journal of Numerical Analysis 7 *(1987), 283–300.*

[9] BOS, F., AND GRAVEMEIER, V. *Numerical simulation of premixed combustion using an enriched finite element method.* Journal of Computational Physics 228 *(2009), 3605–3624.*

[10] BOTTI, L., DI PIETRO, D. A., AND DRONIOU, J. *A hybrid high-order method for the incompressible Navier-Stokes equations based on Temam's device.* Journal of Computational Physics 376 *(2019), 786 – 816.*

[11] BOTTI, M., DI PIETRO, D., AND SOCHALA, P. *A hybrid high-order method for nonlinear elasticity.* SIAM Journal on Numerical Analysis 55*, 6 (2017), 2687–2717.*

[12] BRAMBLE, J. H., AND KING, J. T. *A finite element method for interface problems in domains with smooth boundaries and interfaces.* Advances in Computational Mathematics 6*, 1 (1996), 109–138.*

[13] BURMAN, E., AND ERN, A. *An Unfitted Hybrid High-Order Method for Elliptic Interface Problems.* SIAM Journal on Numerical Analysis 56*, 3 (2017), 1525–1546.*

[14] BURMAN, E., AND FERNÁNDEZ, M. *An unfitted Nitsche method for incompressible fluid-structure interaction using overlapping meshes.* Computer Methods in Applied Mechanics and Engineering 279 *(2014), 497–514.*

[15] BUSTINZA, R., GARCÍA, G. C., AND GATICA, G. N. *A mixed finite element method with Lagrange multipliers for nonlinear exterior transmission problems.* Numerische Mathematik 96 *(2004), 481–523.*

[16] BUSTINZA, R., AND GATICA, G. N. *A Local Discontinuous Galerkin Method for Nonlinear Diffusion Problems with Mixed Boundary Conditions.* SIAM Journal Scientific Computing 26 *(2004), 152–177.*

[17] BUSTINZA, R., GATICA, G. N., AND SAYAS, F.-J. A LDG-BEM Coupling for a Class of Nonlinear Exterior Transmission Problems. *Springer, Berlin, Heidelberg, 2006, pp. 1129–1136.*

[18] BUSTINZA, R., GATICA, G. N., AND SAYAS, F.-J. *On the coupling of local discontinuous Galerkin and boundary element methods for non-linear exterior transmission problems.* IMA Journal of Numerical Analysis 28 *(2007), 225–244.*

[19] BUSTINZA, R., AND MUNGUIA-LA-COTERA, J. *A hybrid high-order formulation for a Neumann problem on polytopal meshes.* Numerical Methods for Partial Differential Equations 36*, 3 (2020), 524–551.*

[20] BUSTINZA, R., AND MUNGUIA-LA-COTERA, J. *An a priori error analysis for a class of nonlinear elliptic problems with the hybrid high-order method.* Centro de Investigación en Ingeniería Matemática, Universidad de Concepción, Chile *(2020). Pre-print 2020-08.*

[21] CHEN, L., WEI, H., AND WEN, M. *An interface-fitted mesh generator and virtual element methods for elliptic interface problems.* Journal of Computational Physics 334 *(2017), 327–348.*

[22] CHEN, Z., AND ZOU, J. *Finite element methods and their convergence for elliptic and parabolic interface problems.* Numerische Mathematik 79 *(1998), 175–202.*

[23] CHU, C.-C., GRAHAM, I., AND HOU, T.-Y. *A new multiscale finite element method for high-contrast elliptic interface problems.* Mathematics of Computation 79*, 272 (2010), 1915–1955.*

[24] COCKBURN, B., GOPALAKRISHNAN, J., AND LAZAROV, R. *Unified Hybridization of Discontinuous Galerkin, Mixed, and Continuous Galerkin Methods for Second Order Elliptic Problems.* SIAM Journal on Numerical Analysis 47 *(2009), 1319–1365.*

[25] DEMMEL, J. W., EISENSTAT, S. C., GILBERT, J. R., LI, X. S., AND LIU, J. W. H. *A supernodal approach to sparse partial pivoting.* SIAM Journal of Matrix Analysis and Applications 20*, 3 (1999), 720–755.*

[26] DI PIETRO, D., AND DRONIOU, J. *A Hybrid High-Order method for Leray–Lions elliptic equations on general meshes.* Mathematics of Computation 86*, 307 (2017), 2159–2191.*

[27] DI PIETRO, D., AND DRONIOU, J. *$W^{s,p}$-approximation properties of elliptic projectors on polynomial spaces, with application to the error analysis of a Hybrid High-Order discretisation of Leray-Lions problems.* Mathematical Models and Methods in Applied Sciences 27*, 5 (2017), 879–908.*

[28] DI PIETRO, D., DRONIOU, J., AND ERN, A. *A discontinuous-skeletal method for advection-diffusion-reaction on general meshes.* SIAM Journal on Numerical Analysis 53 *(2015), 2135 – 2157.*

[29] DI PIETRO, D., AND ERN, A. Mathematical Aspects of Discontinuous Galerkin Methods*, vol. 69 of* Mathématiques et Applications*. Springer-Verlag, Berlin, 2012.*

[30] DI PIETRO, D., AND ERN, A. *A hybrid high-order locking-free method for linear elasticity on general meshes.* Computer Methods in Applied Mechanics and Engineering 283 *(2014), 1–21.*

[31] DI PIETRO, D., AND ERN, A. *Hybrid High-Order methods for variable diffusion problems on general meshes.* Comptes Rendus Mathematique 353*, 1 (2015), 31–34.*

[32] DI PIETRO, D., ERN, A., AND LEMAIRE, S. *An Arbitrary-Order and Compact-Stencil Discretization of Diffusion on General Meshes Based on Local Reconstruction Operators.* Computational Methods in Applied Mathematics 14*, 4 (2014), 461–472.*

[33] DI PIETRO, D. A., AND DRONIOU, J. The Hybrid High-Order Method for Polytopal Meshes: Design, Analysis, and Applications*., vol. 19 of* Modeling, Simulation and Applications series*. Springer International Publishing, 2020. 528 pages.*

[34] DI PIETRO, D. A., ERN, A., AND LEMAIRE, S. *A Review of Hybrid High-Order Methods: Formulations, Computational Aspects, Comparison with Other Methods. In* Building Bridges: Connections and Challenges in Modern Approaches to Numerical Partial Differential Equations*, G. R. Barrenechea, F. Brezzi, A. Cangiani, and E. H. Georgoulis, Eds., vol. 114. Springer International Publishing, Cham, 2016, ch. 7, pp. 205–236. Lecture Notes in Computational Science and Engineering.*

[35] DOLBOW, J., AND HARARI, I. *Erratum: An efficient finite element method for embedded interface problems.* International Journal for Numerical Methods in Engineering 78 *(2009), 229–252.*

[36] DONG, H., WANG, B., XIE, Z., AND WANG, L.-L. *An unfitted hybridizable discontinuous Galerkin method for the Poisson interface problem and its error analysis.* IMA Journal of Numerical Analysis 37*, 1 (2016), 444–476.*

[37] ESSER, P., GRANDE, J., AND REUSKEN, A. *An extended finite element method applied to levitated droplet problems.* International Journal for Numerical Methods in Engineering 84 *(2010), 757–773.*

[38] FEISTAUER, M. *Mathematical and numerical study of nonlinear problems in fluid mechanics. In* Proceedings of the International Conference on Differential Equations and their Applications (Equadiff 6) *(1986), vol. 1192, Springer-Verlag Berlin Heidelberg, pp. 3–16.*

[39] FEISTAUER, M. *On the finite element approximation of a cascade flow problem.* Numerische Mathematik 50 *(1987), 655–684.*

[40] G. GUENNEBAUD AND B. JACOB. *Eigen v3. http://eigen.tuxfamily.org, 2010.*

[41] GATICA, G. N. Introducción al Análisis Funcional. Teoría y Aplicaciones. *Reverté Ediciones S.A. de C.V., 2014.*

[42] GATICA, G. N. A simple introduction to the mixed finite element method. Theory and applications. *SpringerBriefs in Mathematics. Springer, Cham, 2014.*

[43] GATICA, G. N., AND MEDDAHI, S. *A dual-dual mixed formulation for nonlinear exterior transmission problems.* Mathematics of Computation 70 *(2001), 1461–1480.*

[44] GATICA, G. N., AND SAYAS, F.-J. *A note on the local approximation properties of piecewise polynomials with applications to LDG methods.* Complex Variables 51 *(2006), 109–117.*

[45] GATICA, G. N., AND SAYAS, F.-J. *An a priori error analysis for the coupling of local discontinuous Galerkin and boundary element methods.* Mathematics of Computation 75 *(2006), 1675–1696.*

[46] GONG, Y., LI, B., AND LI, Z. *Immersed interface finite element methods for elliptic interface problems with nonhomogeneous jump conditions.* SIAM Journal on Numerical Analysis 46*, 1 (2008), 472–495.*

[47] GRISVARD, P. Elliptic problems in nonsmooth domains. *Classics in Applied Mathematics. SIAM, USA, 2011. Reprint of the 1983 edition.*

[48] GUYOMARC'H, G., LEE, C.-O., AND JEON, K. *A discontinuous Galerkin method for elliptic interface problems with application to electroporation.* Communications in Numerical Methods in Engineering 25*, 10 (2009), 991 – 1008.*

[49] HANSBO, A., AND HANSBO, P. *An unfitted finite element method based on Nitsche's method for elliptic interface problems.* Computer Methods in Applied Mechanics and Engineering 191 *(2002), 5537–5552.*

[50] HANSBO, P., LOVADINA, C., PERUGIA, I., AND SANGALLI, G. *A Lagrange multiplier method for the finite element solution of elliptic interface problems using non-matching meshes.* Numerische Mathematik 100*, 1 (2005), 91–115.*

[51] HEISE, B. *Nonlinear Field Calculations with Multigrid-Newton Methods.* IMPACT of Computing in Science and Engineering 5*, 2 (1993), 75 – 110.*

[52] HEISE, B. *Analysis of a Fully Discrete Finite Element Method for a Nonlinear Magnetic Field Problem.* SIAM Journal on Numerical Analysis 31*, 3 (1994), 745–759.*

[53] HU, W.-F., LAI, M.-C., AND YOUNG, Y.-N. *A hybrid immersed boundary and immersed interface method for electrohydrodynamic simulations.* Journal of Computational Physics 282 *(2015), 47–61.*

[54] HUYNH, L., NGUYEN, N., PERAIRE, J., AND KHOO, B. *A high-order hybridizable discontinuous Galerkin method for elliptic interface problems.* International Journal for Numerical Methods in Engineering 93 *(2013), 183–200.*

[55] KUMMER, F., AND OBERLACK, M. *An Extension of the Discontinuous Galerkin Method for the Singular Poisson Equation.* SIAM Journal on Scientific Computing 35*, 2 (2013), A603–A622.*

[56] LEMAIRE, S. *Bridging the hybrid high-order and virtual element methods.* IMA Journal of Numerical Analysis *(Published online).*

[57] LEVEQUE, R. J., AND LI, Z. *The immersed interface method for elliptic equations with discontinuous coefficients and singular sources.* SIAM Journal on Numerical Analysis 31*, 4 (1994), 1019–1044.*

[58] LIPNIKOV, K., AND MANZINI, G. *A high-order mimetic method on unstructured polyhedral meshes for the diffusion equation.* Journal of Computational Physics 272 *(2014), 360 – 385.*

[59] MOES, N., DOLBOW, J., AND BELYTSCHKO, T. *A finite element method for crack growth without remeshing.* International Journal for Numerical Methods in Engineering 46*, 1 (1999), 131–150.*

[60] SAYAS, F. J., BROWN, T. S., AND HASSEL, M. E. Variational techniques for elliptic partial differential equations. Theoretical tools and advanced applications. *CRC Press. TAYLOR & Francis Group, LCC, 2019.*

[61] SETHIAN, J. Level Set Methods and Fast Marching Methods Evolving Interfaces in Computational Geometry, Fluid Mechanics, Computer Vision, and Materials Science. *Cambridge University Press, 1999.*

[62] VEIGA, L., BREZZI, F., CANGIANI, A., MANZINI, G., MARINI, L., AND RUSSO, A. *Basic principles of virtual element methods.* Mathematical Models and Methods in Applied Sciences 23 *(2012).*

[63] WANG, B., AND KHOO, B. *Hybridizable discontinuous Galerkin method (HDG) for Stokes interface flow.* Journal of Computational Physics 247 *(2013), 262 – 278.*

[64] WANG, Q., AND CHEN, J. *An unfitted discontinuous Galerkin method for elliptic interface problems.* J. Appl. Math. *(2014), Art. ID 241890, 9.*

[65] ZHENG, X., AND LOWENGRUB, J. *An interface-fitted adaptive mesh method for elliptic problems and its application in free interface problems with surface tension.* Advances in Computational Mathematics 42 *(2016).*

Centro de Investigación en Ingeniería Matemática (CI^{2}MA)

PRE-PUBLICACIONES 2019 - 2020

2019-47 Raimund Bürger, Sarvesh Kumar, David Mora, Ricardo Ruiz-Baier, Nitesh Verma: *Virtual element methods for the three-field formulation of time-dependent linear poroelasticity*

2019-48 Gabriel R. Barrenechea, Fabrice Jaillet, Diego Paredes, Frederic Valentin: *The multiscale hybrid mixed method in general polygonal meshes*

2020-01 Sergio Caucao, Gabriel N. Gatica, Ricardo Oyarzúa, Nestor Sánchez: *A fully-mixed formulation for the steady double-diffusive convection system based upon Brinkman–Forchheimer equations*

2020-02 Gonzalo A. Benavides, Leonardo E. Figueroa: *Orthogonal polynomial projection error in Dunkl-Sobolev norms in the ball*

2020-03 Rodolfo Araya, Abner Poza, Frederic Valentin: *An adaptative multiscale hybrid-mixed method for the Oseen equations*

2020-04 Carlos Parés, David Zorío: *Lax Wendroff approximate Taylor methods with fast and optimized weighted essentially non-oscillatory reconstructions*

2020-05 Julio Aracena, Lilian Salinas: *Finding the fixed points of a Boolean network from a positive feedback vertex set*

2020-06 Tomás Barrios, Rommel Bustinza, Camila Campos: *A note on a posteriori error estimates for dual mixed methods*

2020-07 Raimund Bürger, Elvis Gavilán, Daniel Inzunza, Pep Mulet, Luis M. Villada: *Numerical simulation of forest fires by IMEX methods*

2020-08 Rommel Bustinza, Jonathan Munguia: *An a priori error analysis for a class of nonlinear elliptic problems applying the hybrid high-order method*

2020-09 Ngoc-Cuong Nguyen, Jaime Peraire, Manuel Solano, Sébastien Terrana: *An HDG method for non-matching meshes*

2020-10 Rommel Bustinza, Jonathan Munguia: *A mixed Hybrid High-Order formulation for linear interior transmission elliptic problems*

Para obtener copias de las Pre-Publicaciones, escribir o llamar a: Director, Centro de Investigación en Ingeniería Matemática, Universidad de Concepción, Casilla 160-C, Concepción, Chile, Tel.: 41-2661324, o bien, visitar la página web del centro: http://www.ci2ma.udec.cl







Centro de Investigación en
Ingeniería Matemática (CI²MA)
Universidad de Concepción

Casilla 160-C, Concepción, Chile
Tel.: 56-41-2661324/2661554/2661316
http://www.ci2ma.udec.cl